



SCHOOL of
GRADUATE STUDIES
EAST TENNESSEE STATE UNIVERSITY

East Tennessee State University
**Digital Commons @ East
Tennessee State University**

Electronic Theses and Dissertations

Student Works

12-2011

New Test Set for Video Quality Benchmarking

Joaquin Raventos
East Tennessee State University

Follow this and additional works at: <https://dc.etsu.edu/etd>

 Part of the [Engineering Commons](#)

Recommended Citation

Raventos, Joaquin, "New Test Set for Video Quality Benchmarking" (2011). *Electronic Theses and Dissertations*. Paper 1226.
<https://dc.etsu.edu/etd/1226>

This Thesis - Open Access is brought to you for free and open access by the Student Works at Digital Commons @ East Tennessee State University. It has been accepted for inclusion in Electronic Theses and Dissertations by an authorized administrator of Digital Commons @ East Tennessee State University. For more information, please contact digilib@etsu.edu.

New Test Set for Video Quality Benchmarking

A thesis

presented to

the faculty of the Department of Engineering Technology, Surveying, and Digital Media

East Tennessee State University

In partial fulfillment

of the requirements for the degree

Master of Science in Technology

Concentration Engineering Technology

by

Joaquin Raventos

December 2011

J. Paul Sims, Chair

Andrew J. Czuchry

Keith V. Johnson

Michael Seek

Key words: video image quality; low light camera; image quality benchmarking

ABSTRACT

New Test Set for Video Quality Benchmarking

by

Joaquin Raventos

A new test set design and benchmarking approach (US Patent pending) allows a “standard observer” to assess the end-to-end image quality characteristics of video imaging systems operating in day time or low-light conditions.

It uses randomized targets based on extensive application of Photometry, Geometrical Optics, and Digital Media.

The benchmarking takes into account the target’s contrast sensitivity, its color characteristics, and several aspects of human vision such as visual acuity and dynamic response. The standard observer is part of the “extended video imaging system” (EVIS).

The new test set allows image quality benchmarking by a panel of standard observers at the same time. The new approach shows that an unbiased assessment can be guaranteed.

Manufacturers, system integrators, and end users will assess end-to-end performance by simulating a choice of different colors, luminance levels, and dynamic conditions in the laboratory or in permanent video systems installations.

US Patent Pending Sep 21, 2011

Copyright © 2011 Joaquin Raventos

All Rights Reserved

ACKNOWLEDGMENTS

This project was undertaken in fulfillment of ENTC 5960, *Thesis of Master of Science in Technology -- Concentration: Engineering Technology*, Fall Semester 2011.



I would like to thank to Dr. Sims and the committee members for the time spent reviewing and assisting me in writing the thesis. I would also like to thank Mr. Lee Grasheim, President/CEO of Nightline, Inc. for his support and to my fiancée Isabel for her patience and encouragement while I was dedicated to the intense activity of research and development required to elaborate this thesis. And thank God for being a radiant source of inspiration that is always there regardless the distance.

CONTENTS

	Page
ABSTRACT	2
ACKNOWLEDGMENTS	4
LIST OF TABLES	9
LIST OF FIGURES	10
LIST OF UNITS AND ABBREVIATIONS	13
Chapter	
1. INTRODUCTION	16
Background	16
Problem Statement	20
2. METHOD	23
Subjects: Extended Video Imaging Systems (EVIS)	23
Image Quality	24
Apparatus (New Test Set)	25
Procedure	28
Color Capability	31
Standard Vision	32
Visual Acuity	32
Field of View	34
Aperture Stop	37
Exit Pupil & Entrance Pupil	38
Field Stop – System Field of View	38
<i>F-Stop</i>	38
Vignetting	41
Optical Vignetting	41
Mechanical Vignetting	42
Natural Vignetting	44
Lens Aberrations	46

Spherical Aberration	47
Chromatic Aberration	48
Astigmatism	48
Solid Angle (ω) – Steradian (sr)	49
Hemisphere Definition	52
Luminous Flux (Φ)	53
Definition of Lumen	55
Luminous Intensity (I)	56
Definition of Candela	56
Isotropic Source Definition	58
Extended Source Definition	58
Luminance (L)	58
Lambertian Source – Luminance	59
Luminous Exitance (Emittance) (M)	60
Illuminance (E)	60
Standard Observer Defined.....	63
Visual Acuity.....	63
Equal Legibility Letters.....	63
Tumbling Es Used in Optometry	64
Minimum Angle Resolution (MAR)	64
Normal Color Vision	67
Dynamic Searching Time	68
Target Detection & Recognition Model	69
Angular Threshold of the Human Eye	72
Tumbling Es Spatial Frequency	72
20/20 Tumbling E – LCD Monitor Calibration	74
20/20 Tumbling E Optotype Dimensions	74
Tumbling Es and USAF1951 Bar Chart	76
Tumbling Cs versus Tumbling Es	77

Contrast Sensitivity	77
Asphalt Reflectivity	79
Modulation Transfer Function	80
Contrast Sensitivity Patterns	81
Video Imaging System Analytics	87
CCTV Camera Formats	87
FOV, CCTV, and Objective Lens Format	88
Lenses for Use With TV-Type Systems	91
Radiant Power Transfer from Source to Detector	91
Lambertian Source	92
Illuminance E_d – Exact & Approximate Figures	93
The Cosine-To-The-Fourth Law	95
Reflectance of a Lambertian Source	95
Sensor Format SNR.....	96
Irradiance Levels at Different Stages of a Video Imaging System	96
Irradiance E_d in Terms of E_{lens} and Lens FOV	99
Calibration: The Need for Color Management	99
Open-Loop Color Management	99
Color Gamut	101
Device Calibration and Characterization	101
Laptop Screen Luminance	103
Apparatus Setup (New Test Set)	103
3. RESULTS	111
Traditional Optotypes vs New Optotypes	111
Grey Es / Cs	112
Day & Night E-Chart / C-Chart	112
Color Es / Cs	112
Random Es / Cs	112
Grey Tumbling Es/Cs Main Characteristics	113

Dynamic Es / Cs	114
LCD Photometric Parameters - Measurements & Estimates	115
Screen Display Luminance L_s – Estimate	115
Screen Display Luminance Control	119
Screen Display Illuminance E_d – Estimate	122
Illuminance E_d – Estimate for $d \geq 2$ m	124
ω_s Estimate Validation for $d \geq 2$ m	125
Luminous Intensity I_s - Estimate for $d \geq 2$ m	126
Luminous Power Φ_s - Estimate for $d \geq 2$ m.....	127
Luminous Emittance M – Estimate	127
Illuminance E_d in Terms of the Objective Lens F-Stop	128
Illuminance E_d in Terms of E_{lens} and Lens FOV	130
Lux Meter LX1010B Linearity	130
LCD Viewing Angle	132
LCD Refresh Rate	139
4. CONCLUSIONS AND RECOMMENDATIONS	140
Limitations and Recommendations for Future Research	140
Conclusions	140
REFERENCES	142
APPENDIXES.....	145
Appendix A: Language of Light - Definitions	145
Appendix B: Optical Vignetting	150
Appendix C: Natural Vignetting	151
Appendix D: Solid Angle Equations	153
Appendix E: Radiant Power Transfer from Source to Detector	157
Appendix F: Irradiance Levels at Different Stages of a Video System	166
Appendix G: Summary of Key Equations and Relationships	174
VITA	175

LIST OF TABLES

Table	Page
1. Tumbling Es Used in ASTM E2566 – 08. Main Characteristics	22
2. Light Transmittance.....	40
3. Summary of Units Used in Radiometry and Photometry	62
4. Contrast Index Based on HSL Measures of Snapshot in Figure 29	79
5. System Angle of View θ as Function of the CCD Format	90
6. Illuminance E_d - Exact Calculation and Lux Meter LX1010B Readings.....	94
7. LCL-217HS Settings	107
8. LCL-217HS CCD Camera Specifications.....	108
9. Digital Lux Meter LX1010B Specifications.....	118
10. LX1010B Lux Meter - E_d (lx) Measurements Linearity Test.....	131
11. Cosine-To-The-Fourth Power - E_d Estimate at Short Distance.....	135
12. Cosine-To-The-Fourth Power - E_d Correct Readings at Short Distance	137
13. Solid Angle ω - Apex Angle 2θ - Validity of $\omega \approx \pi(\theta)^2$ Approximation.....	156

LIST OF FIGURES

Figure		Page
1.	Tumbling Es Used in ASTM E2566 – 08	21
2.	Extended Video Imaging System (EVIS)	23
3.	Layout for Benchmarking an Extended Video Imaging System (EVIS)	27
4.	Terms Used in Radiometry and Photometry	29
5.	The USAF1951 Resolution Test Chart	30
6.	Thin Lens Field of View (FOV): $H \approx H' \cdot d/f$ for $1/d \ll 0$	35
7.	Thin Lens Angle of View (AOV) θ for Target Located at Infinity	36
8.	Simple Lens System and Aperture Stop	37
9.	Entrance Pupil	38
10.	Optical Vignetting: Common Intersection Area of Three Lenses at an Angle...	42
11.	Mechanical Vignetting Affects the Field of View	42
12.	Image Affected By Mechanical Vignetting	43
13.	Mechanical Vignetting Avoided by Increasing the Lens <i>F-Stop</i>	43
14.	Picture Showing Natural Vignetting	44
15.	Performance Diagram of Natural Vignetting for a Commercial Lens	45
16.	Thin Lens Focal Point	46
17.	Solid Angle Definition	49
18.	Steradian Definition	50
19.	Hemisphere Definition	52
20.	Photopic Luminous Efficiency is a Function of the Wavelength	54
21.	Photometry is a Subset of Radiometry in the Visible Spectrum	55
22.	The Definition of Candela Includes Units of Radiometry and Photometry	57
23.	Summary of Photometric Units	59

24. Luminous Flux Φ and Illuminance E	61
25. The 20/20 Tumbling E has a Spatial Frequency of 1.7 cy/mR.....	64
26. The 20/20 Tumbling E Scaled Up and Down.....	66
27. Probability P_2 of Detection.....	71
28. Designing the Tumbling Es Chart	75
29. Hue, Saturation, Luminance for Different Spots in a Scene	78
30. Square Wave Generated by a Fourier Series	80
31. Blurred Edges Generate a Sine-Wave Optotype Grating.....	82
32. MTF Curve for a Commercial Device.....	83
33. Output LCD Displays Tumbling Es as Sine-Wave Gratings	83
34. MTF for One Cycle Composed of One White Bar and One Black Bar	84
35. MTF Reduces: Sharpness (Effect #1) and Image Contrast (Effect #2)	85
36. Input / Output Tumbling C-charts Used in the EVIS.....	86
37. Different CCD Sensor Array Formats Available in the Marketplace.....	87
38. Increased System Magnification: 2/3” Format Lens on a 1/3” CCD Sensor...	89
39. Lambertian Source Approximation	92
40. Illuminance E_d Estimated at the Detector for $d \gg q \approx f$	97
41. Color Management Option in Windows 7 Professional Edition	100
42. Luminance Adjustment of the Dell Latitude D620 Laptop Video Card	102
43. Tumbling C Used for Screen Calibration / Tumbling Cs Generator	104
44. Display Setup Using the Calibrated C Optotype	105
45. LCL-217HS Settings for Video Quality Benchmarking.....	107
46. Digital Filter A_s 40% White/60% Black for Luminance L_s Adjustment	109
47. Digital Filter A_s 50% White/50% Black for Luminance L_s Adjustment	110
48. Tumbling Es: Dark Optotypes on Dark Background	113

49. 20/20 Tumbling Cs for C-Gap Identification.....	114
50. Solid Angle ω_s Subtended by a Lambertian Source	116
51. Spectrum Relative Sensitivity	118
52. Digital Filters for a Lambertian Source A_s from 100% to 70%.....	120
53. Digital Filters for a Lambertian Source A_s from 65% to 50%	121
54. Dell UltraSharp 1708-BLK/1908-BLK Monitor	123
55. Approximation of a Sphere Cap by a Flat Surface for 2θ Small $\leq 94^\circ$	125
56. Dell Latitude D620 Can Be Approximated to a Lambertian Source.....	126
57. The Geometrical Center in the Dell Latitude D620 Monitor	133
58. Same Illuminance E_{di} for Symmetric Cells Around the Geometric Center	134
59. The Radii r_1 to r_{20} and r_a to r_b Directly Measured on the Dell D620 Screen	136
60. A Lux Meter Placed at $d = 30$ cm Is Not Affected by Corner Screen Cells	138
61. Natural Vignetting	151
62. The approximation $\omega \approx \pi(\theta)^2 \rightarrow A$ (cone cap) $\approx A_s$ (flat circle) $= \pi r^2$	155
63. Solid Angle ω_d Subtended by the Detector	161
64. Solid Angle ω_{lens} Subtended by the Lens	167
65. Solid Angle ω_s Subtended by the Source.....	168
66. Image Formation by a Converging Thin Lens	169

LIST OF UNITS AND ABBREVIATIONS

Distance

nm	nanometer
μm	micrometer
mm	millimeter
cm	centimeter
m	meter
km	kilometer
in.	inch
“	inch
ft	foot
yd	yard

Radiant Power

W	watt
mW	milliwatts
μW	microwatts

Light

lm	lumen
cd	candela
fL	foot-lambert
fc	foot-candle
lx	lux
nit	nit

Planar Angle

rad	Radian
mR	milliradian
MOA	Minute Of Angle
MAR	Minimum Angle Resolution
deg	degree
°	degree

Solid Angle

sr	Steradian
----	-----------

Spatial Resolution

lp/mm	linepairs/millimeter
cy/mR	cycles/milliradian
cy/deg	cycles/degree

Colorimetry

H	Hue
S	Saturation
L	Luminance

Signal to Noise

dB	decibels
----	----------

Electricity

V	volts
mV	millivolts
VDC	volts direct current
VAC	volts alternate current
V _{p-p}	voltage peak to peak
A	amperes
mA	milliamperes
W	watts
mW	milliwatts
Ω	ohm

Time

sec	seconds
hr	hour

Weight

g	gram
kg	kilogram

CHAPTER 1

INTRODUCTION

The convergence of technological advances in optics, semiconductors, electronics, and embedded processing has led video imaging systems to become an integral component in an enormous variety of electronic solutions. Markets that are currently benefiting from video imaging system technology include:

- Security and Surveillance
- Network / IP Cameras for broadband videoconferencing
- Machine Vision

Closed-Circuit Television (CCTV) is typically used for Security and Surveillance applications. It differs from broadcast television in that the signal is not openly transmitted though it may employ point to point (P2P), point to multipoint, or mesh wireless links.

CCTV applications have blossomed in the last 2 decades. It is estimated that only in the U.K. more than 1.85 million CCTV systems are currently in operation (CCTV Image, 2011). At the same time, technology advances in video imaging has made it more difficult to compare the performance of various CCTV systems simply by looking at their specifications.

Background

Can Image Quality Be Usefully Quantified? One challenge faced by research scientists in the field of image quality is convincing product engineers, marketing personnel, management, and other scientists that image quality can be characterized in a quantitative fashion (Keelan, 2002).

Upon hearing a claim that image quality can be quantified, a skeptic is likely to cite certain factors that influence the satisfaction that different viewers derive from a particular image (Keelan, 2002).

Although there is a range of opinions regarding what is aesthetically pleasing in an image, just as in other art forms such as music and painting, *there actually is a good deal of agreement about desirable aspects of composition and lighting*. For instance, contrast might be correlated with some average gradient of the system tone scale and because preferences vary, the optimal contrast must be described as a statistical distribution.

Scientists and engineers, rather than psychologists, have sought to quantify various aspects of image quality. Keelan refers to some authors quantifying image quality, namely, Bartleson (1982) who modeled overall quality as a Minkowski sum (n^{th} root of the sum of n^{th} powers) of sharpness and the complement of graininess, each expressed on a 1-9 interval scale or De Ridder (1992) who combined digital encoding impairments expressed as fractions of maximum quality loss using a re-normalized Minkowski metric. But Engeldrum (1999) pointed out that none of these methods, nor others previously proposed, have proven to be extensible and generally applicable.

Other scientists investigated the image structure to *describe the ability to discriminate fine detail* in images produced by optical instruments. In the case of astronomical observations, resolving power was useful because it accurately described the ability of a telescope to distinguish stars having small angular separations as seen from the earth.

Image noise was first characterized in terms of blending distance (the viewing distance at which the noise became visually imperceptible), and later by root-mean square (RMS) granularity. Fourier theory began to permeate the field of optics in the

1940s, leading to the generalization of resolving power, a single-frequency metric, to the modulation transfer function (MTF), and of RMS granularity, an integrated quantity, to the noise power spectrum (NPS).

In 1964 Crane proposed the system modulation transfer (SMT) metric that was based upon system component MTFs and an assumed visual frequency response and was stated to have Just Noticeable Difference (JND) units. In 1975 Zwick and Brothers enhanced the usefulness of the RMS granularity metric by the determination of its JND increment (Keelan, 2002).

The final survey relates to the study of color and tone reproduction. There was a great deal of work done in the 1960s involving scaling of perceived brightness as a function of light level (controlling direct adaptation) and type of surround (controlling lateral adaptation).

The trichromatic nature of color vision was well known by the mid-1800s. Color matching functions and tristimulus values were standardized by the CIE in 1931, and subsequently more perceptually uniform color spaces were sought, leading to the definition of CIE $L^* u^* v^*$ and CIE $L^* a^* b^*$ coordinate systems (CIE Publication 15.2, 1986).

As mentioned in Keelan, recent studies - Buhr and Franchino, 1994, 1995; de Ridder, 1996; and Janssen, 2001 - have found *a preference for overall color and tone reproduction that differs systematically from accurate reproduction in having higher contrast and colorfulness.*

With the emergence of digital imaging, a great deal of attention has been focused on the properties of digital components including image processing algorithms and their effects on image quality.

Areas of current interest include:

- sampling, resampling, and reconstruction of images
- compression of digital images
- algorithms for correcting defects or enhancing images
- digital encoding of color information
- rendering of images for half-tone output
- standardization of measurements (ISO 14524:1997; ISO 12233:1998)

Recently some efforts have been made by the Image Quality Circle of Engeldrum, the Document Appearance Characterization (DAC) system used at Xerox or the European Adonis project to develop more integrated approaches based upon a general perceptually relevant framework.

In order to equally assess different displays and display technologies, image quality must be carefully defined in tangible and measurable terms. When characterizing a display, sensory qualities such as luminance, contrast, color, and spatial frequency depend and interact with each other. In understanding image quality it is important that the limits of the display and that of the human-eye system are comprehended.

It is important to understand how we process and perceive visual stimuli to understand how image quality is defined. The human eye is composed of two photoreceptors; rods and cones. Rods have greater sensitivity to light, can only "see" shades of grey, and are more sensitive to luminance and flicker. Cones have greater resolving capabilities.

When the intensity of a multi-color display or image is lowered, the colors drop out sequentially into grey levels. The first colors to shift to grey are blues and reds

with the last being greens. This shifting of colors to grey is known as the Purkinje shift.

The two primary measurements used in display image quality characteristics are luminance and spectral radiance.

Resolution is also important in defining the interaction between the information density on the display and the resolving capability of the human visual system (Sharp Corporation, 1993).

Problem Statement

Hence, tests were developed that allowed comparison of different architectures such as the ASTM E2566-08 Standard Test Method that covers the measurement of end-to-end capability of Visual Acuity and the Field of View for remotely operated video systems:

- Visual Acuity in Light and Dark Environments
 - at near distances
 - at far distances with both ambient lighting and lighting on-board
 - with zoom lens capability
- Field of View of the camera system

This test determines the visual acuity available to the operator at control unit when the camera on the robot is focused on distant objects (more than a few meters or so distant from the robot).

The display on the screen at the operator control unit integrates the effects of camera; the sensor array within the camera; digitization of the signals; transmission of the data; reconstruction of the images; and resolution of the display screen.

There is no need from the user's perspective to resolve these various contributing factors because the visual image as presented to the operator is the key issue in remote operation.

Developers of robots and video imaging systems, on the other hand, may need to analyze each of these factors separately.

The ASTM E2566-08 Standard is written from the standpoint of evaluation and procurement by the user.

Nevertheless some characteristics of human vision need to be taken into account because measurement of end-to-end capability considers visual acuity that involves the human eye.

In this sense, this standard has serious limitations and does not provide an effective comparison among modern CCTV systems.

The ASTM E2566-08 basically compares system resolution without including contrast sensitivity or randomly generated characters (optotypes) to eliminate the possibility of bias in selecting the best CCTV system, see Figure 1 and Table 1.



Figure 1. Tumbling Es Used in ASTM E2566 – 08

Table 1

Tumbling Es Used in ASTM E2566 – 08. Main Characteristics

Black Tumbling E's:	on White Background
Different E-Chart for Day & Night:	NO
Contrast Sensitivity:	Not Considered
Color E's:	NO
E-Chart Computer Generated:	NO
Tumbling E's Randomly Generated:	NO
Standard Observer Dynamic Searching	NO

The purpose of this thesis is to develop a new test set for end-to-end video quality testing that takes into account all the factors that intervene in the benchmarking carried out by a “standard observer” of video imaging systems in high light or low-light conditions.

The “standard observer” is defined in detail in CHAPTER 2 as the observer is an integral contributor to the EVIS.

The main characteristics affecting “standard vision” are visual acuity and normal color vision:

- Visual acuity

The spatial resolving capacity of the human visual system

- Normal color vision

The standard assumed to represent the average of the human population according to the standard developed by CIE.

CHAPTER 2

METHOD

Subjects: Extended Video Imaging Systems (EVIS)

The subjects considered in this thesis are the Extended Video Imaging Systems (EVIS) that typically consist of the following, see Figure 2:

- a) Objective Lens
- b) CCD or CMOS camera
- c) LCD display
- d) Standard Observer (trained and with good or corrected 20/20 vision)

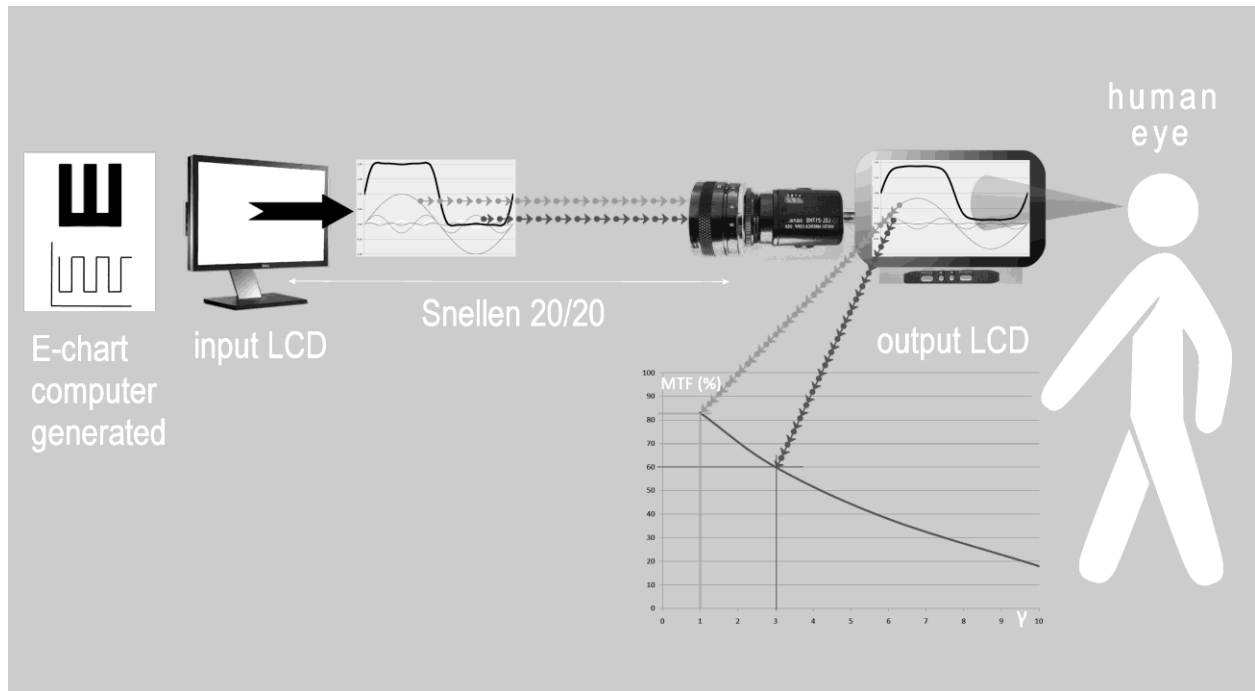


Figure 2. Extended Video Imaging System (EVIS)

The performance of the whole system is subject to the characteristics of the human eye of the “standard observer”. Each component of the EVIS affects the quality of the image assessed by the observer.

There are numerous Charged-Coupled Device (CCD) or Complementary Metal-Oxide Semiconductor (CMOS) sensor arrays and objective lenses available to the market.

Before proceeding to the installation in the permanent location, the selection and testing of an appropriate configuration requires a video quality benchmarking test set and a comprehensive approach that includes the multiple aspects affecting the end-to-end assessment of Extended Video Imaging Systems (EVIS).

If an incorrect objective lens or CCD / CMOS video camera is selected because a limited benchmarking approach has been used, the overall performance of the EVIS will be drastically reduced.

This is particularly noticeable when the video imaging system is used under low-light conditions, for instance full moon or quarter moon, because the benchmarking approach currently used in the market does not provide an accurate measure of testing the performance of video imaging systems in a simulated low-light environment.

Image Quality

The design of the new test and the definition of the new benchmarking approach developed in this thesis are based on extensive use of principles and key measurement units defined in the fields of Geometrical Optics, Radiometry, and Photometry.

Also the Modulation Transfer Function (MTF) and the Contrast Transfer Function (CTF) are considered.

The main characteristics affecting the video image quality are:

- 1) Visual Acuity
- 2) Field of View
- 3) *F-Stop*
- 4) Solid Angle subtended by the source
- 5) Luminance of a Lambertian source
- 6) Illuminance on the sensor array
- 7) Vignetting
- 8) Lens Aberrations
- 9) Standard Observer - Definition

The next section discusses the various factors that reduce the visual acuity offered by the video imaging system to the “standard observer” and how the different types of vignetting are the main contributors to reducing the field of view.

Also, it is shown that if the luminance L_s of the radiant source can be approximated to a Lambertian radiator, useful approximate equations to calculate the illuminance E_d on the sensor array can be obtained.

Apparatus (New Test Set)

The new test set includes items already available in the market, such as a Dell Laptop Computer or Microsoft Windows 7 Professional Edition, and new items designed specifically for operation and calibration of the test such as Tumbling Cs Generator and Luminance Digital Filters.

The items required for the new test set, see Figure 2 and Figure 3, used for video benchmarking are:

- Dell Latitude D620 Laptop Computer or similar
- Windows 7 Professional Edition
- Adobe Reader X
- Adobe Photoshop CS3 or later
- Tumbling Es Generator
- Tumbling Cs Generator
- Lux Meter LX1010B or similar
- Photosensor Holder
- Luminance Digital Filters to Calibrate the LCD Radiant Surface:

100%

85%

75%

70%

65%

60%

55%

50%

40%

- Measuring Tape 25' x 1"
- Metric Ruler 30 cm
- Lens, 1X Magnification
- C-CS Mount Adapter
- LCL-217HS CCD video camera or similar
- 5" LCD Monitor
- 12 VDC Power Supply
- Dark Room Environment

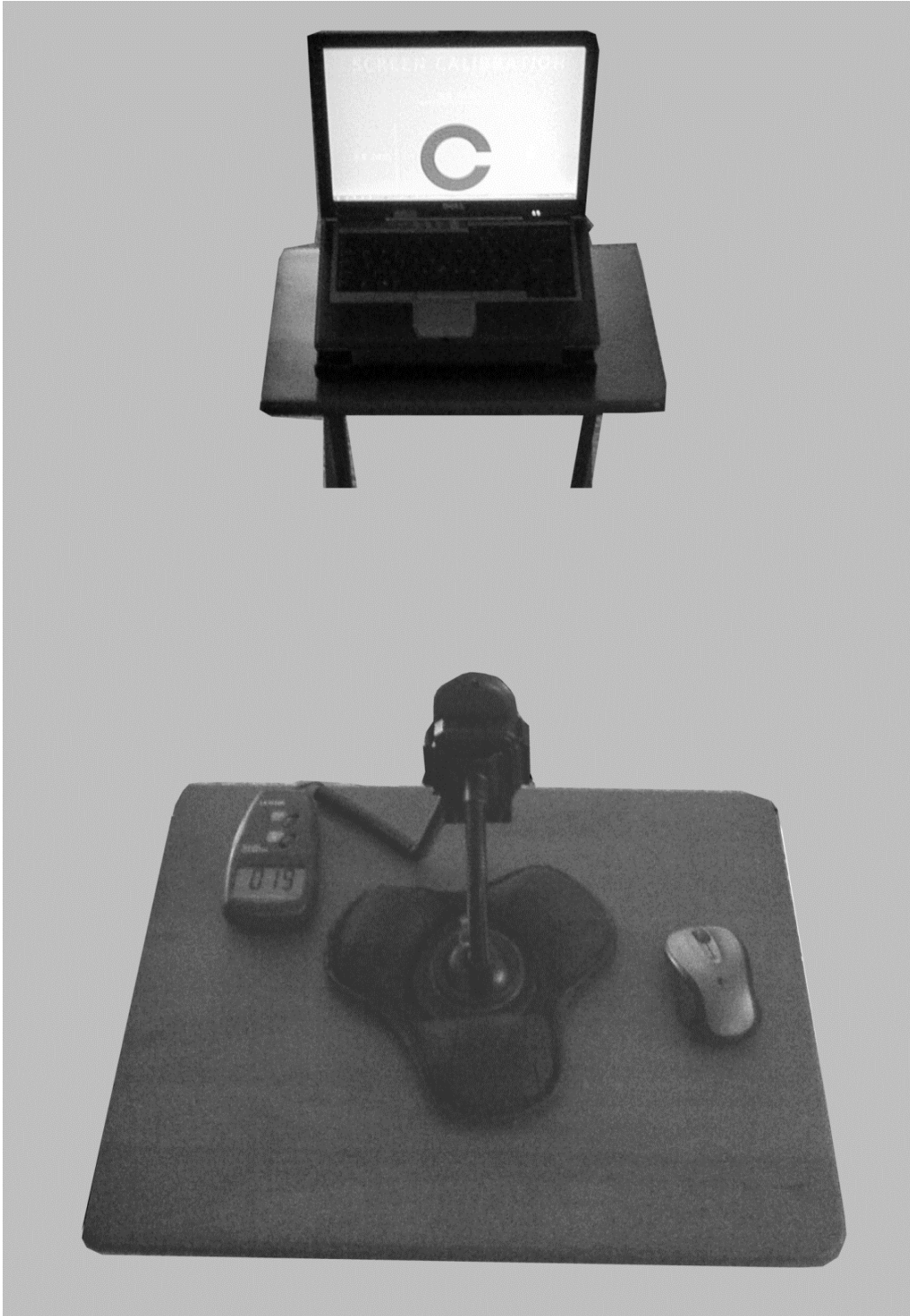


Figure 3. Layout for Benchmarking an Extended Video Imaging System (EVIS)

Procedure

The basic configuration of a video imaging system starts with a light source that illuminates (illuminance) an object which then generates an image throughout the optical system projected onto the sensor array of a CCD or CMOS. It will convey a video signal to a display screen that transforms the signal into a visible image where finally it is processed by the human eye.

It also should be noted that according to the “standard observer” mentioned in ASTM 2855-08 and the principles of visual measurements in Photometry, the human eye is part of what can be described as an “extended video imaging system” (EVIS), see Figure 2.

An End-To-End Testing Method considers an EVIS composed of:

- a) Input LCD
- b) Objective Lens
- c) CCD or CMOS camera
- d) Output LCD
- e) Human Eye

Each component of the EVIS affects the quality of the image assessed by the observer. The performance of the EVIS is not evaluated using laboratory instruments and mathematical models for objective video quality metrics but by a human observer who may introduce subjectivity and bias in the assessment of the image quality of the video imaging system.

In order to minimize the impact of human errors in the EVIS benchmarking process, a discussion of the different variables affecting the image quality of EVIS follows.

This section describes the main units and definitions considered in Photometry, Geometrical Optics, and Human Vision, sometimes referred altogether as “the language of light” see Figure 4 and also Appendix A.

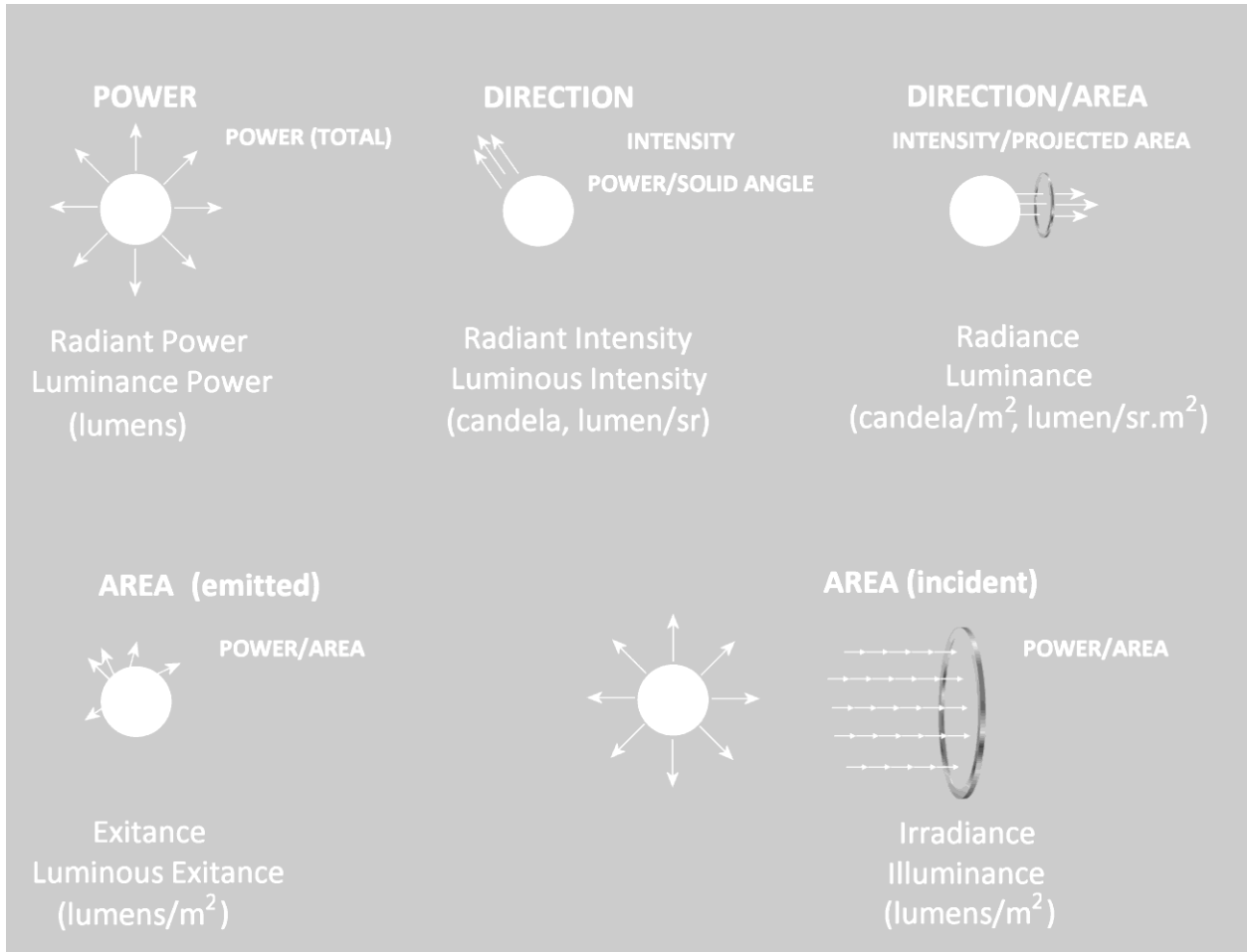


Figure 4. Terms Used in Radiometry and Photometry

Figure 4 shows the photometric units: Lumen; Lumen/sr; Lumen/sr.m²; and Lumen/m². Understanding the “language of light” is essential to figure out the limitations, improvements, and validations of any image benchmarking methods:

- a) Limitations: Of the ASTM 2855-08 standard and other standards such as the USAF1951 Bar Chart, see Figure 5, currently used for end-to-end video imaging testing;

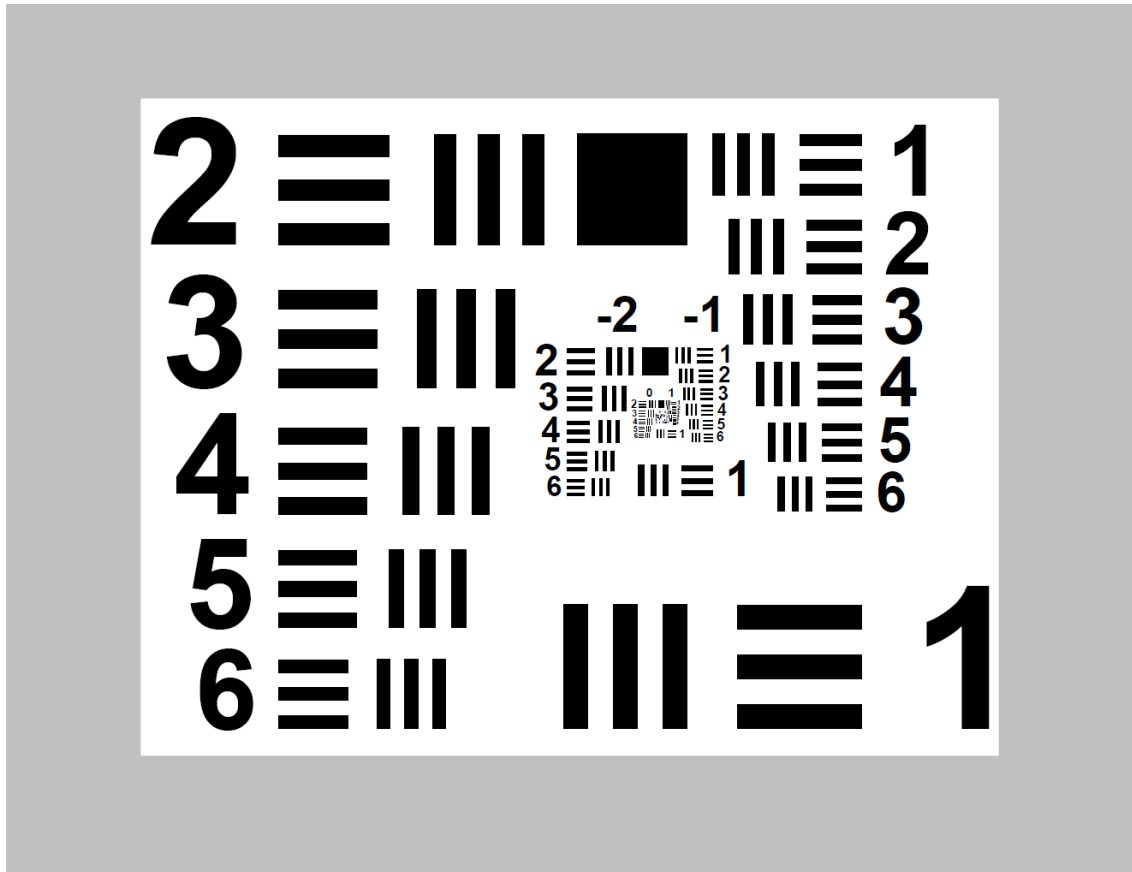


Figure 5. The USAF1951 Resolution Test Chart

- b) Improvements: That can be achieved with the new test set and benchmarking method described in this thesis;
- c) Validations: Of the design and calibration of the test set used to develop the new video quality benchmarking approach.

Color Capability

Color capability feature is needed in low light conditions to compare video imaging systems as most of them have automatic color correction and back light compensation.

To ascertain which one is the best video imaging system when the targets are illuminated by street lights or other types of artificial lights, a color target feature is needed.

In some applications monochrome (black-and-white) processing is enough to assess the alarm condition, However, for other applications the ability to recognize the color of clothing, the color of vehicles, and so forth is often more important than a more detailed image.

In surveillance (airports, car parks, industrial areas) shadow detection is critical. The goal of algorithms for shadows detection is to prevent moving shadows from being misclassified as moving objects or part of them, and all of these algorithms rely on color features (Lukac & Plataniotis, 2006).

The measurement of luminous parameters, luminance and illuminance, is confusing due to the large numbers of new names for units and also because complex definitions are simplified by making reference to an ideal Lambertian source. For instance when discussing topics in photometry the term intensity has been found frequently misused in publications (Palmer, 1995). In addition, the totally arbitrary peak values of the standard photopic and scotopic curves used in photometry have been modified several times since they were initially adopted in 1924 and 1951.

In addition, using some units such as foot-candle units when referring to luminous exitance may be confusing because candle is an old unit of intensity, not flux (Roberts, 1996).

So, in order to clarify the “language of light” a description of the units and definitions regarding the technologies of radiometry and photometry used to elaborate this thesis are discussed. A complete set of the currently approved photometric terms and definitions can be found in the ANSI Standard ANSI/IES RP-16-1980.

Standard Vision

By definition in Geometrical Optics, it is considered that an angle measurement of 1 degree has 60 MOA (minute of arc).

The standard vision of the human eye was defined in 1862 by Hermann Snellen, a Dutch Ophthalmologist, and he stated that standard vision is the ability to resolve (i.e. to identify) target features subtending an angle equal to 1 MOA.

Standard vision depends on visual acuity.

Visual Acuity. According to ASTM E2566-08, visual acuity is the ability to resolve features subtending some angle, as compared with “standard vision” measured at the same distance.

When benchmarking an EVIS, visual acuity is affected by both the video imaging system performance and the human vision characteristics of the “standard observer”. The main factors reducing the performance of the video imaging system or the response of the human eye are:

- Video Imaging System (ASTM E2566-08):
 - objective lens
 - the sensor array within the CCD / CMOS camera
 - digitization of the signals
 - data transmission
 - reconstruction of the images and
 - resolution of the LCD monitor

- Human Eye:
 - Angular Threshold of Eye
 - Contrast
 - Perception
 - Visual Effectiveness
 - Relative brightness
 - Threshold detection
 - Recognition
 - Conspicuity
 - Reaction time
 - Visual performance

In defining visual effectiveness, historically several options were considered (DiLaura, 2011), but at the time it was decided that visual effectiveness in photopic mode (luminance $L > 10 \text{ cd/m}^2$ what generates an illuminance $E > 32 \text{ lux}$) was better represented in terms of the relative brightness (luminance) produced by radiant power at different wavelengths.

In the photopic mode the light impinges the fovea, which is the very center of the human eye field of view.

As a matter of fact, in the design of the new test set it has been estimated that when the EVIS operator is observing a scene in the LCD monitor at an approximate distance of 24 in. (60 cm), the mode of vision is photopic because the illuminance level on the eye E_{eye} generated by for instance, the display screen of a Dell Latitude D620 is about 32 lux.

The E_{eye} figure of 32 lx can be determined by extrapolating the illuminance E_d on the detector (in this case the eye) between $d = 0.30 \text{ m}$ and $d = 1.0 \text{ m}$ in Table 6.

The “standard vision” is based on the ophthalmologic analysis of the human emmetropic eye (a state in which the eye is relaxed and focused on an object more than 6 meters or 20 feet away).

For the human eye entrance-pupil diameter is controlled by muscle fibers of the iris. In total darkness the iris is about 8 mm in diameter, whereas in bright light it is reduced to 2 mm in diameter (Laikin, 2007).

According to the ASTM E2566-08, the visual image as presented to the operator is the key issue in remote surveillance, so in order to propose an alternative to the current ASTM E2566-08 standard itself, a review of the various factors affecting the visual acuity of the observer is required.

Field of View

Imaging optical systems have three main components—the object, the optic, and the image it forms.

The object is considered as a set of points that emit light in all directions. The light (or part of it) from each point on the object is captured by the optical system and concentrated onto a point in the image. The distances between points on the image may be scaled relative to those on the object resulting in magnification (Chaves, 2008).

Field of View is the maximum height (or width) of the object as seen from the position of the entrance pupil.

It is the shooting range H that can be viewed by the video system if the distance d to the object is finite and is calculated as, see Figure 6:

$$H = H' \cdot d / f \tag{01}$$

H' : horizontal dimension of the CCD or CMOS sensor array

f : focal length of the objective lens

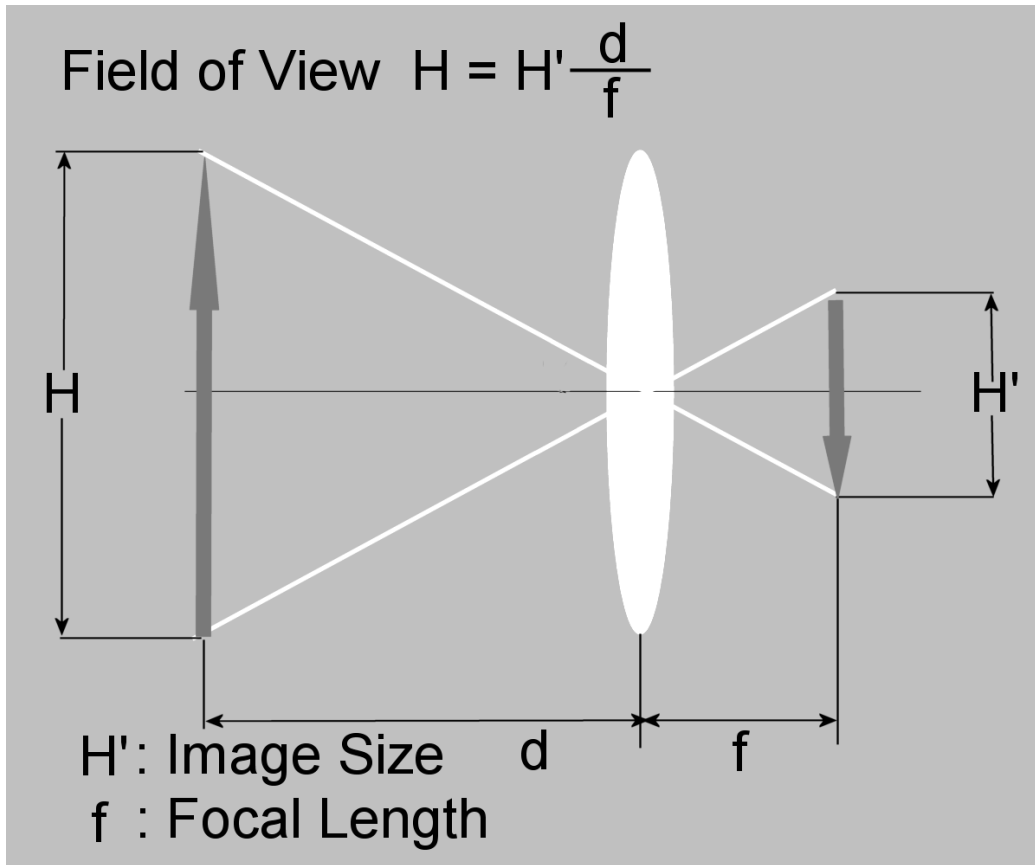


Figure 6. Thin Lens Field of View (FOV): $H \approx H' \cdot d / f$ for $1/d \ll 0$

When the object is located at a very far distance, in practice $d \geq 60$ ft, it can be considered that the lens is focused at infinity and instead of the Field of View (FOV), another parameter, the Angle of View (AOV) θ is measured, see Figure 7.

In this case the shooting range that can be covered by the video system is given a specified image size of the CCD sensor array ($H' = 1''$, $2/3''$, $1/2''$ or $1/3''$) and it is usually expressed in degrees. From Figure 7:

$$\tan(\theta/2) = (H'/2)/f \Rightarrow \theta = 2 \tan^{-1} H'/2f \quad (02)$$

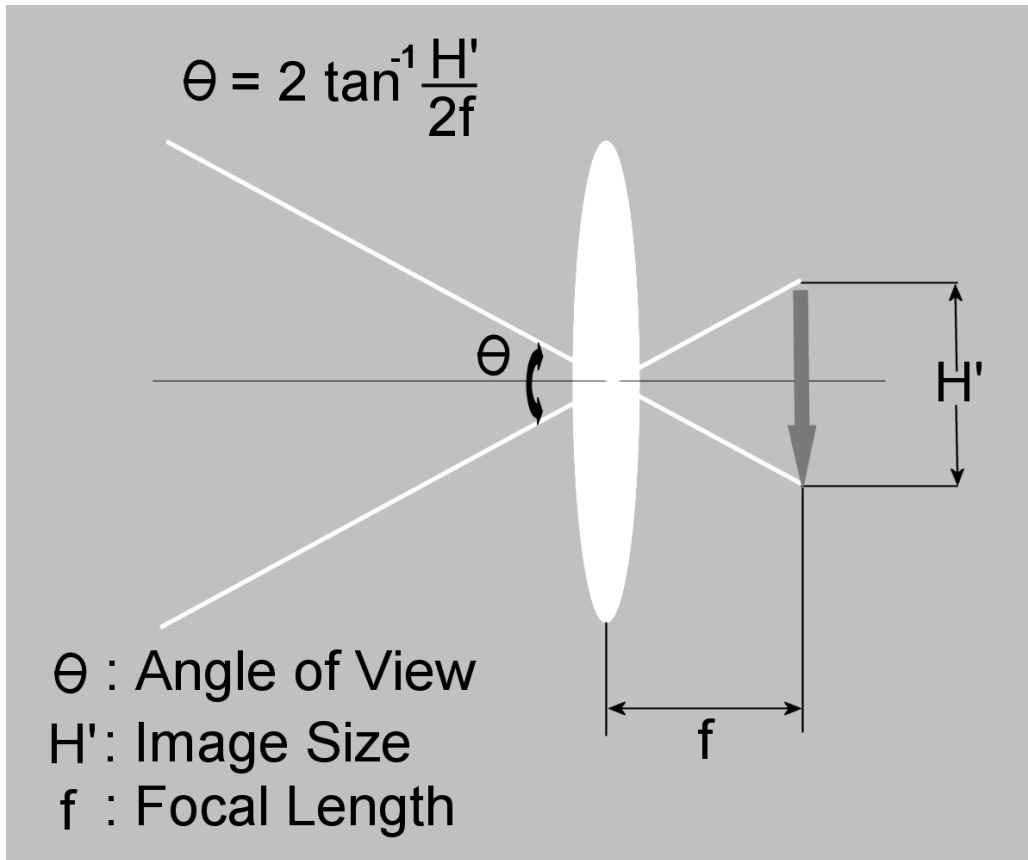


Figure 7. Thin Lens Angle of View (AOV) θ for Target Located at Infinity

In this case the shooting range that can be covered by the video system is given by a specified image size of the CCD sensor array ($H' = 1''$, $2/3''$, $1/2''$ or $1/3''$) and it is usually expressed in degrees.

From Figure 7 the lens AOV θ is calculated by:

$$\tan \frac{\theta}{2} = \frac{H'/2}{f} \implies \theta = 2 \cdot \text{atan} \left(\frac{H'/2}{f} \right) \quad (02)$$

The Field of View is an important characteristic of a video system, as it determines the ability of the operator to obtain information from a scene.

Looking at the world through a zoom lens is like “looking through a soda straw.” Looking with a 30° or 40° FOV lens is like “driving with blinders on.”

On the other hand, using a very wide field of view lens (with a field of view of 120 or 150°), the operator’s use of optic flow to cue depth perception is severely degraded and navigating in a tight environment is very difficult, ASTM E2566-08.

Aperture Stop

The *aperture stop* of an optical system is an aperture near the entrance that determines the size of the bundle of rays leaving the source that can enter the optical system, see Figure 8.

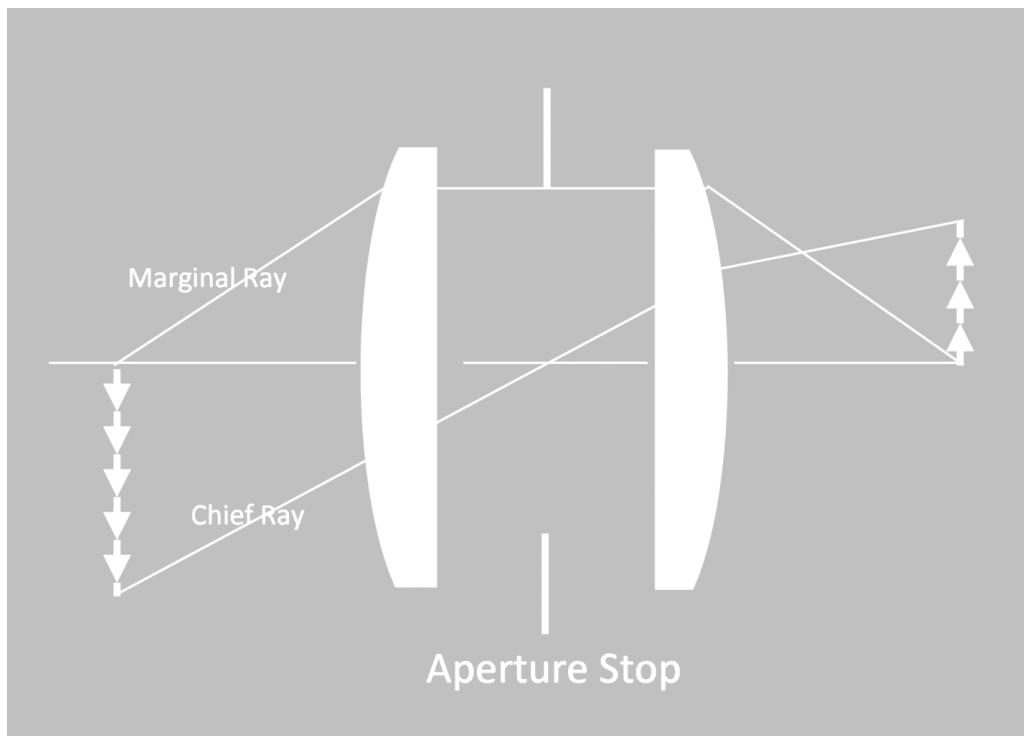


Figure 8. Simple Lens System and Aperture Stop

Exit Pupil & Entrance Pupil. The image of the aperture stop in the region of the detector is the *exit pupil*. The image of the aperture stop in the region of the source is the *entrance pupil*, see Figure 9.



Figure 9. Entrance Pupil

In the left image of Figure 9 the entrance pupil is the aperture stop of the lens; in the right image the entrance pupil is reduced by the *F-Stop* of the lens.

Field Stop – System Field of View. The *field stop* is an aperture within the optical system. The field stop defines the solid angle within the optical system, called the *system field of view*, and is a useful radiometric concept because a complex optical system can often be approximated as an exit pupil having the same radiance as the object being imaged.

F-Stop. The *F-Stop* also called *f*-number (abbreviated $f_{\#}$) or *relative aperture* is an indication of the brightness of a lens, namely its capacity to transfer luminous flux onto a detector or another lens. The smaller the value, the brighter the image produced by the lens.

The *F-Stop* is the ratio between the diameter D of the entrance pupil of the lens and its focal length f (in image space) and can also be described as function of the maximum aperture angle as indicated by Zalewski (as cited in Bass, 1994) and that for small angle α the value of $\tan\alpha$ can be approximated by $\sin\alpha$ (Lenhardt & Kreuznach, 2005):

$$F\text{-Stop} = \frac{f}{D} = \frac{1}{2r/f} = \frac{1}{2\tan\alpha_{max}} \approx \frac{1}{2\sin\alpha_{max}} \quad (03)$$

α_{max} is half of aperture angle between the optic axis and the ray pencil from the on-axis object point to the edge of the entrance pupil in the object space.

The scale on the iris ring of the lens uses a ratio of $\sqrt{2}$ because the value of incident light (irradiance in Radiometry or illuminance in Photometry) transferred by a lens see Appendix F, is:

$$E_d \approx \frac{\pi}{4} \frac{L_s}{(F_{stop})^2} \quad (04)$$

Thus, the irradiance or illuminance E_d in the film of a still camera or sensor array of a video imaging system, decreases by half each time the *F-Stop* is increased by one *F-Stop*.

For instance: *F-Stop* 2.8 incremented by one *F-Stop* \implies *F-Stop* = 2.8 x $\sqrt{2}$ = 4

$$E_d(F/4) \approx \frac{\pi}{4} \frac{L_s}{(2.8 \times \sqrt{2})^2} = 1/2 \frac{\pi}{4} \frac{L_s}{(2.8)^2} = 1/2 E_d(F/2.8)$$

Camera lenses are stopped in irradiance steps of 2, 4, 8, 16, 32, 64, 128 that correspond to *F-Stop* numbers of 1.4 ; 2 ; 2.8 ; 4 ; 5.6 ; 8 ; 11 so one stop change produces a factor increasing or decreasing by 2 the irradiance on the sensor array.

See Table 2 for a complete chart of typical *F-Stop* scales and light transmittance percentages for objective lenses.

Table 2

Light Transmittance.

F-Stop measures the aperture of a given lens. Each F-Stop jump indicates a 50% reduction in the amount of light a lens is able to transmit (transmittance).

Light Transmittance	F-Stop				
100%	0.8	1.2	1.3	1.4	2.8
50%	1.1	1.7	1.8	2	4
25%	1.6	2.4	2.6	2.8	5.6
12.50%	2.3	3.4	3.7	4	8
6.25%	3.2	4.8	5.2	5.6	11
3.0%	4.5	7	7.4	8	16
1.6%	6.4	10	10.4	11	22
0.8%	9	14	15	16	32
0.4%	12	19	21	22	45
0.2%	18	27	29	32	64
0.1%	25	38	41	45	90
0.05%	36	54	59	64	128
Transmittance Reduced by 1/10					
0.006%	102	154	166	181	362
Transmittance Reduced by 1/10					
0.0007%	290	434	471	512	1440

Vignetting

Benchmarking the image quality of video imaging systems, considers several factors affecting the Field of View and Visual Acuity.

In optics vignetting refers to the effect of reducing an image's brightness or saturation at the periphery compared to the image center. It is an important factor affecting the field of view in video imaging systems.

There are several types of vignetting:

- Optical Vignetting
- Mechanical Vignetting
- Natural Vignetting

Another type of vignetting that distorts the radiometric fidelity of video imagery is spectrum-related vignetting, and it is typically introduced at larger incident angles by an interference filter located in front of a lens, but this type of filter is mainly used in airborne video imagery (Edirisinghe, 2001) and is not common in CCTV systems.

Optical Vignetting. It is caused by the reduction of the cross-sectional area of an oblique beam traversing the lens in comparison to that of an equivalent axial beam, see Appendix B.

The result is (Thompson & Malacara, 2001) a gradual decrease in light intensity towards the image periphery due to physical length of the lens, the position of the aperture stop, and the diameter of the front and rear elements, see Figure 8.

The amount of optical vignetting depends on the *F-Stop* in use; for an aperture with low *F-Stop*, the effect of optical vignetting may be high (Ray, 1988). It can be completely cured by a reduction in aperture of 2–3 stops, i.e. an *increase* in the *F-Stop* see Figure 10.

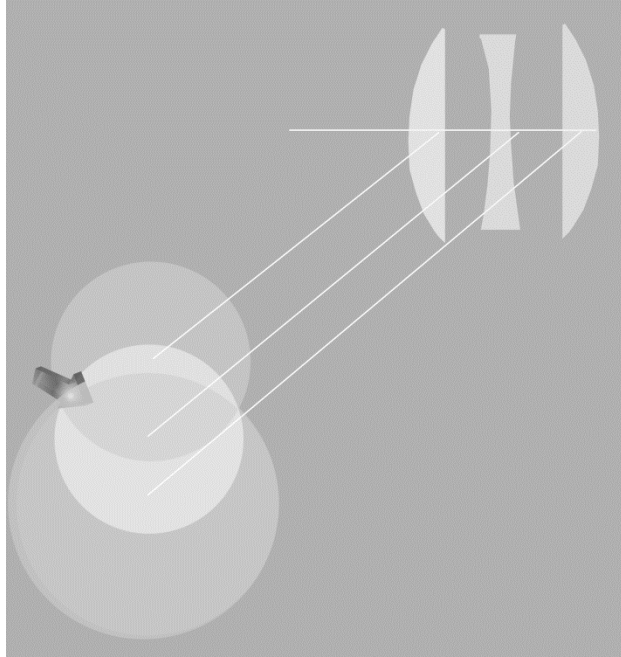


Figure 10. Optical Vignetting: Common Intersection Area of Three Lenses at an Angle

Mechanical Vignetting. It is caused by an obstruction of light in the corner area of the lens, see Figure 11 creating the effect shown in Figure 12 (Ray, 1988).

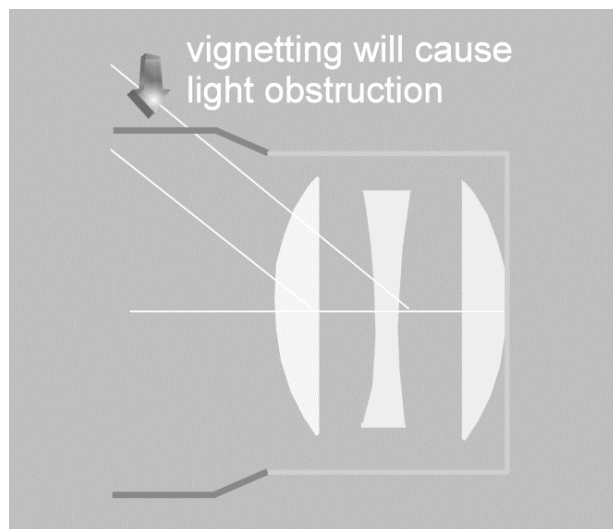


Figure 11. Mechanical Vignetting Affects the Field of View



Figure 12. Image Affected by Mechanical Vignetting

Mechanical Vignetting is sensitive to the lens aperture and can be completely cured by a reduction in aperture of 2–3 stops, i.e. an *increase* in the *F-Stop*:

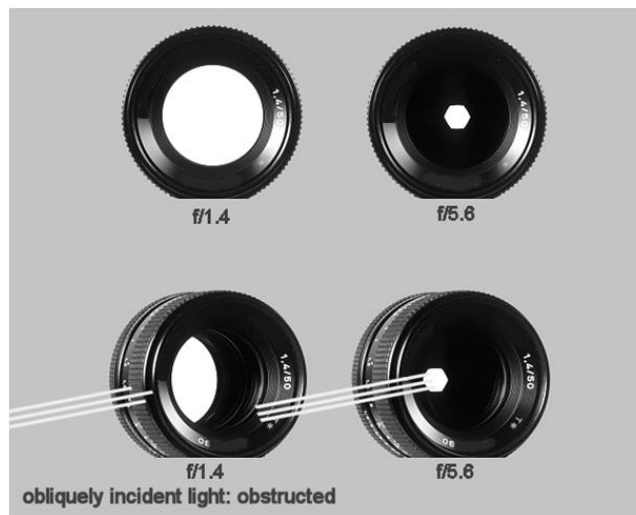


Figure 13. Mechanical Vignetting Avoided by Increasing the Lens *F-Stop*

Natural Vignetting. Most objective lenses exhibit natural vignetting to some degree. This term indicates an unintended darkening of the image corners and it is caused by the cosine-to-the-fourth power law, see Figure 14:



Figure 14. Picture Showing Natural Vignetting

Obliquely incident light is confronted with a smaller lens opening compared to the lens opening offered by light approaching the lens head-on.

All types of vignetting are at their worst with the lens focused at infinity (Walree, 2011) and the lens aperture wide open.

For practical purposes, a lens focused at a target farther than 60 feet, which is the usual condition for a CCTV system, is considered to be focused at infinity.

The effect is strongest when the lens is used wide open, i.e. for an aperture with low F -Stop.

Thus a Zeiss $F/2.8$ lens is equivalent to an $F/5.6$ lens when looking at the borders, see Figure 15.

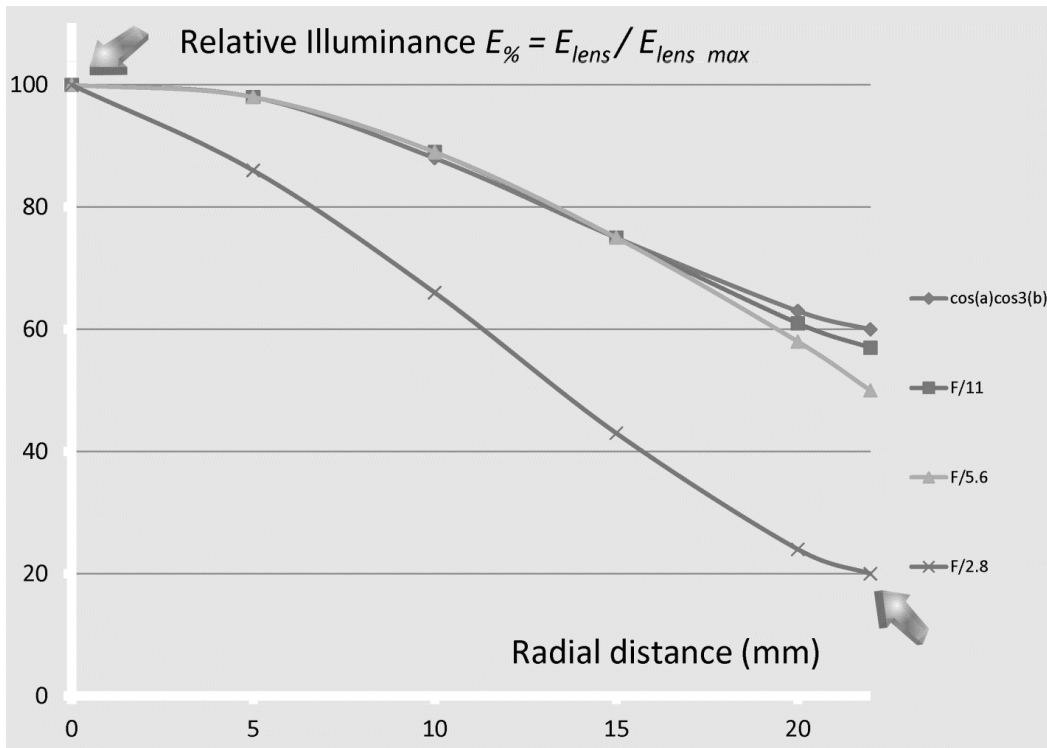


Figure 15. Performance Diagram of Natural Vignetting for a Commercial Lens

At full aperture the lens provides a corner illuminance of 20%. The center receives 100% namely five times the amount of light of the corner.

The lens performance at F -Stop = $F/11$ & $F/5.6$ follows very closely, see Appendix C, the cosine-to-the-fourth power curve:

$$\cos(a)\cos^3(b) = \cos^4(\theta)$$

Lens Aberrations

The most common types of thin lenses are: convergent and divergent. As the objective lenses used in CCTV systems are based on the convergent type, the focal length definition will consider the convergence lens.

When a convergent lens is focused to infinity, it is considered that the light rays are parallel and they converge thru a convex lens to a point on the optical axis: the Focal Point, see Figure 16.

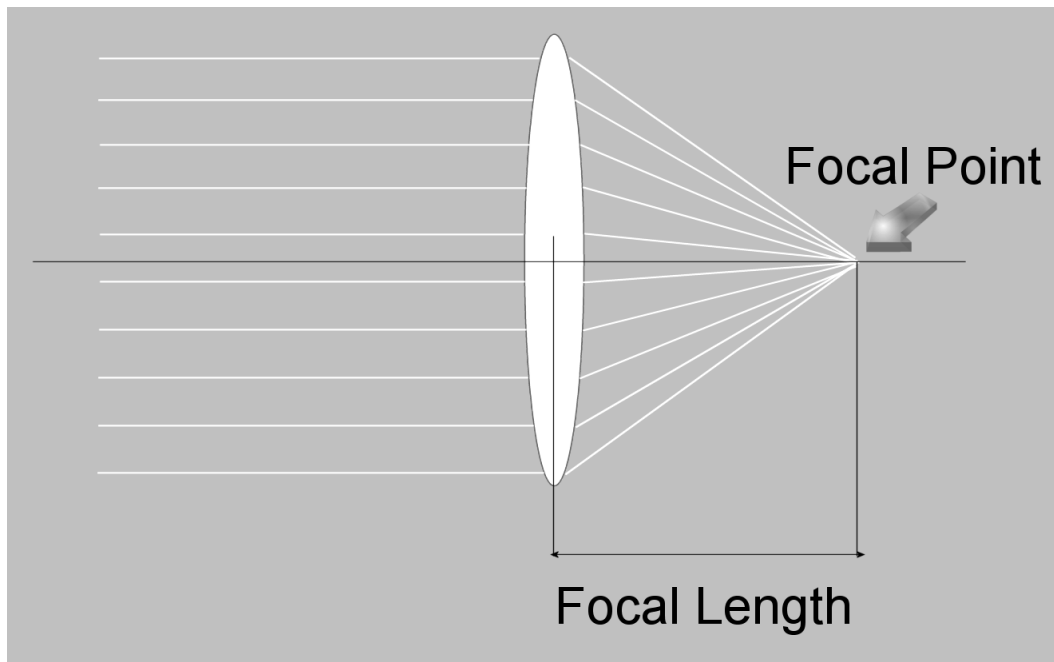


Figure 16. Thin Lens Focal Point

A thin lens is an ideal convergent lens without aberration. The rays are parallel when distance to the target is infinite.

In practice, rays are considered parallel when distance to the target is longer than 20 ft (6.1 m). This approximation is also used in human vision and then it is called emmetropic vision.

Geometrical Optics is the study of First-Order Optics, namely perfect optical systems without light diffraction or interference. The analysis methods include Gaussian Optics and Paraxial Optics, which are extensively been used in this thesis.

Aberration is a deviation from the ideal focusing of light by a lens. As a result, the image is not sharply focused. These aberrations are inherent to the design of the optical system, even when perfectly manufactured (Greivenkamp, 2204) and their study includes the Third-Optics and higher-order optics.

Some of the problems may lie with the geometry of the lens in use. Other aberrations may occur because different wavelengths of light are not refracted equally at the same time. The latter problem is called dispersion of light.

The spherical shape of any lens surface causes spherical aberration and the manufacturers of the lenses use multiple surfaces to overcome spherical aberration.

There are several types of spherical aberrations that may be detected when evaluating a video imaging system with the Tumbling Es Test Method:

- Spherical
- Chromatic (Dispersion)
- Astigmatism (Distorsion)

Spherical Aberration. Light rays that are far from the principal axis focus at different focal points and produce spherical aberration. It can be minimized by using

an aperture to reduce the effective area of the lens as in most cameras equipped with an adjustable aperture to control the light intensity.

Chromatic Aberration. Rays of different wavelengths (colors) do not refract at the same angle; there is no common focal point for all the wavelengths. Then, the rays focus at different points and chromatic aberration is formed.

Chromatic aberration can be greatly reduced by the use of a combination of two different types of glass with differing indexes of refraction.

Astigmatism. Is the imaging of a point offset from the axis as two perpendicular lines in different planes: The horizontal rays to a line called the primary image and the vertical rays to a second line, called the secondary image.

First-Order Optical Systems image points to points, lines to lines, and planes to planes even if the lines or planes are not perpendicular to the optical axis.

For a thin lens, the line of intersection lies in the plane of the lens, but for a tilted plane image even though the image is in focus, it will exhibit keystone distortion as the lateral magnification varies along the tilted object. This condition easily extends to a thick lens or system (Greivenkamp, 2004).

The circle of least confusion (greatest convergence) appears between these two positions. The image of a straight line that does not pass through the optic axis may be curved.

As a result, the image of a square with the axis through its centre may resemble a barrel (sides bent outward) or a pincushion (sides bent inward).

This effect is called distortion and can be minimized by using properly designed, nonspherical surfaces or specific lens combinations (Al-Azzawi, 2007).

Solid Angle (ω) – Steradian (sr)

Whereas in Geometrical Optics a two dimensional system is used for the study of light without diffraction or interference (Greivenkamp, 2004), for instance to calculate a lens field of view, a three dimensional system is necessary to analyze the propagation of radiant energy through an optical system (Radiometry) or when visual measurements are considered (Photometry).

Thus, instead of the planar angle θ used in Geometrical Optics, a new unit is defined: the Solid Angle ω and it is measured in *Steradian*, abbreviated *sr*.

Solid Angle is the ratio of a portion of the area *on the surface of a sphere* to the square of the sphere radius R . The sphere is defined by the vertex (usually the center of a luminous body) and the center of the surface (usually an aperture detector), see Figure 17.

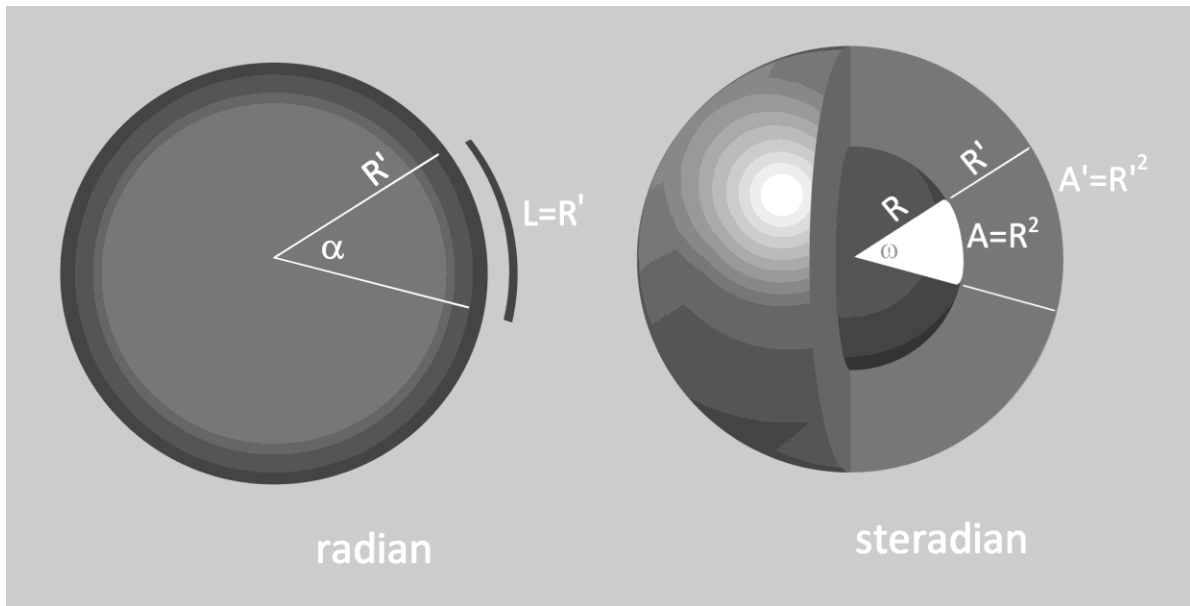


Figure 17. Solid Angle Definition

The portion of the whole space of a sphere of radius R about a given point (the center of the sphere) bounded by a conical surface with its vertex at that point is *measured by the area cut by the bounding surface from the sphere*.

If a unit radius is considered, a solid angle ω defines a sector of unit sphere ($R = 1$) in analog manner a planar angle θ defines the length of an arc on a unit circle (Sharp Corporation, 1993), see Figure 18.

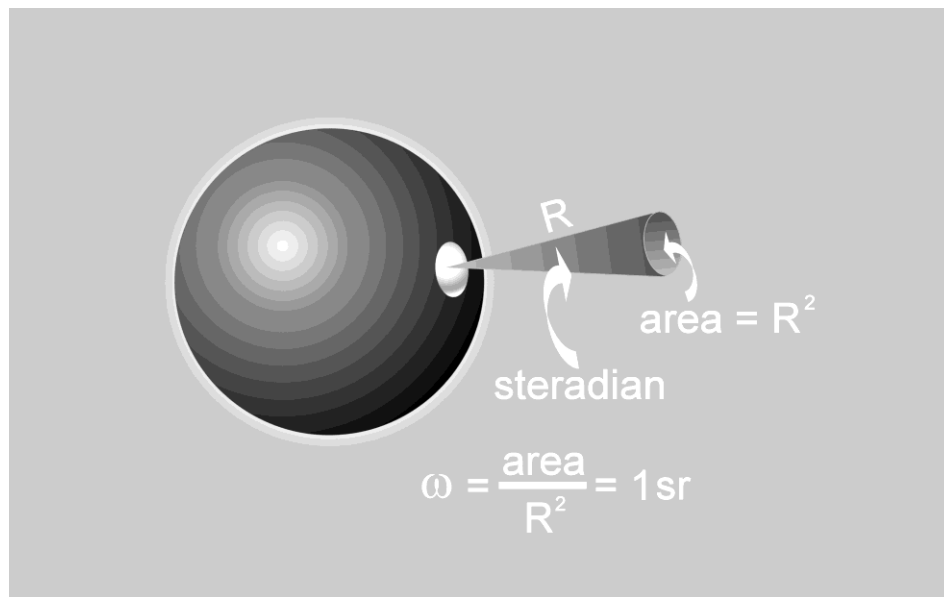


Figure 18. Steradian Definition

A cone with apex angle 2θ defines a solid angle ω and sets a spherical cap in a sphere of radius R in analog manner a planar angle α defines the length L of an arc in a circle of radius R .

$$\text{Planar Angle } \alpha = \frac{L}{R} \xrightarrow{L=R'} \alpha = \frac{R'}{R'} = 1 \text{ radian}; \quad \text{Solid Angle } \omega = \frac{A}{R^2} \xrightarrow{A=R^2} \omega = \frac{R^2}{R^2} = 1 \text{ Steradian}$$

$$1 \text{ radian} = 57.3^\circ$$

$$\text{Solid Angle } \omega = \frac{A}{R^2} = \frac{A'}{R'^2}$$

The planar angle θ is measured in degrees or radians and the solid angle ω in Steradians (sr).

A circumference of length L has a planar angle:

$$\alpha = L/R = 2\pi R/R = 2\pi \text{ radians} \quad (05)$$

and a sphere of area A has a solid angle:

$$\omega = A/R^2 = 4\pi R^2/R^2 = 4\pi \text{ Steradians} \quad (06)$$

The solid angle ω of a cone with apex angle 2θ (planar angle), sets a spherical cap on the unit sphere with a solid angle:

$$\omega = 2\pi (1 - \cos\theta) \quad (07)$$

where θ is half the apex angle (Greivenkamp, 2004)

For $R = 1$ the following equivalent identities can be considered:

$$\omega = 2\pi (1 - \cos\theta) = 4\pi \sin^2(\theta/2) \quad (08)$$

The mathematical equivalence for the solid angle ω is demonstrated in Appendix D.

For $R \neq 1$ the area of the spherical cap is:

$$A = 4\pi R^2 \sin^2(\theta/2) \quad (09)$$

although the solid angle is independent of the distance R as by definition:

$$\omega = A/R^2 = 4\pi \sin^2(\theta/2) \quad (10)$$

A cone with apex angle 2θ (planar angle) sets in a sphere of radius R a spherical cap of area $A = R^2 \cdot 2\pi(1 - \cos\theta)$ and the solid angle is defined as $\omega = \frac{A}{R^2}$ and given in steradians (sr) which is a dimensionless figure.

When the cap area $A = R^2$ then $\omega = 1$ Steradian (sr). If the cap area A is 0.5 m^2 and the radius R is 1 m then $\omega = 0.5$ Steradian (sr).

Thus an entire sphere, regardless its radius' size, has a solid angle:

$$\omega = 4\pi \text{ Steradians} = 12.56 \text{ sr} \quad (11)$$

Defining the solid angle ω by making reference to $\theta/2$ (half angle) as indicated by Zalewski (as cited in Bass, 1994) or θ the entire angle (Ray, 2002), leads to two equivalent definitions, see Appendix D:

considering a cone with apex angle 2θ

$$\omega = 4\pi\sin^2(\theta/2) \quad (12)$$

considering a cone with apex angle θ

$$\omega = \pi\sin^2(\theta) \quad (13)$$

In fact, when θ is small, $\omega = 4\pi\sin^2(\theta/2) \approx 4\pi(\theta/2)^2 = 4\pi(\theta)^2/4 = \pi(\theta)^2$ and using the alternative definition: $\omega = \pi\sin^2(\theta) \approx \pi(\theta)^2$.

Both definitions are found in technical literature and when comparing mathematical derivations among different authors, the reference used for the apex angle θ in books or papers has to be figured out to avoid confusing the equations.

Hemisphere Definition

Figure 19 shows a cone with a planar angle increased up to $\theta = 90^\circ$ and the ensuing planar surface rotated around its vertical axle, namely $\varphi = 360^\circ$:

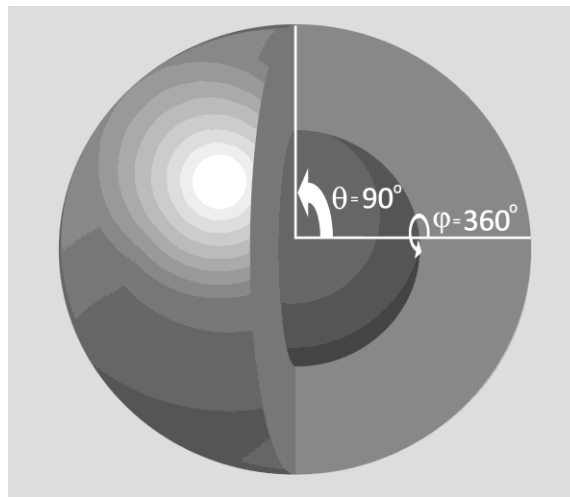


Figure 19. Hemisphere Definition

and the three dimensional object obtained is called a hemisphere.

Thus, when the planar angle increases up to a value $\theta = 90^\circ$ (equal to $\pi/2$ radians) and the ensuing planar surface is rotated around either its vertical or horizontal axle so $\varphi = 360^\circ$ (equal to 2π radians), a hemisphere is obtained and its solid angle is:

$$\omega = 4\pi \sin^2(\theta/2) = 4\pi \sin^2(\pi/4) = 4\pi \left(\frac{1}{\sqrt{2}}\right)^2 = 2\pi.$$

If the planar angle $\theta = 180^\circ$ (equal to π radians) the resulting object is the sphere and its solid angle is:

$$\omega = 4\pi \sin^2(\theta/2) = 4\pi \sin^2(\pi/2) = 4\pi(1)^2 = 4\pi.$$

Thus the following general definition for the solid angle:

$$\omega = \int_0^{2\pi} d\varphi \int_0^{\theta_{max}} \sin \theta d\theta \quad \text{where } 0 \leq \theta_{max} \leq 180^\circ$$

If $\theta = 180^\circ$ then the object is the sphere and $\omega = 4\pi$.

Thus the solid angles for the hemisphere and sphere are:

$$\text{Hemisphere} \quad \omega = 2\pi \quad (14)$$

$$\text{Sphere:} \quad \omega = 4\pi \quad (15)$$

Luminous Flux (Φ)

Once the solid angle is defined, radiometry and photometry units can be discussed.

Radiometry units measure the electromagnetic radiation (EMR), whereas Photometry is actually an attempt to define the amount by which EMR stimulates the sensation of *brightness* in the human eye (Roberts, 1996).

The transfer from radiometry to photometry requires only *defining the Lumen, a unit of luminous flux*.

Luminous Flux (or visible energy) is similar to Radiant Flux except that it only includes those wavelengths that are visible to the human eye and each wavelength is scaled by the photopic curve, see Figure 20, which considers the response of the human eye, see Figure 21.

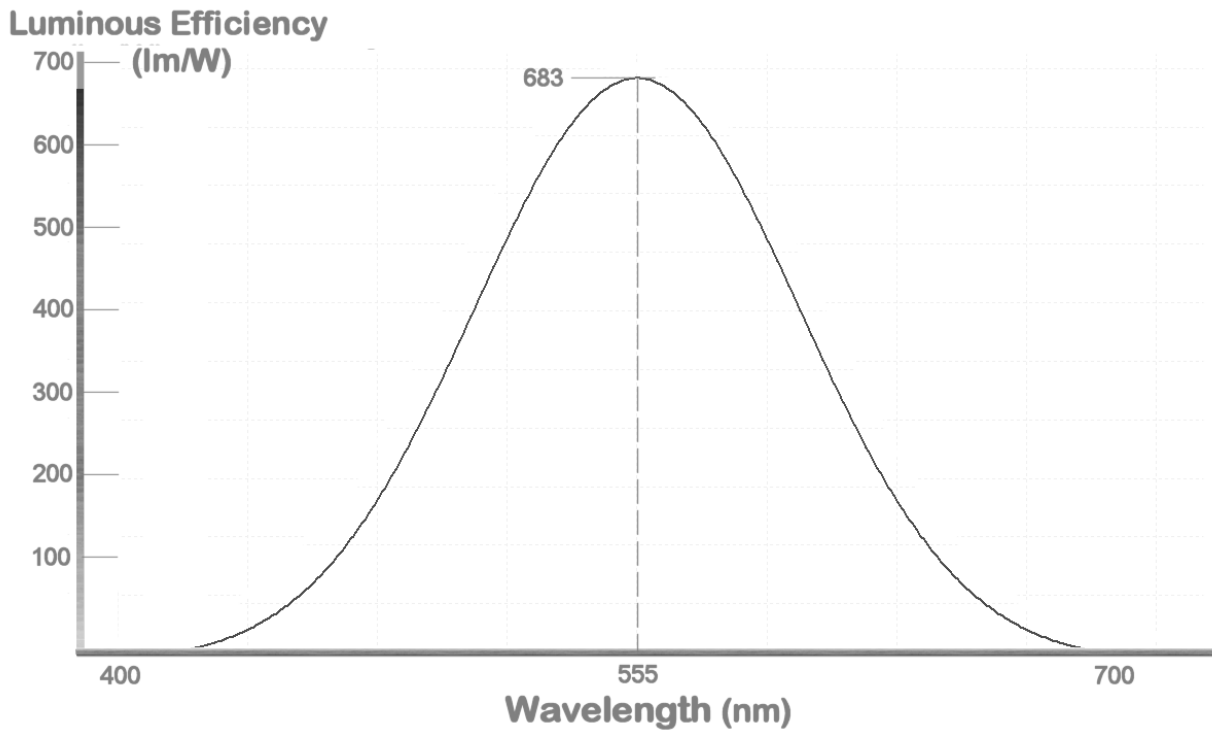


Figure 20. Photopic Luminous Efficiency is a Function of the Wavelength

In Radiometry, radiant flux is synonymous of power, and as such it is measured in watts, thus in Photometry, Lumens is the unit for luminous power. In 1980, the peak of the curve was set arbitrarily to 683 lm/W at 555 nm.

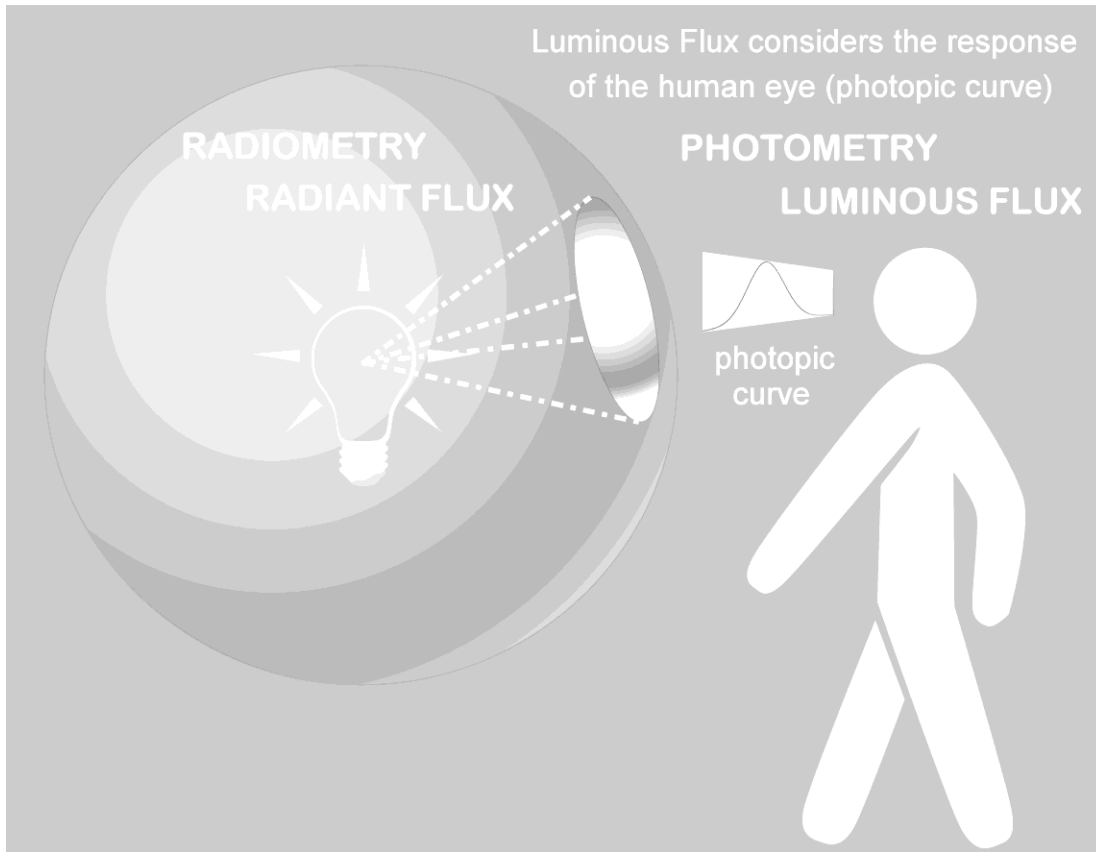


Figure 21. Photometry is a Subset of Radiometry in the Visible Spectrum

Definition of Lumen. The Lumen (abbreviated lm), based on the photopic curve, is the power-like unit of brightness-sensation-producing ability (Roberts, 1996).

In radiometry radiant flux is synonymous of power, and as such it is measured in watts, thus in photometry Lumens is the unit for luminous power.

The definition of Lumen is derived from the Candela (the unit of *I* luminous intensity).

Thus, to provide a more thorough understanding of the Lumen, the definition of Candela has to be introduced first (see definition below) and the following statement is applicable (Al-Azzawi, 2007):

A Lumen is equivalent to about 1.5 mW of radiant power generated by a source of yellow-green light of wavelength 555 nm.

Light bulbs and projection devices are also characterized by Lumens to indicate how much luminous flux they can deliver to a screen (Palmer, 2003).

The total number of Lumens (luminous flux) emitted from a source is usually not a concern, because a detector can collect only the luminous flux within a limited solid angle. Thus a new unit *I* luminous intensity it introduced.

Luminous Intensity (*I*)

Total number of Lumens (luminous flux) *emanating* from a source *in a specific direction*.

The unit of luminous intensity is the *Candela* and it is equivalent to:

$$\text{Candela} = \text{Lumen}/\text{sr}$$

The Candela is sometimes called *new candle* (Roberts, 1996).

$$1 \text{ Candela} = 0.98 \text{ candle}$$

An isotropic light source of one Candela has a constant Luminous Intensity in every direction of 1 *Lumen/sr* and thus a luminous flux $\Phi = 12.56 \text{ Lumens}$ calculated:

$$\begin{aligned}\Phi &= I \cdot \omega (\text{sphere}) = 1 \text{ Lumen}/\text{sr} \cdot 4\pi \text{ sr (solid angle of the sphere)} = \\ &= 4\pi \text{ Lumens} = 12.56 \text{ Lumens}\end{aligned}$$

An aperture is used to limit the light for measurement and the size of the aperture and its distance from the source define a solid angle relative to the source.

Definition of Candela. The ANSI standard defines the Candela as the luminous intensity, *in a given direction*, of a source emitting monochromatic radiation frequency 540 THz and whose radiant intensity in this direction is $\frac{1}{683} \text{ W}/\text{sr}$.

The constant $\frac{1}{683} \text{ W}$ is based on the photopic curve's peak value, which was set at 683 lm/W in 1980.

A radiation frequency of 540 THz has a wavelength of 555 nm and if emitting a radiant intensity of $\frac{1}{683}$ W/sr \approx 1.5 mW/sr allows the definition of Candela be described in the following terms:

Candela is the luminous intensity, in a given direction, of a source emitting monochromatic radiation wavelength of 555 nm (thus it is a photometric radiation as it falls within the visible spectrum) and whose radiant intensity (a radiometric unit) in this direction is \approx 1.5 mW/sr.

The definition of Candela includes a reference to radiant intensity (a radiometric unit) and a wavelength of 555 nm (yellow green color), located right in the middle of the visible spectrum, as it was shown in Figure 13. This way a link between Radiometry and Photometry was established, see Figure 22.

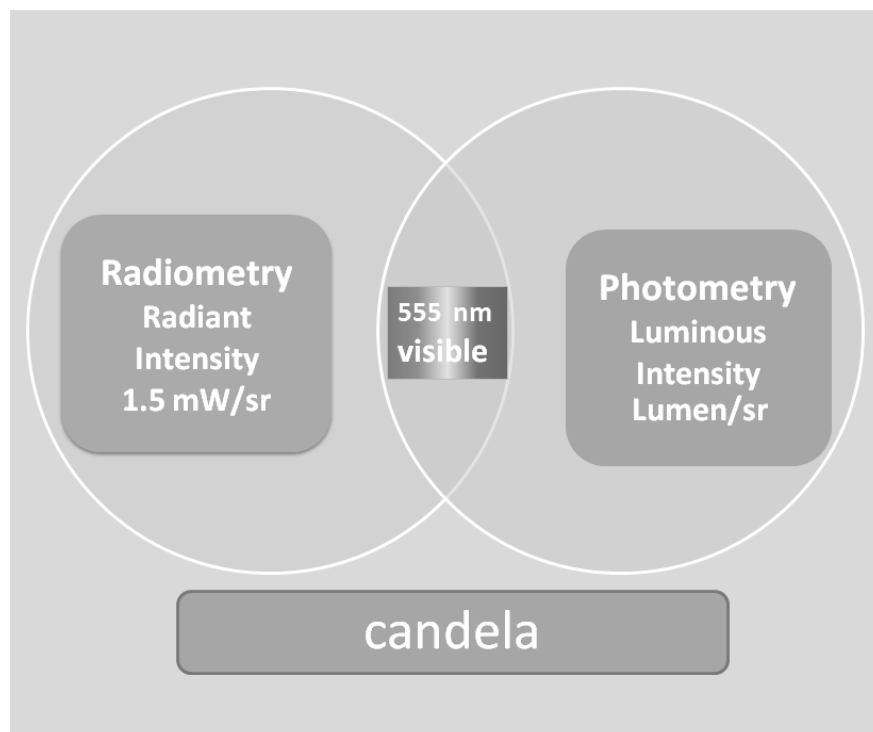


Figure 22. The Definition of Candela Includes Units of Radiometry and Photometry

Isotropic Source Definition. Although luminous intensity is often associated with an isotropic point source, a small, uniform sphere comes very close.

An isotropic light source of one Candela has a luminous flux $\Phi = 12.56$ Lumens

Furthermore, isotropic implies a spherical source that radiates the same in all directions, but still it is a valid specification for characterizing highly directional light sources such as LEDs, automotive lighting, and searchlights (Palmer, 2003).

Extended Source Definition. To characterize an extended source, namely one that has appreciable area compared to R^2 (the observation distance), a new unit is defined: Luminance L .

Luminance (L)

Luminance is a measure of the flux *emitted or reflected* from a surface and it is commonly referred to as *brightness*. Although the term *brightness* is inappropriate because it describes a sensation caused by the human eye and as such it has no measure units.

Basically luminance is a simple measure (K-Light, 2011) of luminous intensity I per unit projected area, for instance candelas per m^2 abbreviated $\frac{cd}{m^2}$.

The moon reflecting the sunlight has a luminance that varies between 2 cd/m^2 and 4200 cd/m^2 depending on the altitude - the angle of the center moon above the horizon - (Conrad, 2000).

By definition Candela = $\frac{lumen}{sr}$ so L can be given in (Greivenkamp, 2004):

a) L in $\frac{cd}{m^2}$

b) L in $\frac{lm}{m^2 \cdot sr}$ because $\frac{cd}{m^2} = \frac{lm}{m^2 \cdot sr}$.

Sometimes the *nit* is used instead of $\frac{cd}{m^2}$ which is an old unit to refer $\frac{cd}{m^2}$.

In the past, luminance L has been typically measured in *foot-lambert* (abbreviated fL):

$$\text{fL} = \text{Lumen}/\text{ft}^2$$

but nowadays $\frac{\text{cd}}{\text{m}^2}$ is more commonly used.

Lambertian Source - Luminance. A Lambertian source is defined as a radiator that L is constant across its surface.

Example is a surface painted with a good “matte” or “flat” white paint. If it is uniformly illuminated, like from the sun, it appears equally bright from whatever direction you view it (Palmer, 2003), see Figure 23.

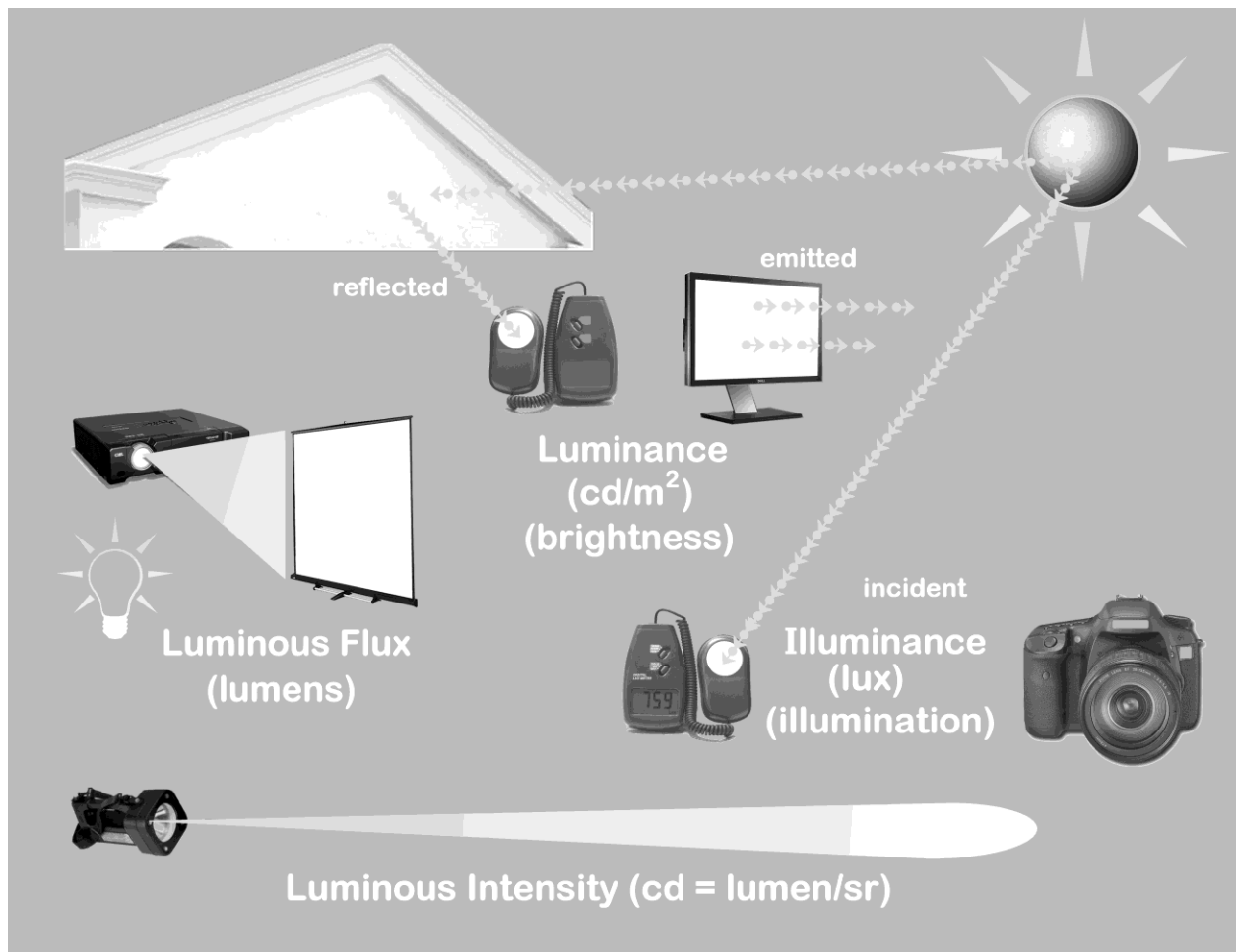


Figure 23. Summary of Photometric Units

A surface painted with a good “matte” or “flat” white paint, uniformly illuminated from the sun, appears equally bright from whatever direction it is seen, and can be approximated by a Lambertian source; in this case on the surface:

$$M \text{ (Exitance)} = \pi L \text{ (Luminance)}$$

and a new Photometric unit: Luminous Exitance is introduced.

Luminous Exitance (Emittance) (M)

Luminous Exitance a new term replacing Luminous Emittance is defined as the luminous flux directly *emitted* by a radiant surface plus the *reflected* from and transmitted through the surface *divided by that area*.

Exitance is measured in *Lumen/m²*.

Using foot-candle (abbreviated fc) units when referring to luminous exitance may be confusing because “candle is an old unit of intensity, not flux, and the term *foot-candle* can thus be very misleading” Roberts (1996).

A Lambertian source with a luminance L of 1 *Candela/m²* (by definition equivalent to 1 *lm/m²·sr*) has a luminous exitance M of $\pi \text{lm/m}^2$.

Thus, in the case of a Lambertian radiator:

$$M \text{ (lm/m}^2\text{)} = \pi(\text{sr}) \cdot L \text{ (lm/m}^2\text{·sr)} = \pi L \text{ (cd/m}^2\text{)} = \pi L \text{ (nit)} \quad (16)$$

Lambertian refers to a flat radiating surface; it can be an active surface or a passive reflective surface.

The relationship $M = \pi L$ contains π instead of the expected 2π because of the falloff ($I = I_0 \cdot \cos\theta$) of the projected area with θ (Greivenkamp, 2004).

Illuminance (E)

It is the result of luminous flux striking a surface and it is *commonly referred to as illumination* (K-Light, 2011). It is the luminous flux *incident* on a surface per unit area, see Figure 24. It is the luminous flux incident on a surface from all directions.

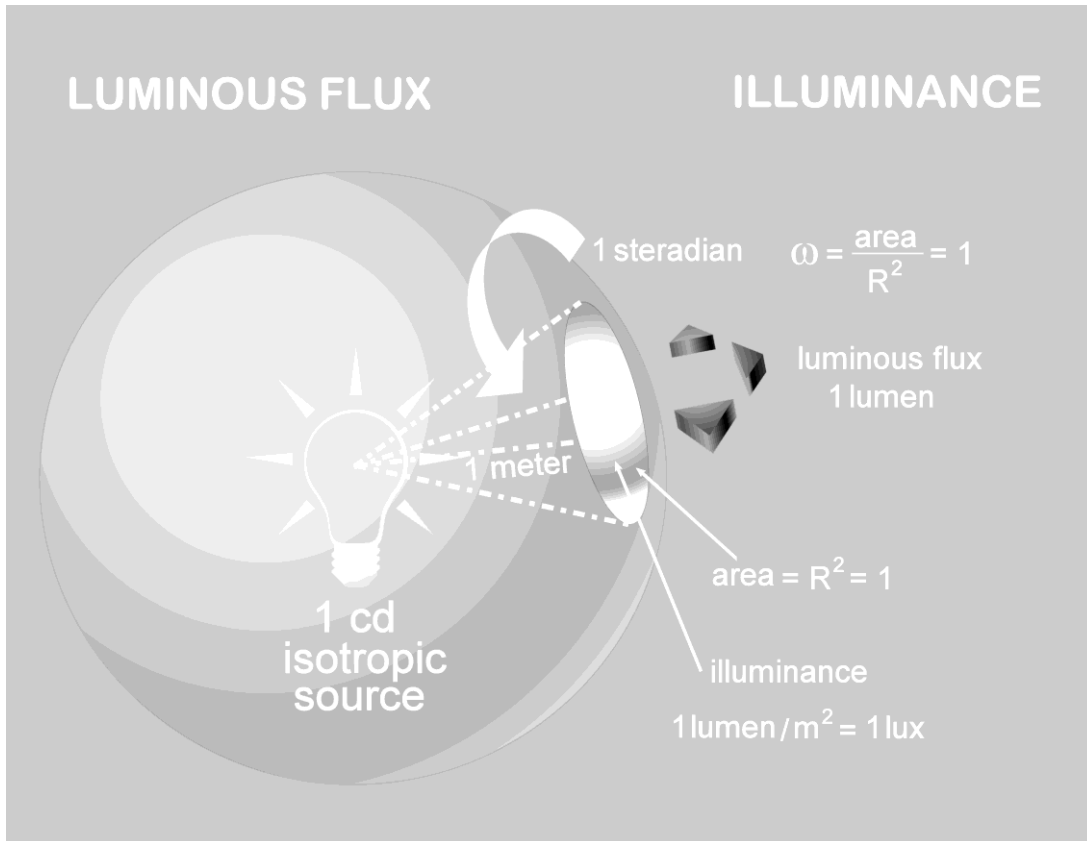


Figure 24. Luminous Flux Φ and Illuminance E

In SI units Illuminance is measured as:

$$\text{Lumen/m}^2 = 1 \text{ lux (abbreviated lx)}$$

and in English units it is measured as:

$$\text{Lumen/ft}^2 = 1 \text{ foot-candle}$$

Illuminance E and Luminous Exitance M have different interpretations:

E refers to luminous flux striking a surface

M refers to luminous flux leaving a surface

Illuminance E and Luminous Exitance M are also related (Greivenkamp, 2004)

by the *reflectance* ρ of the surface $M (\text{lm/m}^2) = \rho \cdot E (\text{lm/m}^2) = \rho \cdot E (\text{lx})$.

What indicates that only a percentage ρ of the flux striking (illuminance E) a surface is reflected (emitted luminous exitance M) by the surface. Thus:

$$\pi(sr)L(\text{lm}/\text{m}^2\cdot\text{sr}) = M (\text{lm}/\text{m}^2) = \rho E(\text{lm}/\text{m}^2)$$

or in terms of candelas and lux:

$$\pi(sr)L(\text{cd}/\text{m}^2) = \rho E(\text{lx}) \quad (17)$$

Equation (17) is a fundamental relationship between Luminance L and Illuminance E and when applied to an ideal Lambertian radiator/reflector that by definition has $\rho = 1$ gives for the surface of the radiator the known equation:

$$L(\text{cd}/\text{m}^2) = \frac{E(\text{lx})}{\pi(sr)} \quad (18)$$

Table 3 shows a summary of units in Radiometry and Photometry:

Table 3

Summary of Units Used in Radiometry and Photometry

Radiometry		Units	Photometry		Units
Φ	Flux	W	Luminous Power		Lumens
M	Exitance	W/m ²	Luminous Exitance		Lumen/m ²
I	Intensity	W/sr	Luminous Intensity		Lumen/sr = Candela (cd)
L	Radiance	W/m ² ·sr	Luminance (“Brightness”)		Lumen/m ² ·sr = cd/m ²
E	Irradiance	W/m ²	Illuminance (“Illumination”)		Lumen/m ² = lux

Standard Observer Defined

The standard observer is an integral contributor to the EVIS. Thus, the main characteristics: Visual Acuity and Normal Color Vision should be defined.

Visual Acuity. It is the spatial resolving capacity of the human visual system and is a fundamental characteristic of the “standard human vision”. It is limited by diffraction, aberrations, and photoreceptor density in the eye (see also page 32).

A number of factors affect visual acuity such as refractive error, illuminance, contrast, and the location of the retina being stimulated (Kalloniatis & Luu, 2007).

Its measurement also depends on the type of test a person is asked to perform. In 1955 measurement of visual acuity was classified by Weymouth based on testing three main categories (Tyler, “n.d.”): minimum distinguishable, minimum separable, and minimum cognizable.

- **Minimum Distinguishable:** To see something as being distinguishable from the background. For instance asking what is the smallest dot one can see.
- **Minimum Separable:** To determine if a group of targets are separate and distinct by using grating type charts: contrast sensitivity charts.
- **Minimum Cognizable:** To be able to separate and distinguish forms, by testing in which a simple form as the letter E (or the letter C) depends on orientation identification to measure acuity.

Equal Legibility of Letters. In 1862 a Dutch Ophthalmologist, Hermann Snellen devised a test chart consisting of a series of letters or letters and numbers with the largest at the top to assess human eye visual acuity.

More recently, the British Standard BS 4274-1:2003 "Test charts for clinical determination of distance visual acuity — Specification" recommended only the letters

C, D, E, F, H, K, N, P, R, U, V, and Z to be used for the testing of vision based upon equal legibility of the letters.

Other versions of the Snellen chart are used, for instance, the Tumbling Es that have the capital letter "E" facing in different directions and the person being tested must determine which direction the "E" is pointing, up, down, left, or right or the Landolt Cs.

Tumbling Es Used in Optometry. The notation 20/20 or 6/6 is used in Optometry and refers to the set of fractions originally defined in the Snellen Chart.

The original design of the Tumbling E Chart took into account the distribution of cone-shaped elements in the retina that are primarily responsible for acute vision, so the width of one black bar was set to have an angle of view of 1 MOA (abbreviation for minutes of arc) and each letter was enclosed in a square of 5 MOA, with the width of its arms and interstices subtending 1 MOA, see Figure 25.

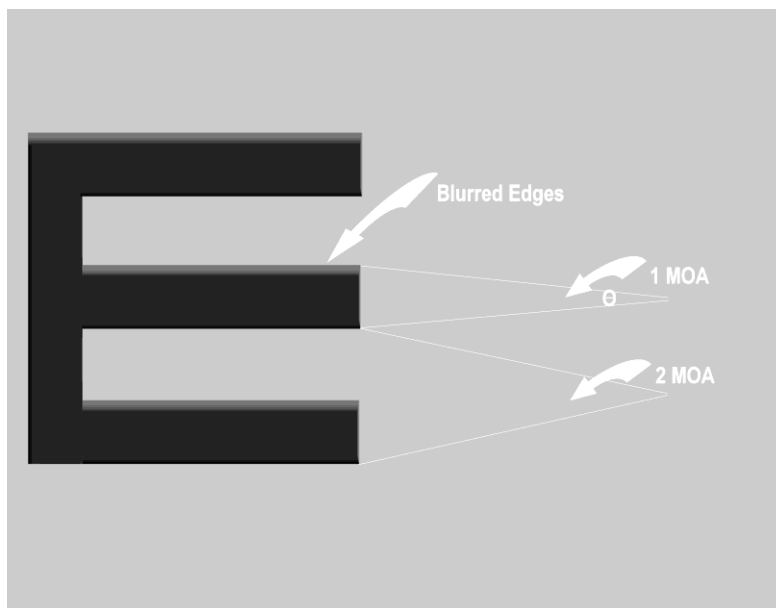


Figure 25. The 20/20 Tumbling E has a Spatial Frequency of 1.7 cy/mR

Snellen chose this design because of the belief that an individual could not separate images (minimum separable acuity) unless the images were at least 1 MOA in size.

In addition, because the English alphabet has letters with a maximum of 5 details in one orientation, 5 MOA was used for the Snellen optotype total size.

Thus, if a person is able to resolve the "detail" of 1 MOA in an optotype that subtends 5 MOA at 20 feet, that person's visual acuity would be 20/20 (Tyler, "n.d.").

There are 60 MOA in 1 degree, so 1 MOA = $1/60 = 0.017$ degree (abbr. 0.017°)

It has been determined that the eye effective focal length (EFL) is 16.63 mm and the spot radius on axis for a 3-mm pupil is $5 \mu\text{m} = 0.005$ mm (in bright light the iris is reduced to 2 mm in diameter). Thus using equation (02):

$$\tan\theta = (0.005/16.63) = 0.0003 \implies \theta \approx 0.0003 \text{ radians} = 0.017^\circ = 1 \text{ MOA}$$

At 21° off-axis, the spot radius increases to $25 \mu\text{m}$, yielding a resolution in photopic vision of $\theta = 5$ MOA (Laikin, 2007):

$$\tan\theta = (0.025/16.63) = 0.0015 \implies \theta \approx 0.0015 \text{ radians} = 0.086^\circ = 5 \text{ MOA}$$

So off-axis the eye resolution is lower.

Minimum Angle Resolution (MAR). The unit 1 MOA is also known as the Minimum Angle Resolution, abbreviated MAR and it can also be given in \log_{10} form, abbreviated as logMAR that in this case for an angle $\theta = 1$ MOA the associated logMAR = 0.0 (Kalloniatis & Luu, 2007).

The Snellen fractions, 20/20; 20/40; etc. are measures of sharpness of sight and they relate to the ability to identify small letters with high contrast at a specified distance.

If the magnification needed to identify the 20/20 optotype is 2x, then the visual acuity of that person is 1/2 namely 20/40, see Figure 26.

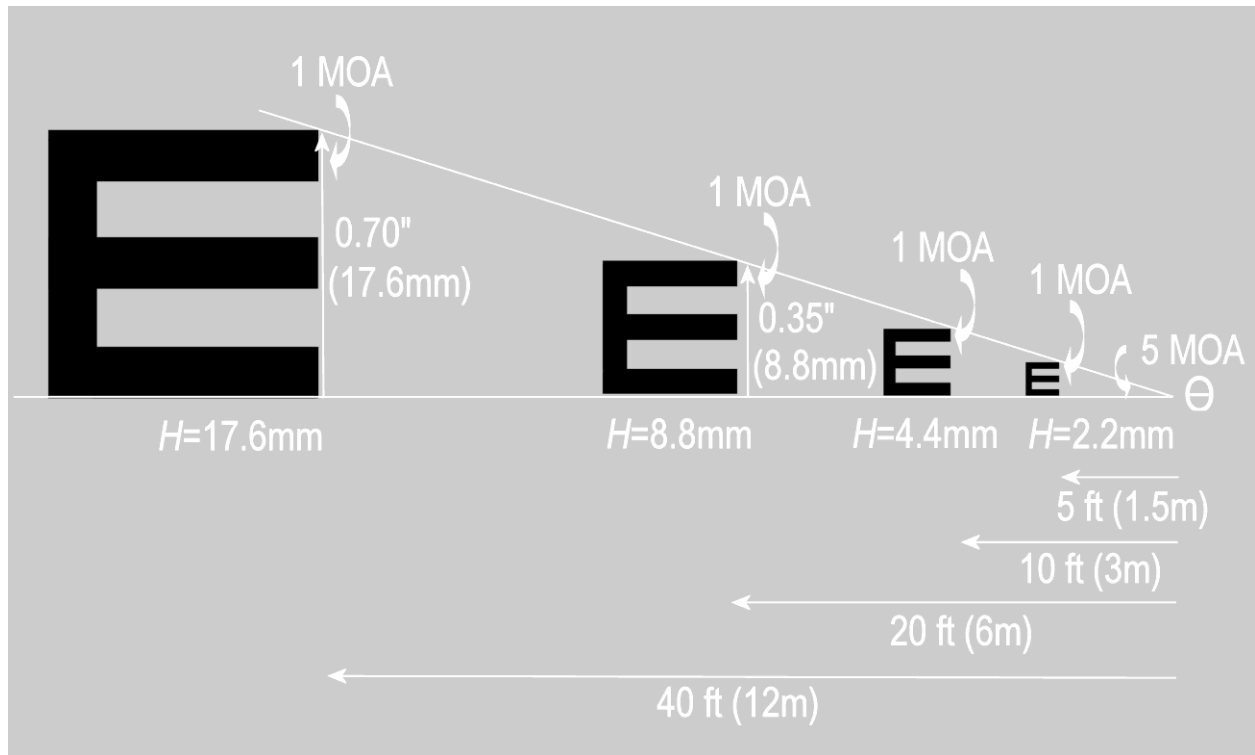


Figure 26. The 20/20 Tumbling E Scaled Up and Down

The dimensions of the 20/20 Tumbling E in Figure 26 are scaled up to a 40 ft optotype and scaled down to 10 ft and 5 ft optotypes.

The optotypes at 20 ft, 40 ft, 10 ft, and at 5 ft subtend the same 5 MOA angle.

The stroke of the Es at 20 ft, 40 ft, 10 ft, and 5 ft subtends the same 1 MOA angle.

The height of the E is:

17.6mm at 40 ft

8.8mm at 20 ft

4.4mm at 10 ft

2.2mm at 5 ft

Contrary to popular belief, 20/20 is not actually normal or average, normal acuity in healthy adults is one or two lines better, i.e. 20/15 or 20/10 (Strouse, 2003).

More recent work of Curcio et al., Miller et al., and Roorda and Williams (as cited in Kallionatis & Luu, 2007) on photoreceptor density and spatial resolution has shown that the receptor array in the human visual system can resolve in the order of $20/3$ (6/1) equivalent to 150 cycles/degree approx.

Optical infinity is the distance at which no accommodation (focusing) is being used by a person to clear that distance and all distances further (Tyler, “n.d.”).

In practice, 20 ft is the ideal test distance for determining a person’s visual acuity because rays of light emanating from a distance of 20 feet or more from the eye are considered to be coming from optical infinity in which the rays are parallel to each other, see Figure 16. This condition is called emmetropic vision.

In emmetropic vision parallel rays coming from 20 feet or more focus clearly on the retina.

The basic principle of the modern Snellen Chart is that if a person is placed at a distance of 20 ft, see Figure 26, he or she should be able to recognize the very same letter if it's twice the size when viewed at double distance of 40 ft (Weber, Humphrey, & Silver, 1998).

Normal Color Vision. CIE stands for Commission Internationale de l’Eclairage, and one of the most useful CIE systems is CIE 1976 L^* , a^* , b^* , with the official abbreviation of CIELAB.

The CIE developed the concept of the “standard observer” assumed to represent the average of the human population having normal color vision (Lukac & Plataniotis, 2006).

CIE color specification systems are scientifically proven, well-established methods of color measurement.

There are three things that affect the way a color is perceived by humans:

- illuminance
- the object
- interpretation of this information in the eye/brain system

The original primaries were transformed into new primaries called the color-matching functions designated \bar{x} , \bar{y} , \bar{z} that allowed the measurement of color be derived from purely physical data (easily measured spectrophotometric data) *and be based entirely on instrumental measurement*. The starting point for all color specification is CIE XYZ.

XYZ are known as tristimulus values. The CIE 1931 chromaticity diagram, called the x, y chromaticity diagram, and x, y are known as chromaticity coordinates.

$$x = X/(X + Y + Z) \quad (19)$$

$$y = Y/(X + Y + Z) \quad (20)$$

The human eye is less sensitive to changes in lightness and more sensitive to changes in chroma.

ICC is a regulatory body that supervises color management protocols between software vendors, equipment manufacturers, and users.

The ICC profile is a data file that represents the color characteristics of an imaging device, for instance laptop computers, printers, and scanners.

Dynamic Searching Time. The time required by the “standard observer” to search a particular target may be computed analytically from knowledge of the eye’s fixation time and the angular size of the display.

Three assumptions are made:

- (1) a single fixation requires approximately three-tenths of a second (0.3 sec)
- (2) the circular field of clear vision subtends 5 degrees (Simon, 1965)

In fact, it has been measured that at 21° off-axis, the spot radius in the eye increases to 25 μm, yielding a resolution in photopic vision of $\theta = 5$ MOA much lower than $\theta = 1$ MOA on axis at the fovea, the region of highest visual acuity in the center of the retina (Laikin, 2007).

(3) the random target may remain static for a short period of time (3 sec or less)

The length of time required to search an entire display field once through is computed by determining the number of nonoverlapping 5° fixations required to cover the field.

A display subtending 16° x 16° at the eye would thereby be predicted to require:

$$[(16^\circ \times 16^\circ) / (5^\circ \times 5^\circ)] \times 0.3 \text{ sec} = 3.1 \text{ sec}$$

Thus, *in selecting the output LCD display for the Video Imaging System, its size must be small enough as to allow a low visual searching time.*

For instance, the new test set designed for this thesis uses an output LCD display of 5.5 in.

The limited visual searching time may be simulated with tumbling Es or Cs by allowing the “standard observer” to recognize their orientation in only 3 seconds.

Target Detection & Recognition Model. Benchmarking the video imaging quality of an EVIS should also consider the effect of a target detection & recognition model to the observer suggested by Rand Corporation (Bailey, 1970):

$$P_r = P_1 P_2 P_3 \eta \tag{24}$$

P_r is the probability that a target will be recognized on the display

P_1 is the probability that “standard observers” searching an area that is known to contain a target looks with their foveal vision for a specified glimpse time (0.3s) in the direction of the target.

P_2 is the probability that if the displayed target image is viewed foveally for one glimpse period it will, in the absence of noise, *have sufficient contrast and size to be detected.*

P_3 is the probability that if a target is detected, there will be *enough detail shown for it to be recognized* (again during a single glimpse and in the absence of noise)

η is an overall degradation factor arising from noise

An expression for the probability of detection alone (without recognition) is obtained by considering only three factors:

$$P_d = P_1 P_2 \eta \quad (25)$$

$$\eta = 1 - e^{-(\text{SNR} - 1)} \approx 0.9 \text{ to } 1.0 \text{ for } \text{SNR} \geq 3 \quad (26)$$

Thus P_d could be approximated by:

$$P_d \approx 0.9 P_1 P_2 \quad (27)$$

The probability of detection P_2 at the threshold contrast $C = C_T$ is by definition 50% and for $C > C_T$ it has a sharp increase, see Figure 27.

A value of $P_2 \geq 0.8$ can be considered for most scenarios, *with high contrast sensitivity values.*

Hence we approximate:

$$P_d \geq P_1 \times 0.8 \times 0.9 = 0.72P_1 \quad (28)$$

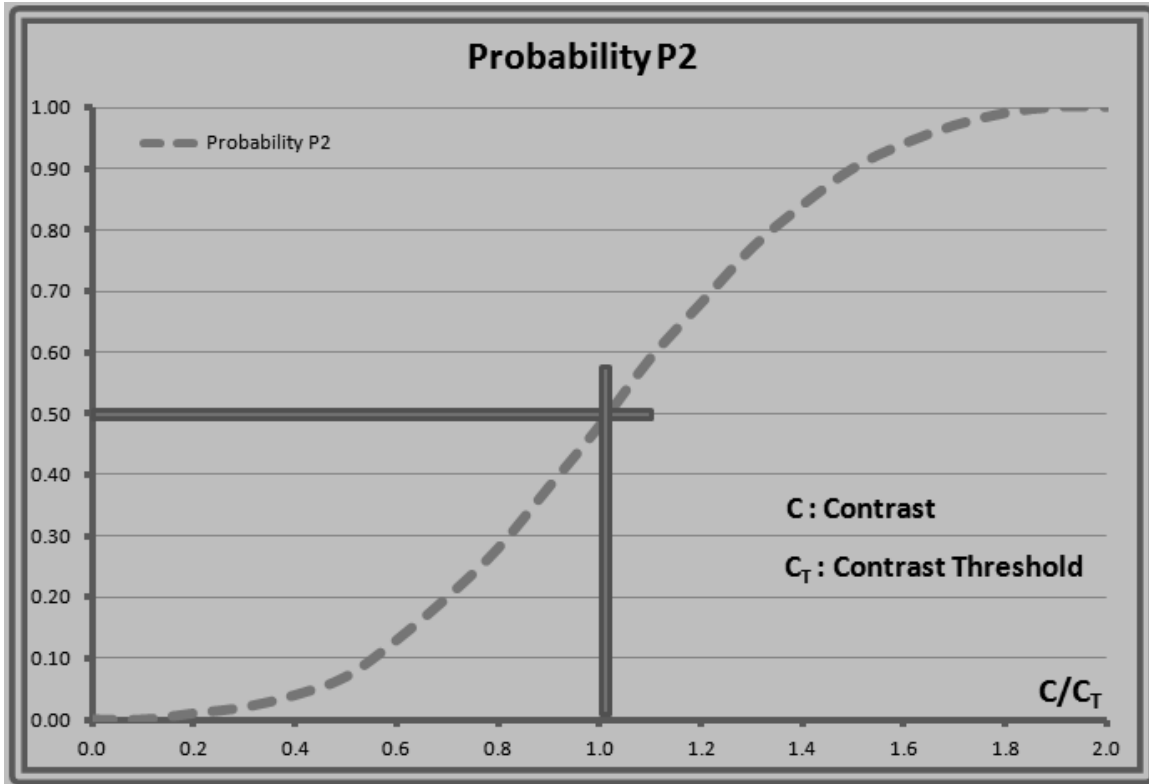


Figure 27. Probability P_2 of Detection

The probability P_1 is difficult to estimate because it is affected:

- 1) by the solid angle presented to the eye of the search field
- 2) by the time available to search it
- 3) by the number of confusing elements within the scene, and
- 4) by the availability of any “cues” or a priori information as to where to look in the display

The Rand model employs the relation:

$$P_1 = 1 - \exp \left[- \left(\frac{700}{G} \right) \left(\frac{a}{A} \right) t \right] \quad (29)$$

where:

a = area of target A = area to be searched t = time

G = congestion factor, usually between 1 and 10.

Angular Threshold of the Human Eye. The probabilities P_1 , P_2 , and P_3 of seeing an object are influenced not only by the field luminance, the contrast of the object with respect to the scene background, and the complexity of the scene, but also by the angle subtended by that object at the eye of the observer.

Under ideal conditions the eye can resolve about 30 seconds of arc (there are 60 seconds in 1 minute of arc) equivalent to 0.5 MOA. In most practical situations; however, the angular threshold of the eye is much larger than that.

For example, it has been shown (Steedman & Backer, 1960) that a target appearing in a complex field of confusion elements must subtend about 12 MOA (minutes of arc) to enable a high (97 percent) probability of recognition.

Tumbling Es Spatial Frequency

To be consistent with a previous standard generally agreed in the field of Optometry, when using the Tumbling E Chart in the new method for testing video imaging systems the 20/20 reference will also be considered.

The Tumbling E Chart used in the ASTM E2566-08 standard, is also used in the video imaging testing described in this thesis, but instead of using the 20/20 Snellen fraction, more accurate units for the visual acuity measurement will be needed. This is due to the overall performance of a video imaging system.

In testing a video imaging system, Visual Acuity should be measured in cy/mR. The spatial frequency for a 20/20 E optotype (6/6 in the European Snellen scale) is 1.7 cy/mR and it is calculated as follows:

$$1 \text{ degree has } 60 \text{ MOA} \Rightarrow 1 \text{ MOA} = 0.0175^\circ \Rightarrow 5 \text{ MOA} = 0.0873^\circ$$

1 cycle has two consecutive bars (one black and one grey) thus:

20/20 Tumbling E: 2.5 cycles (black/white bars; black/white bars; black)

therefore the 20/20 Tumbling E Spatial Frequency is:

20/20 Tumbling E Angular Size: 5 MOA = 0.0873° = 2.5 cycles

20/20 Tumbling E Spatial Frequency: 29 cycles/deg

Nevertheless spatial frequencies are preferably indicated in cycles/milliradian (abbreviates cy/mR) units, so the figure for the 20/20 Tumbling E follows:

There are 2π radians in 360 degrees, and 60 MOA in 1 degree, thus 6.2832 radians in 21,600 MOA. Using the conversion factor 1,000 mR (milliradians) in 1 radian, it can be stated that:

6283.2 mR in 21,600 MOA

what gives the conversion factor:

0.291 mR/MOA

The spatial resolution of 1 cycle (one black and one grey bar) for the 20/20 Tumbling E shown in Figure 25 is: 2 MOA and applying the conversion factor 0.291 mR/MOA it gives: 2 MOA = 0.582 mR thus:

20/20 Tumbling E Spatial Frequency: 1.7 cy/mR

For quick calculations, it is convenient to use the approximation that:

1 MOA is just about 1 inch at 100 yards

what in the metric system is: 2.54 cm at 9144 cm. The approximation is valid because in fact, θ in Figure 25 can be determined as: $\theta/2 = \text{atan} [(2.54/2)/9144] = \text{atan} [0.0001388] = 0.000139$ radians = 0.139 mR $\Rightarrow \theta = 2 \times 0.139 = 0.278$ mR which is very approximated to the exact figure of 0.291 mR.

The practical rule of 1 MOA equivalent to 1 inch at 100 yards has a low error because 1 MOA = 0.291 mR and it can be approximated to 0.278 mR that differs from the more precise figure ($0.278/0.291 \approx 0.96$) less than 4%.

20/20 Tumbling E – LCD Monitor Calibration. To calibrate an LCD monitor, the practical rule 1 inch at 100 yards is very convenient, as in fact applying the definition of the Snellen Chart 1 MOA at 100 yards means that the 20/20 E optotype should be 5 in. height and have 1 in. strokes. This approximate calibration has an error < 4%.

If a shorter distance is needed, the exact calculation for 1 inch stroke Es should be used: 1 MOA = 0.000291 radians and for a distance D not equal to 100 yards (9144 cm) the practical formula can be stated as : $\theta/2 = \text{atan} [(2.54/2)/D] =$

$$\frac{1}{2} \text{ MOA} = \frac{1}{2} 0.000291 \text{ radians} \Rightarrow 1.27/D = \tan [0.0001455] \Rightarrow D = 1.27/\tan [0.0001455]$$

$$= 1.27/0.0001455 = 8,728 \text{ cm} = 286.4 \text{ ft which is equivalent to } 96 \text{ yd} \approx 100 \text{ yd.}$$

20/20 Tumbling E optotype Dimensions. The exact dimensions used in the practical rule are: 1 MOA is the angle subtended by 1 inch at 286.4 ft. Now the 20/20 E can be scaled up or down as needed.

The angle subtended by the 20/20 E is 5 MOA, and its height at 20 ft according to Figure 26 is: $H = 5 \text{ MOA} = 5 \left(\frac{1 \text{ in.}}{286.4 \text{ ft}} \right) \times 20 \text{ ft} = 0.349'' \approx 0.35'' = 8.8\text{mm}$

To calibrate an LCD display with the E-Chart, the following figures will be used:

20/20 Es of 8.8 mm height and 1.8 mm strokes placed at 20 feet distance

One inch in a ruler is divided in 16 fractions of an inch, thus 1 division of the ruler, namely 1/16 inch will be equivalent to $\frac{286.4 \text{ ft}}{1 \text{ inch}} * \frac{1 \text{ inch}}{16 \text{ divisions}} = 17.9 \text{ ft/division.}$

Thus, another practical rule for shorter distance can be developed stating that: 1 MOA is the angle of view subtended by E optotypes with strokes of 1 inch seen at 100 yards or of 1/16" in. seen at 17.9 ft \approx 20 ft distance.

The spatial frequency of the tumbling Es still is 1.7 cy/mR and the error in the estimate is 20 ft/17.9 ft \approx 12%

Figure 28 shows the design of the Tumbling Es Chart including the spatial frequencies figures when different optotype Es are placed at 20 ft distance.

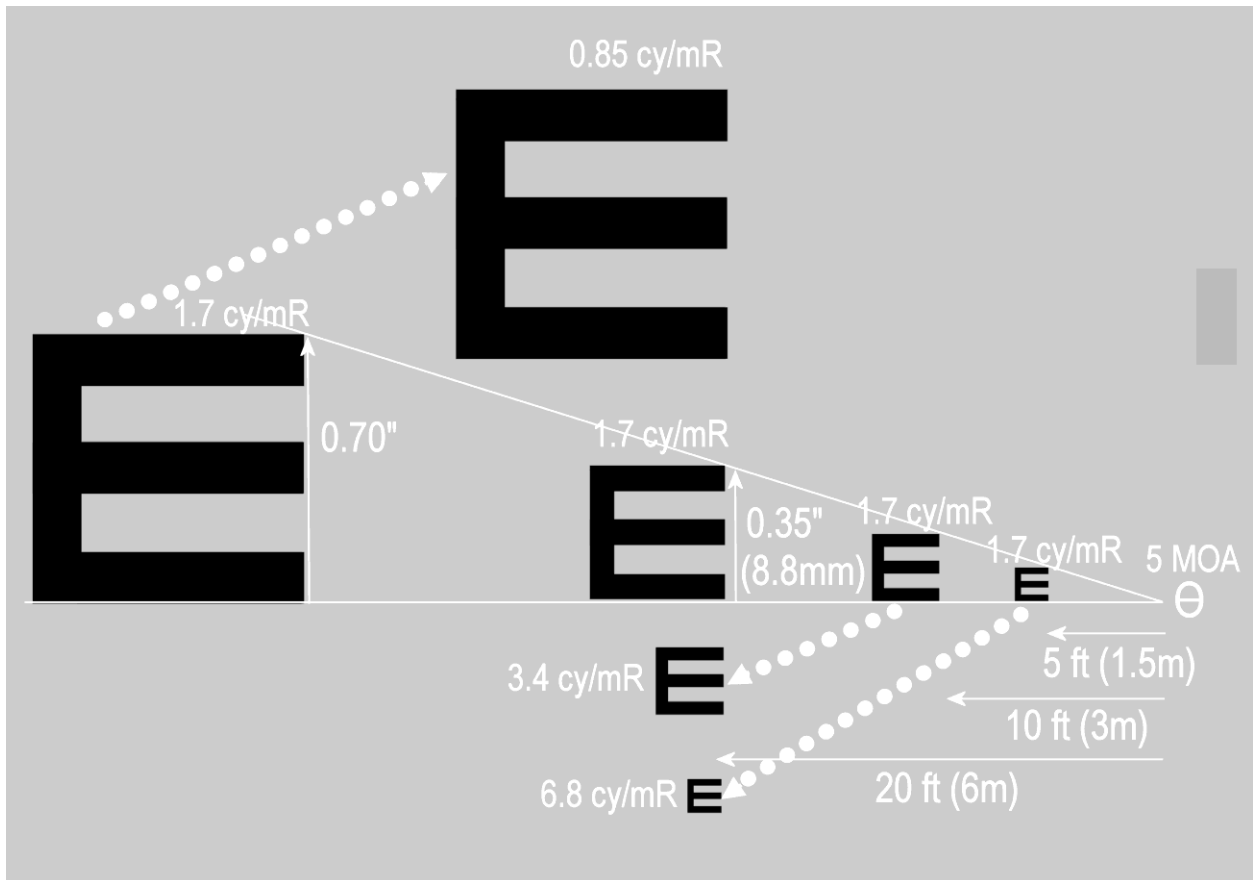


Figure 28. Designing the Tumbling Es Chart

The spatial frequency increases when the 5 ft E and the 10 ft E are moved forward to 20 ft distance from the observer and decreases when 40 ft E is moved backward to 20 ft distance.

Thus, the Tumbling Es Chart can be placed at 20 ft from the observer and the smallest size of the E will determine the spatial resolution of the human observer's eye or the video imaging system.

The height of the 40 ft, 20 ft, 10 ft, and 5 ft Es are 17.6mm, 8.8mm, 4.4mm, and 2.2mm respectively and when they are located at 20 ft distance, i.e. in the same plane, the spatial resolutions are 0.85; 1.7; 3.4; and 6.8 cy/mR respectively.

Tumbling Es and USAF1951 Bar Chart

The tumbling Es test can be compared to another measuring system with extended use: the USAF1951 bar chart according to MIL-STD-150A, see Figure 5.

USAF1951 targets consists of a series of elements having two sets of lines at right angles.

Each set of lines consists of three lines separated by spaces equal to the line width and each bar has a length to width ratio of 5:1 (same ratio as for 20/20 Tumbling E which is 5 MOA height and has 1 MOA strokes).

Elements are arranged in groups of six each and Groups are arranged in pairs.

Spatial frequencies in cycles/mm (cy/mm) increase between each Element by the sixth root of two (approximately 12.25% per step).

The general formula (MIL-STD-150A, 1959) for the line frequency of any target Element can be expressed as $2^{\text{Group} + \frac{(\text{Element}-1)}{6}}$ so for Group 1 and Element 1 line frequency is:

$$2^{1+\frac{(1-1)}{6}} = 2^1 = 2 \text{ cy/mm}$$

The USAF1951 is typically used in determining the resolving power of optical systems and imaging materials at a close distance, such as the resolution power of a 35mm film-camera system, and the spatial frequency is then indicated in line pairs per millimeter abbreviated lp/mm (where a line pair is equivalent to one cycle, i.e. one

black bar and one consecutive white bar), although the large spatial frequency range makes it applicable for the evaluation of almost any imaging system.

When used for long distant targets, the calculations applied to determine the spatial frequency of the tumbling Es shown in the previous section, can also be considered. Namely, 1 MOA is the angle of view subtended by one bar of 1/16" in. seen at 20 ft distance.

For instance the Group 1 Element 6 indicated in Figure 5, has a spatial frequency of 1.7 cy/mR provided the black bar in the computer screen measures 1/16" in.

Tumbling Cs versus Tumbling Es

Tumbling Cs is a subset of the Landolt Cs and are similar optotypes to Tumbling Es. They can also be used to test a video imaging system.

Tumbling Cs for video testing will only have four positions as the Tumbling Es: up, down, left, and right.

In practice, the Tumbling Es may provide clues as to the orientation of the gap in the Es but the Tumbling Cs, because of their circular shape, do not allow any possibility for guessing where the gap is located. For that reason, the Tumbling Cs are the preferred optotypes in the new test set presented in this thesis.

Contrast Sensitivity

In addition to the factors affecting the measurement of visual acuity, the stimulus-response of a visual system is analogous to a filter function and the Snellen or similar traditional acuity charts such as the Black/White Tumbling Es, fail to adequately consider the concurrent effects of contrast sensitivity and spatial frequency on visual sensitivity (Ginsburg, 1982).

Contrast Sensitivity refers to the ability of the visual system to distinguish between an object and its background. Figure 29 shows Hue, Saturation and Luminance (HSL), the Tristimulus Colorimetric Values for different spots in the scene of the original photography taken with a digital color camera.

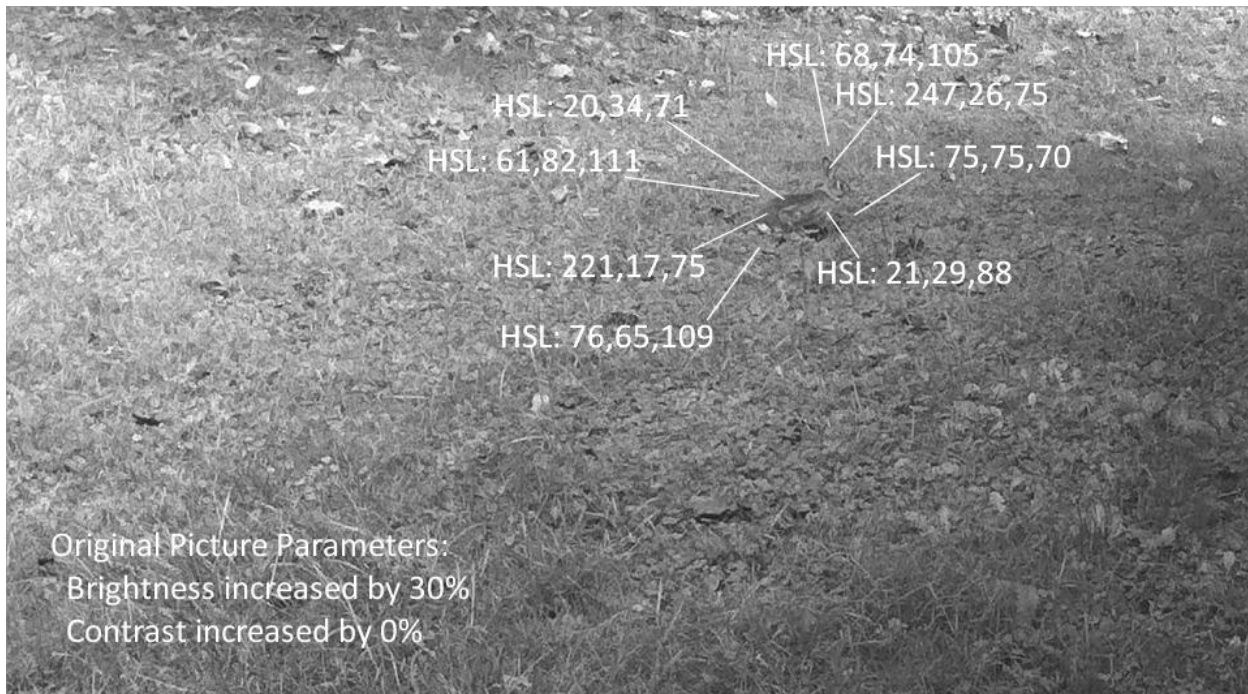


Figure 29. Hue, Saturation, Luminance for Different Spots in a Scene

The tristimulus colorimetric values at different spots are given for a sample picture taken to a rabbit on the grass. The original picture was in color. Later on it was rendered in grey scale and its brightness (luminance level) increased by 30% for a better printing, nevertheless the contrast level was not changed to preserve the contrast from the original picture.

The Average Contrast Index is $C = 0.17$, see Table 4, where C is defined as:

$$C = \frac{L_{max} - L_{min}}{L_{max} + L_{min}} \text{ and its range is } 0 \leq C \leq 1 \quad (21)$$

Table 4

Contrast Index Based on HSL Measures of Snapshot in Figure 29

HSL Rabbit *	HSL Grass *	$ L_R - L_G $	$L_R + L_G$	Contrast Index
221, 17, 75	76, 65, 109	34	184	0.19
20, 34, 71	61, 82, 111	40	182	0.22
247, 26, 75	68, 74, 105	27	180	0.15
21, 29, 88	75, 75, 70	18	158	0.12
	Σ	119	704	0.17

* Original Color Snapshot Tristimulus Values: HSL (Hue, Saturation, Luminance)

Asphalt Reflectivity. Asphalt has a 5% reflectance factor ρ what considerably decreases its luminance as according to formula (17):

$$\pi(sr)L(\text{cd/m}^2) = \rho E(\text{lx}) = 5\% E(\text{lx}) \quad (22)$$

The reduced asphalt reflectance and contrast levels have a significant impact in the amount of light that impinges the sensor array of a video imaging system.

Modulation Transfer Function. Any periodic waveform, from a square wave to a triangle wave can be represented by a sum of sine waves: the fundamental wave and the harmonics.

The amplitude and phase relationship of each harmonic is determined by the mathematical principles of the Fourier series (Cowan, 1982).

In particular the luminance L of a square wave can be represented by the following Fourier series, see Figure 30:

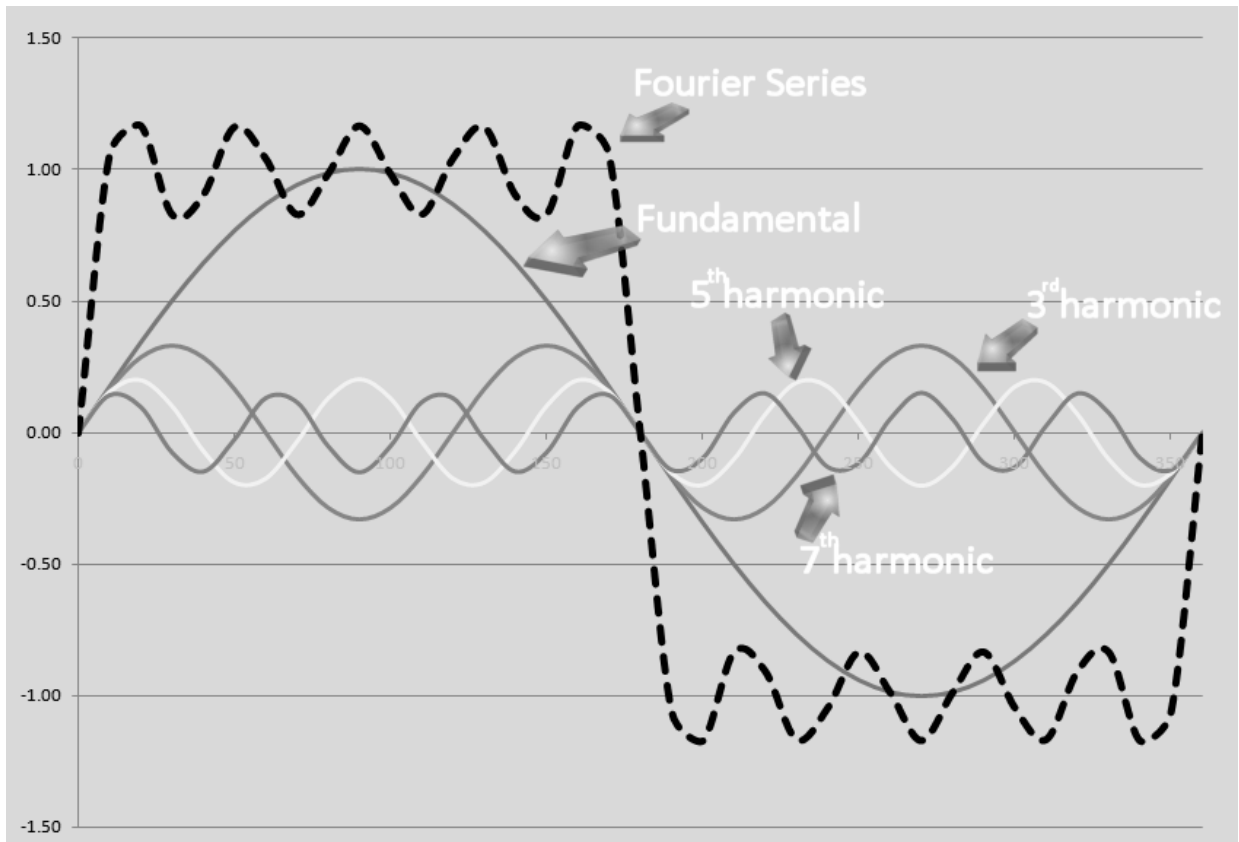


Figure 30. Square Wave Generated by a Fourier Series

The Luminance L may be represented as:

$$L = L_0 \left[\sin \gamma + \frac{1}{3} \sin 3\gamma + \frac{1}{5} \sin 5\gamma + \frac{1}{7} \sin 7\gamma + \dots \right] \quad (23)$$

where:

$L_0 = 4L_{max}/\pi \approx 1.27 L_{max}$ and L_{max} is the maximum value of the square-wave

γ is the spatial frequency of the fundamental sine-wave

$3\gamma, 5\gamma, 7\gamma$ etc the spatial frequencies of the 3rd, 5th, 7th harmonic sine-waves

The amplitude of the harmonics ($\frac{1}{3}; \frac{1}{5}; \frac{1}{7}; \dots$) decreases as the frequency increases.

Contrast Sensitivity Patterns. Contrast is the difference in luminance (commonly known as brightness) that separates an object from its background.

Contrast Sensitivity is a person's ability to identify an object from its background or a system's capability to generate an image that differentiates the target from its background.

There are two general types (Vision Sciences Research, 2002) of contrast sensitivity tests:

- sine-wave gratings
- low contrast letter tests

A grating is a set of lines placed at various widths apart in order to determine if the observer can distinguish direction or separation of the lines (Tyler, "n.d.").

The Tumbling Es can also be considered as a particular case of the sine-wave gratings type because when the E-Chart is seen on a LCD monitor, the video imaging system introduces its own degradation of the imaging performance due to the Modulation Transfer Function (MTF).

The bars of a sinusoidal grating do not change abruptly (Kalloniatis & Luu, 2007) as with square wave gratings, see Figure 31.

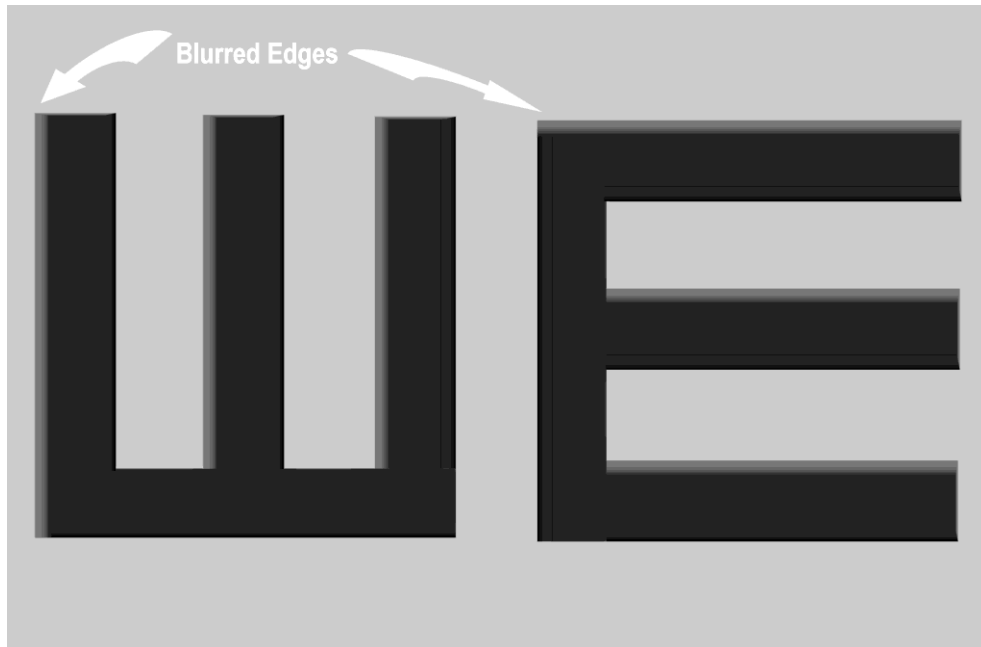


Figure 31. Blurred Edges Generate a Sine-Wave Optotype Grating

When the Tumbling Es shown in Figure 31 are used to test the image quality of a video imaging system, the Es may be considered low contrast letters.

In addition, the Modulation Transfer Function (MTF) affects the image displayed in both the input and output monitors of the video imaging system under test.

The MTF values at different spatial frequencies can be plotted as indicated in Figure 32. They are the actual MTF values for a commercial imaging device:

MTF: 83% for $\gamma = 1$; MTF: 60% for $\gamma = 3$; MTF: 38% for $\gamma = 6$; MTF: 18% for $\gamma = 10$.

Figure 32 shows the normalized spatial frequency γ considering that:

$\gamma = 1$ refers to 2.5 lp/mm

$\gamma = 3$ refers to 7.5 lp/mm

etc.

The MFT values 45% and 34% respectively for $\gamma = 5$ and $\gamma = 7$ were determined by interpolating in the curve (dotted lines) the spatial frequencies $\gamma = 3$ and $\gamma = 7$.

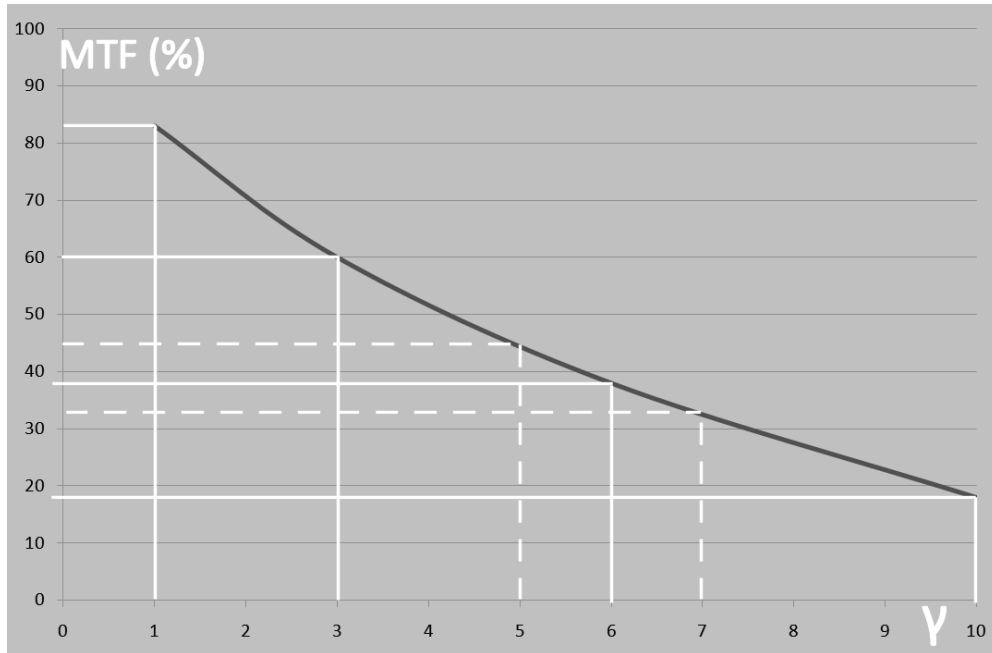


Figure 32. MTF Curve for a Commercial Device

Thus the Es displayed on the EVIS output LCD are no longer square waves but to some extent sine-wave gratings, see Figure 33 and Figure 34

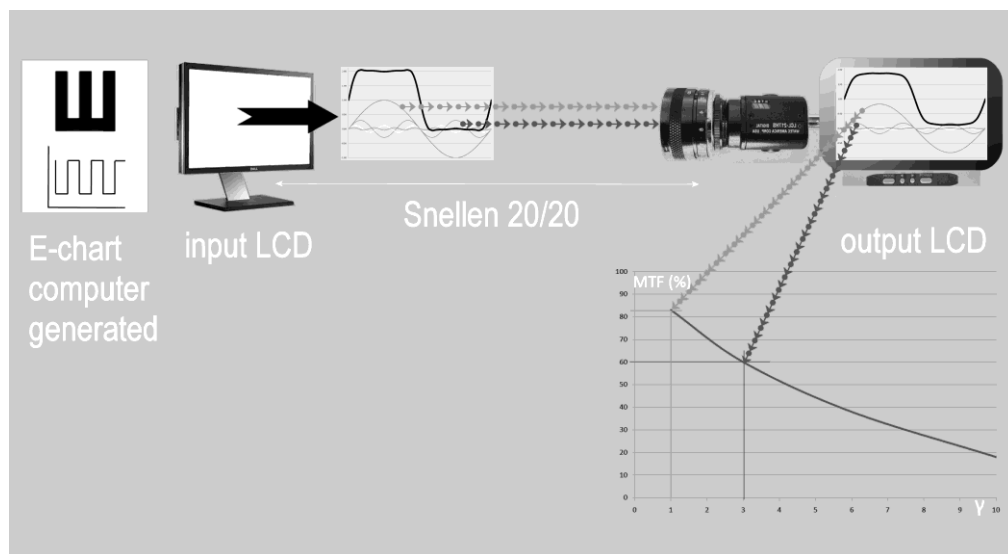


Figure 33. Output LCD Displays Tumbling Es as Sine-Wave Gratings

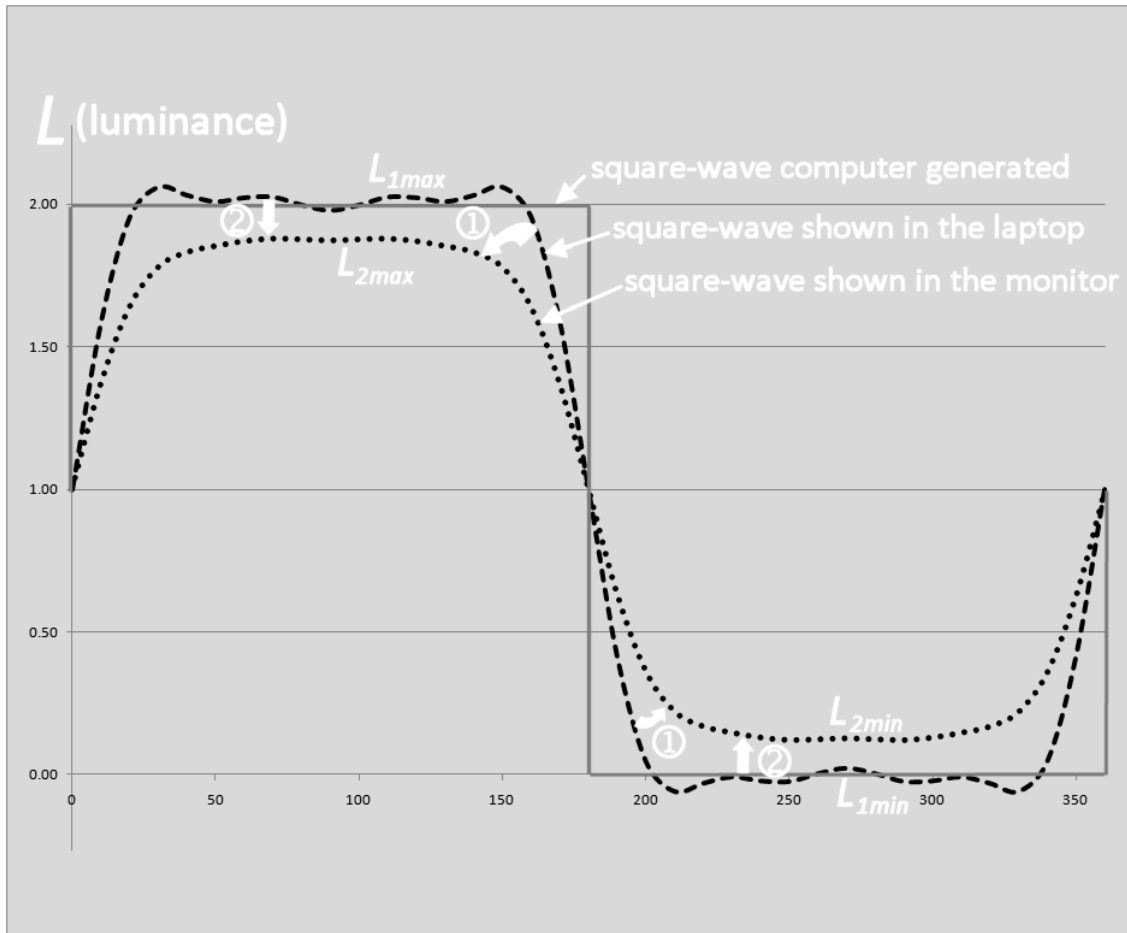


Figure 34. MTF for One Cycle Composed of One White Bar and One Black Bar

Figure 34 shows a square-wave computer generated and displayed by the EVIS input LCD and the square-wave depicted in the output LCD see Figure 33, of the video imaging system.

The MTF causes two effects:

- ① decreases the slope of the output square-wave and thus the sharpness of the image and
- ② decreases L_{1max} (L 's maximum value) and increases L_{1min} (L 's minimum value). Thus the Average Contrast Index defined in equation (21):

$$C = (L_{max} - L_{min}) / (L_{max} + L_{min}) \approx (2 - 0) / (2 + 0) = 1$$

in the case shown in Figure 34 C will have a lower value:

$$C = (1.88 - 0.12) / (1.88 + 0.12) = 0.88$$

Therefore the contrast has been reduced by 12% as shown in Figure 35:

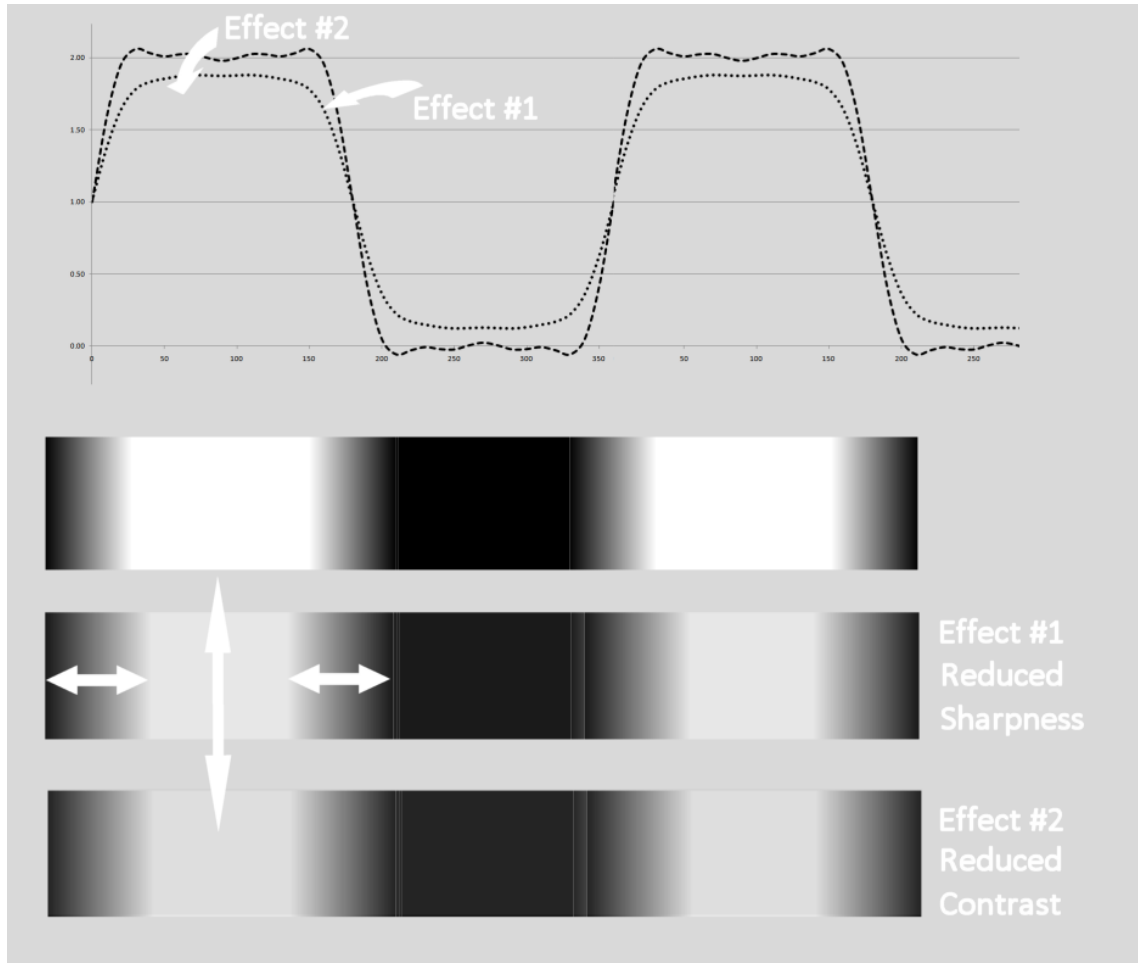


Figure 35. MTF Reduces: Sharpness (Effect #1) and Image Contrast (Effect #2)

The MTF reduces the image sharpness and contrast, see effects #1 and #2 in Figure 35 and makes it more difficult to the “standard observer” to recognize a particular shape, see also Figure 36.

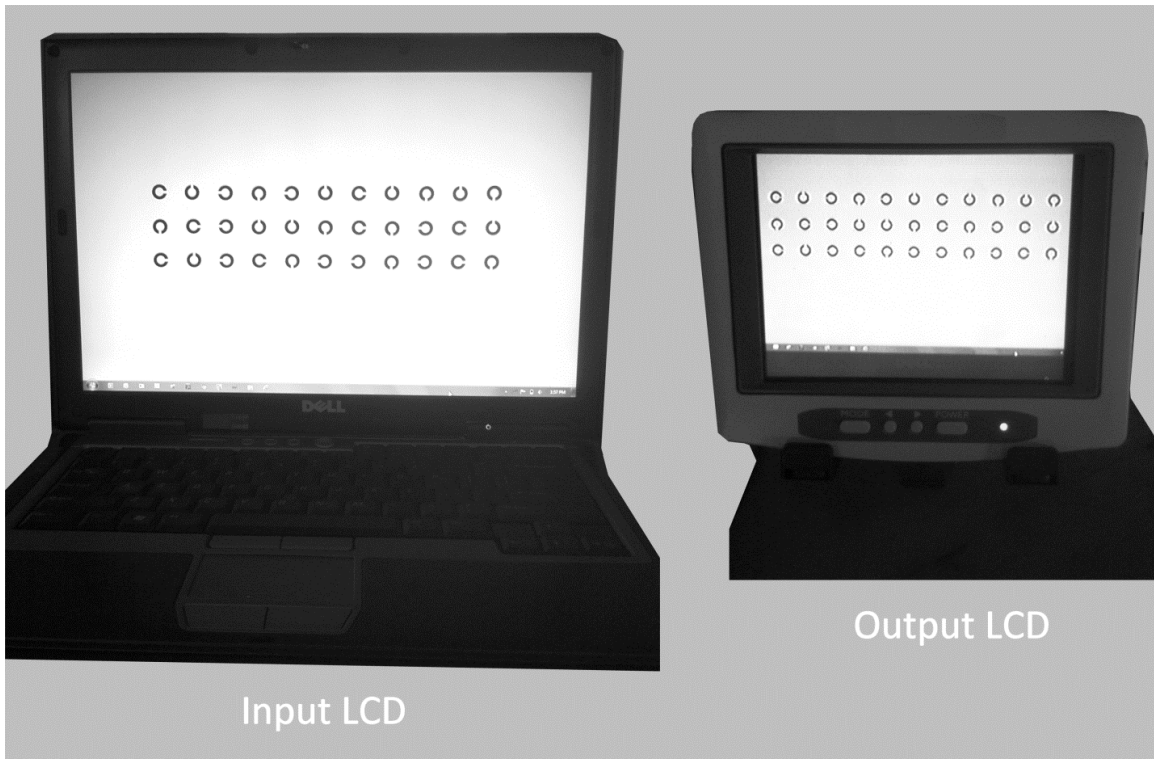


Figure 36. Input / Output Tumbling C-charts Used in the EVIS

In summary there are several factors affecting the human vision of a “standard observer” and they all should be considered when benchmarking end-to-end EVIS:

- visual acuity
- observer’s reaction time
- maximum allowed dynamic searching time
- probability of target detection and recognition
- angular threshold of the human eye
- system modulation transfer function
- scene contrast sensitivity

Video Imaging System Analytics

In this section, the most important optical parameters used in defining a video imaging system and the photometric equations applicable are considered.

CCTV Camera Formats. CCTV cameras have installed either a CCD or CMOS sensor array with one of the following standard formats: 1", 2/3", 1/2", 1/3" or 1/4", see Figure 37.

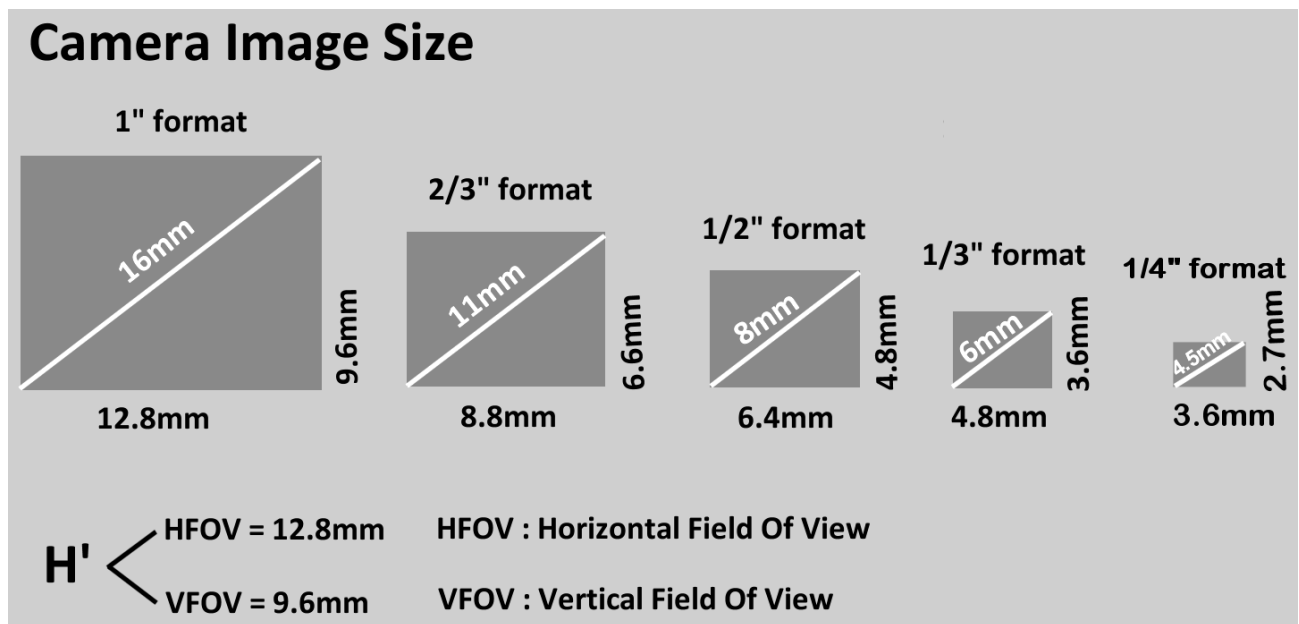


Figure 37. Different CCD Sensor Array Formats Available in the Marketplace

An Objective Lens with 1" Format and Focal Distance 25mm on a 1" Format Camera has the same Angle of View as a 1/2" Format Objective Lens with Focal Distance 12.5mm on a 1/2" Format Camera, see Appendix E, because the Angle Of View $\theta = 2\tan^{-1} H'/2f$ then the two relationships provide the same result:

$$\theta = 2\tan^{-1} H'/2f = 2\tan^{-1} (12.8/2*25) = 2\tan^{-1} (6.4/2*12.5)$$

Throughout the years this relationship has been used to reduce the size of CCTV sensor arrays and objective lenses to get more compact and portable systems, but it also *reduces the total amount of energy the lens is gathering*, because for same Magnification 1X and $F/1.2$ characteristics of the objective lens it can be stated that:

$$F\text{-Stop} = 1.2 = \frac{f}{D} = \frac{25}{21} \text{ (for 1" format)} = \frac{12.5}{11} \text{ (for 1/2" format)}$$

so although the F-Stop is the same, the diameter of a 1/2" format lens is half the size of the 1" format lens and the amount of energy is smaller

FOV, CCTV, and Objective Lens Format. An objective lens of 1" format used in a 1" CCTV camera provides the nominal angle of view indicated for the objective lens.

If it is used with a different CCD format, the angle of view will be different from the lens nominal value and a change of the apparent video imaging system magnification will occur.

For instance, when a 2/3" format objective lens is used with a 1/3" format CCD camera, the nominal magnification of the objective lens will double.

In order for the same target to fill in the entire CCD chip, the objective lens should be moved further away, so the image size decreases and fits a smaller chip area.

Thus there is an apparent increase of system magnification because for the target seen in the LCD monitor the distance from the target has been significantly increased. Figure 38 explains why the distance from the target has been increased.

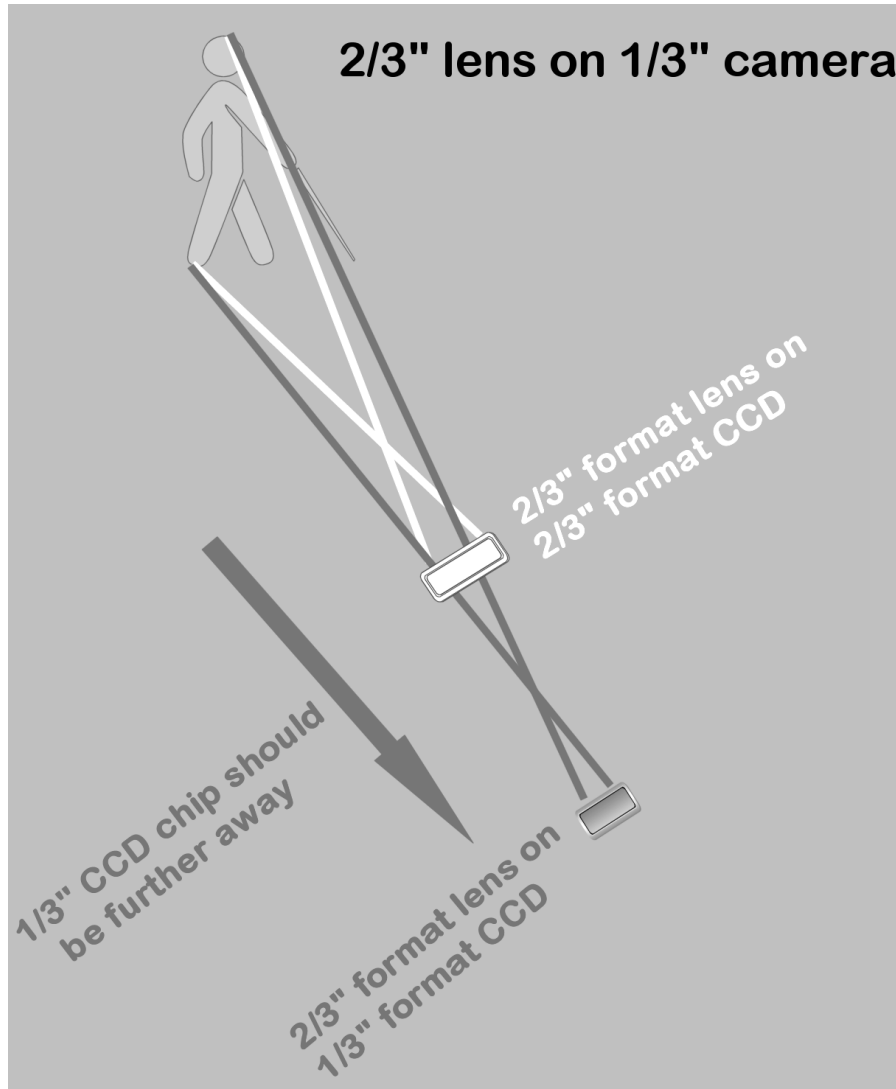


Figure 38. Increased System Magnification: 2/3" Format Lens on a 1/3" CCD Sensor

In Table 5 it is shown a list of CCD formats (1/3", 1/2", 1") and different focal length standards for lens available in the market.

For instance, an objective lens 1" format and 25 mm focal length has an Horizontal x Vertical AOV (Angle of View) $\theta_{1"}$ of 29° x 22° when used with a 1" CCD format and $\theta_{1/2"}$ of 15° x 11° when used with a 1/2" CCD format. Thus $\theta_{1/2"} = 0.5 \theta_{1"}$ what creates the effect of increasing the apparent magnification by a factor of 2X.

Table 5

System Angle of View θ as Function of the CCD Format

The Angle of View θ have been rounded to integer numbers

1/3" CCD	1/2" CCD	1" CCD	ANGLE OF VIEW
Lens Focal Length (mm)			Lens θ (degrees)
9.4	12.5	25	29 x 22
11.3	15	30	24 x 18
13.1	17.5	35	21 x 16
15	20	40	18 x 14
18.8	25	50	15 x 11
20.6	27.5	55	13 x 10
22.5	30	60	12 x 9
24.4	32.5	65	11 x 8
26.3	35	70	10 x 8
28.1	37.5	75	9 x 7
30	40	80	9 x 7
37.5	50	100	7 x 6
41.3	55	110	7 x 5
45	60	120	6 x 5
48.8	65	130	6 x 4
52.5	70	140	5 x 4
56.3	75	150	5 x 4
60	80	160	5 x 3

Lenses for Use with TV-Type Systems. These detectors are generally charge-coupled devices (CCD). Resolution is often expressed as “TV lines.” This represents the actual number of scan lines, not line pairs/mm, as in optical references.

For example, consider a typical 1-in. vidicon (so called because the outside portion of the tube is 1 in. in diameter), it has a vertical height of 0.375 in.

At 525 TV lines, its resolution would be:

$$\frac{525 \text{ lines} / 2 \text{ frames}}{0.375 \text{ in.} \times 25.4 \text{ mm/in.}} = 28 \text{ lp/mm}$$

Therefore, one wants high MTF response at low spatial frequencies. This is accomplished by designing CCTV objective lenses that reduce image flare.

The ray pattern is then adjusted to trace more rays at the outer portion of the pupil (Laikin, 2007 p30).

Radiant Power Transfer from Source to Detector

Non-imaging optics are used to describe some of the characteristics of the video imaging systems (Chaves, 2008) such as the radiant power transfer from the source to the sensor array.

The intensity I of the radiation is defined as the flux per unit solid angle. The radiometric quantity is given in watts per steradian (W/sr).

The photometric quantity is measured in candelas where $1 \text{ cd} = 1 \text{ lm/sr}$.

The radiant flux L per unit projected area and per unit solid angle is called radiance and is measured in watts per square meter per steradian ($W/m^2 \cdot sr$).

The corresponding photometric quantity is the luminance L_s measured in candelas per square meter: $cd/m^2 = 1 \text{ lm}/m^2 \cdot sr$, see Table 3 for a summary of units used in Radiometry and Photometry.

Lambertian source. Consider the particular case in which the radiance L (or luminance L_s) of a surface A is uniform and constant throughout the whole area.

A surface is called Lambertian (Chavez, 2008) if it emits or intercepts radiation with an intensity pattern following only the cosine law (see equation E01 Appendix E):

$$I = LA\cos\theta \quad (30)$$

where:

$$LA = I_s \quad (31)$$

For a Lambertian source L is constant across its surface so the factor LA is constant and the intensity I is only function of the angle θ in a particular direction:

$$I = I_s\cos\theta \quad (32)$$

In practice, if we consider a source located far enough from the observer and that the view angle θ_s varies in a small range from θ_1 to θ_2 , as shown in Figure 39:

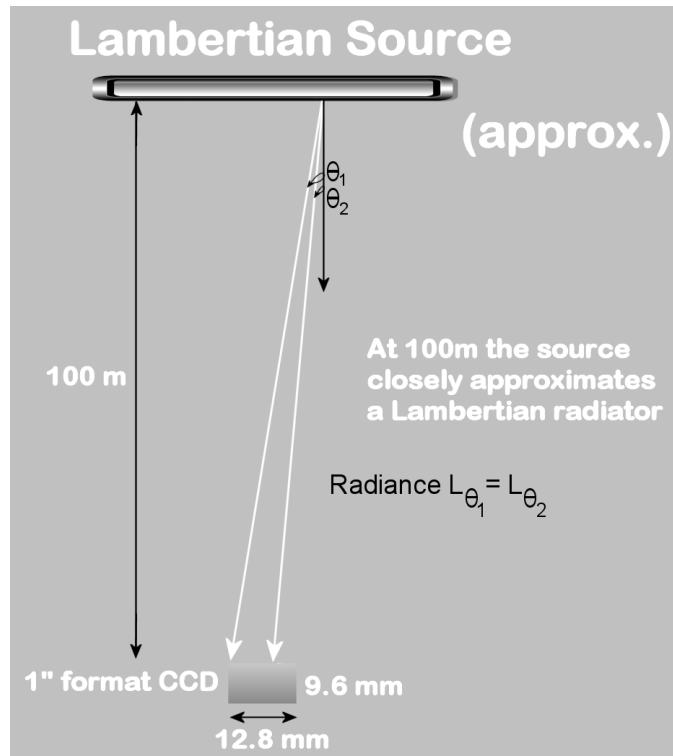


Figure 39. Lambertian Source Approximation

the approximation to a Lambertian source is correct and the radiance exitance $M \approx \pi L$ where L is the radiance (or luminance) of the Lambertian source, see Appendix E.

A radiant source seen from a small detector at a distance $D \geq 20$ ft (6 m) as shown in Figure 39, can be approximated to a Lambertian source.

Illuminance E_d – Exact & Approximate Figures. The power Φ_d from the Lambertian source falling on the detector, see equation (E13) in Appendix E, can be approximated by:

$$\Phi_d \approx L_s A_d \omega_s = L_s A_s \omega_d$$

The exact value of the irradiance at the detector can be calculated using the equation (E11) in Appendix E:

$$E_d = \frac{\Phi_d}{A_d} = \frac{2L_s A_s}{r_s^2 + r_d^2 + d^2 + \sqrt{(r_s^2 + r_d^2 + d^2)^2 - 4r_s^2 r_d^2}}$$

This is the fundamental equation to calculate the illuminance E_d on a detector from a Lambertian radiator of area A_s and luminance L_s located at distance d from the detector.

The equation (E11) can be approximated by:

$$E_d = \frac{\Phi_d}{A_d} \approx L_s \omega_s = L_s \omega_d \frac{A_s}{A_d} \quad (33)$$

It is also demonstrated by comparing the exact calculated figures given by the equation (E11) with the actual readings of the LX1010B lux meter, that the lux meter is quite accurate when used at a distance $d \geq 1$ m from the Dell Laptop D620.

Table 6 shows the calculations and lux meter readings for the new test set, and the distance to the LCD screen: $d = 240$ in. = 20 ft has been included because it is the standard distance for benchmarking the EVIS using 20/20 Tumbling Es / Cs.

Table 6

Illuminance E_d - Exact Calculation and Lux Meter LX1010B Actual Readings

d (distance to LCD screen)			S^2_{sd}	r^2_s	r^2_d	Z	Z²
inch	meter	meter approx.	m ²	m ²	m ²		
0.00	0.000	0.00	0.000000	0.018	0.0004	0.018400	0.000339
1.00	0.025	0.03	0.000645	0.018	0.0004	0.019045	0.000363
2.00	0.051	0.05	0.002581	0.018	0.0004	0.020981	0.000440
4.50	0.114	0.11	0.013064	0.018	0.0004	0.031464	0.000990
5.80	0.147	0.15	0.021703	0.018	0.0004	0.040103	0.001608
11.80	0.300	0.30	0.089832	0.018	0.0004	0.108232	0.011714
39.37	1.000	1.00	0.999996	0.018	0.0004	1.018396	1.037130
78.74	2.000	2.00	3.999984	0.018	0.0004	4.018384	16.147410
102.36	2.600	2.60	6.759709	0.018	0.0004	6.778109	45.942759
107.87	2.740	2.74	7.507041	0.018	0.0004	7.525441	56.632263
185.83	4.720	4.72	22.279174	0.018	0.0004	22.297574	497.181810
240.00	6.096	6.10	37.161216	0.018	0.0004	37.179616	1382.323846

d (distance to LCD screen)			$4r^2_s * r^2_d$	$(Z^2 - 4r^2_s * r^2_d)^{1/2}$	$Z + (Z^2 - 4r^2_s * r^2_d)^{1/2}$
inch	meter	meter approx.			
0.00	0.000	0.00	0.000029	0.017600	0.036000
1.00	0.025	0.03	0.000029	0.018273	0.037319
2.00	0.051	0.05	0.000029	0.020283	0.041263
4.50	0.114	0.11	0.000029	0.031003	0.062468
5.80	0.147	0.15	0.000029	0.039742	0.079846
11.80	0.300	0.30	0.000029	0.108099	0.216331
39.37	1.000	1.00	0.000029	1.018382	2.036778
78.74	2.000	2.00	0.000029	4.018380	8.036764
102.36	2.600	2.60	0.000029	6.778107	13.556215
107.87	2.740	2.74	0.000029	7.525439	15.050880
185.83	4.720	4.72	0.000029	22.297573	44.595148
240.00	6.096	6.10	0.000029	37.179616	74.359232

			$E_d = 2L_s A_s / [Z + (Z^2 - 4r^2_s * r^2_d)^{1/2}]$				
inch	meter	meter approx.	L_s	A_s	E_d (LX) CALCULATED BY FORMULA	E_d (LX) CALCULATED BY πL_s	E_d (LX) LUX METER READING
0.00	0.000	0.00	220	0.05655	691.2	691.2	165
1.00	0.025	0.03	220	0.05655	666.7		159
2.00	0.051	0.05	220	0.05655	603.0	$E_d = \pi L_s$	153
4.50	0.114	0.11	220	0.05655	398.3	<i>is only</i>	127
5.80	0.147	0.15	220	0.05655	311.6	<i>valid on</i>	107
11.80	0.300	0.30	220	0.05655	115.0	<i>the</i>	60
39.37	1.000	1.00	220	0.05655	12.2	<i>surface</i>	10
78.74	2.000	2.00	220	0.05655	3.1	<i>itself</i>	3
102.36	2.600	2.60	220	0.05655	1.8	<i>where</i>	2
107.87	2.740	2.74	220	0.05655	1.7	<i>d = 0</i>	1.5
185.83	4.720	4.72	220	0.05655	0.6		0.5
240.00	6.096	6.10	220	0.05655	0.3		N/A

The Cosine-To-The-Fourth Law. The amount of a viewed area diminishes as it is tilted with respect to the viewer. If the detector is moved off-axis by a distance x the ray from A_s to A_d will then be at an angle θ_s and θ_d with respect to the normal at both surfaces as follows:

$$\theta_s = \theta_d = \theta_x = \text{atan}\left(\frac{x}{d}\right) \quad (34)$$

The radiant power at a distance x away from the axis decreases by the fourth power of the cosine of the angle formed between the normal to the surface and the ray so the radiant power at a position x off-axis, according to Zalewski (as cited in Bass, 1994):

$$\Phi_x \approx \frac{L_s A_s A_d}{d^2} \cos^4 \theta_x \quad (35)$$

Thus, the irradiance at the detector using Φ_d and the cosine-to-the-fourth approximation as described in equation (E18) Appendix E will be:

$$E_d = \frac{\Phi_d}{A_d} \approx L_s \omega_s \cos^4 \theta_x = L_s \omega_d \frac{A_s}{A_d} \cos^4 \theta_x \quad (36)$$

Reflectance of a Lambertian Source. In the particular case of a Lambertian emitter or reflecting source, with a reflection coefficient $\rho = \frac{\Phi_{out}}{\Phi_{in}} \Rightarrow \Phi_{out} = \rho \Phi_{in}$ where Φ_{in} is the incoming radiant power and Φ_{out} is the reflected radiant power.

The following equation between the Exitance M and the Irradiance E applies to a Lambertian source (Greivenkamp, 2004):

$$M = \rho E \quad (37)$$

Thus, the more general equation for the Irradiance E_d at an image when a Lambertian source is tilted at angle θ_x with respect to the viewer and the reflectance of the surface has a coefficient ρ is:

$$E_d = \rho \frac{\Phi_{in}}{A_d} \approx \rho L_s \omega_s \cos^4 \theta_x = \rho L_s \omega_d \frac{A_s}{A_d} \cos^4 \theta_x \quad (38)$$

Sensor Format SNR. The ratio between the areas A_d (mm²) for a 1" CCD format and a 2/3" CCD format sensor arrays is:

$$A_{d_{2/3}}/A_{d_{1}} = 4/9$$

The radiant power (watts) transferred from a Lambertian source to a 2/3" CCD format sensor array is 4/9 of the power transferred to a 1" format:

$$\Phi_{d_{2/3}} / \Phi_{d_{1}} = 4/9 = 0.445$$

considering that $\omega_{s_{2/3}} \approx \omega_{s_{1}}$ because $d = 100\text{m} \gg$ sensor array width (12.8mm).

The SNR of a video imaging system if 2/3" CCD is used instead of 1" will be:

$$\text{SNR}_{2/3} = 10\log_{10}\left(4/9 \frac{P_{\text{signal}}}{P_{\text{noise}}}\right) = \text{SNR}_{1} - 3.52 \text{ dB}$$

where P_{signal} is the useful energy in watts and P_{noise} also in watts is the noise internally created by the CCD, see equations (E20) to (E23) Appendix E.

A similar comparison between the CCD sensor array of a 2/3" format and 1/3" format:

$$\text{SNR}_{1/3} = \text{SNR}_{2/3} - 5.25 \text{ dB}$$

And if a 1/4" CCD format is used instead of 1/3" CCD there is a further reduction:

$$\text{SNR}_{1/4} = \text{SNR}_{1/3} - 2.5 \text{ dB}$$

The cumulative SNR decrease for a 1/4" CCD compared to a 1" CCD format is:

$$\text{SNR}_{1/4} = \text{SNR}_{\text{CCD } 1} - 11.27 \text{ dB}$$

These calculations have important implications when selecting the CCD format to use in the video imaging system (see Appendix E).

Irradiance Levels at Different Stages of a Video Imaging System

The radiant flux Φ_d falling on the detector equals the radiant flux Φ_{lens} falling on the lens considering an ideal lens without energy absorption.

The radiant flux Φ either emitted or reflected from an approximated Lambertian source falling on a detector (CCD sensor) throughout an objective lens, see Figure 40:

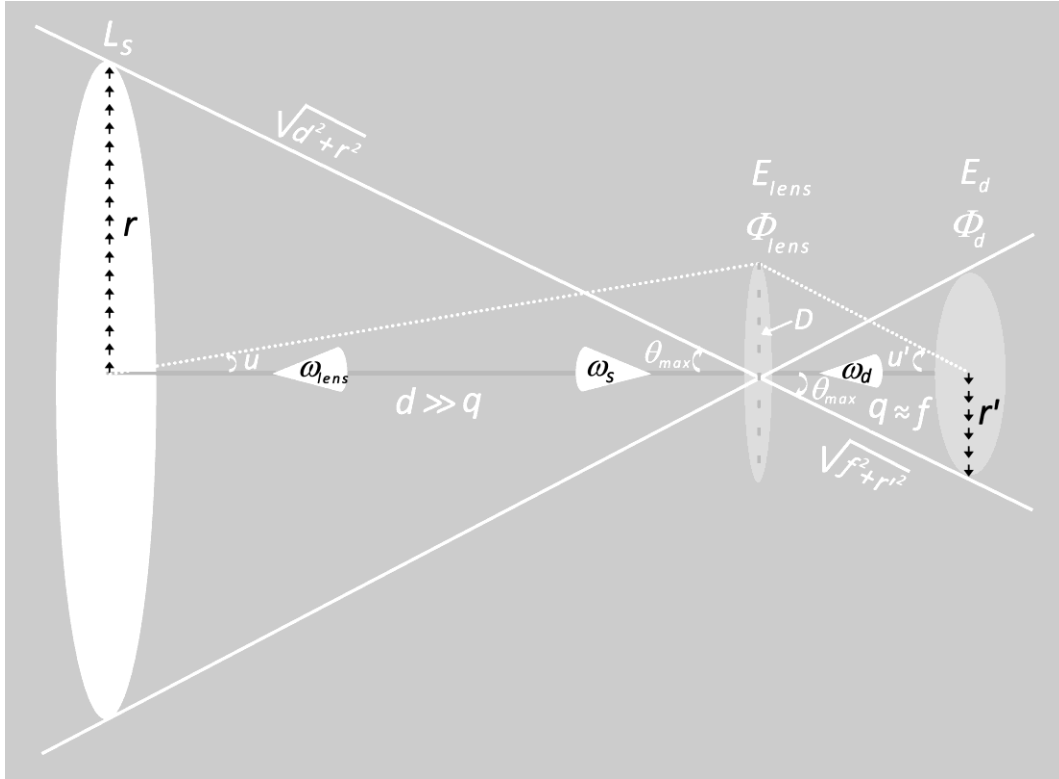


Figure 40. Illuminance E_d Estimated at the Detector for $d \gg q \approx f$

The radiant flux Φ_d falling on the detector is described by, see Appendix F:

$$\Phi_d = \Phi_{lens} = L_s A_{lens} \omega_s = L_s A_s \omega_{lens} \quad (39)$$

L_s : luminance of the Lambertian source; A_s is the area of the source;

A_{lens} is the cross section area of the objective lens; A_d is the area of the detector;

E_{lens} : Illuminance at the lens; E_d : Illuminance at the detector

Φ_{lens} : luminous flux at the lens; Φ_d : luminous flux at the detector

ω_s : solid angle subtended by the source; ω_{lens} : solid angle subtended by the lens;

ω_d : solid angle subtended by the detector;

r : radius of the Lambertian source ; D : lens entrance pupil; r' : radius of the detector;

u and u' are the paraxial angles based on the approximation of small θ values for the

thin lens, in which case (Greivenkamp, 2004):

$$\frac{u}{u'} = \frac{r'}{r} = \frac{q}{d} \quad \text{when } n = n' \quad (n = n' = 1 \text{ in the air})$$

and the thin lens equation (F06) in Appendix F can be approximated as follows:

$$\frac{1}{d} + \frac{1}{q} = \frac{1}{f} \quad \text{for } d \gg q \Rightarrow \frac{1}{q} \approx \frac{1}{f} \Rightarrow q \approx f$$

Now, the irradiance (or illuminance) E_d on the sensor array, see equation (F11) in Appendix F, can be easily calculated:

$$E_d = \frac{\Phi_d}{A_d} \approx \frac{\pi Ls}{4F_{stop}^2 + \left(\frac{2r'}{D}\right)^2} \quad (40)$$

where $2r'$ is the sensor array format and D is the lens entrance pupil.

If the format of the sensor array equals the lens entrance pupil, as it is typically the case in video imaging systems for surveillance that include a 1/2-format fixed objective lens with 1X magnification and 1/2-inch format CCD, then $2r' = D$ and according to equation (F12) in Appendix F:

$$E_d = \frac{\Phi_d}{A_d} \approx \frac{\pi Ls}{4F_{stop}^2 + \left(\frac{2r'}{D}\right)^2} = \frac{\pi Ls}{4F_{stop}^2 + 1} \quad (41)$$

which is a fundamental equation for video imaging systems.

Thus if the Lambertian source is located at a distance $d \geq 20$ ft (6 m) and the area A_s has a constant intensity I across its surface, the irradiance E_d is reduced by the square power of the F -Stop of the objective lens, what is consistent with the statement indicated in Table 2 for the F -Stop section: *Each F-Stop jump indicates a 50% reduction in the amount of light a lens is able to transmit (transmittance).*

Irradiance E_d in terms of E_{lens} and lens FOV. Another useful equation for the irradiance (or illuminance) level E_d at the lens using $\Phi_d = \Phi_{lens}$ will be deduced, see equation (F18) in Appendix F:

$$E_d = \frac{\Phi_d}{A_d} = E_{lens} \frac{A_{lens}}{A_d} \approx \frac{E_{lens}}{(FOV * F_{stop})^2} \quad (42)$$

Calibration: The Need for Color Management

There are differences between two Hewlett-Packard (HP) scanners of the same make and model and even bigger differences between an HP and a Umax scanner. At the scanner stage, the same color gets translated into different pixel values, due to camera or scanner characteristics.

Color management systems seek to quantify the color characteristics of a device and use this to alter the pixel values that must be sent to a device to achieve the desired color.

The same manufacturer would sell a color imaging suite that included the monitor, software, scanner, output, and so on.

These were closed-loop systems in which all devices were designed and installed by one vendor; however, there are many instances in which the demands of the modern imaging industry make closed-loop color appear very expensive, inflexible, proprietary, and personnel dependent and are not recommended in many cases (Lukac & Plataniotis, 2006).

Open-Loop Color Management. An open-loop environment, also known as a color management system, such as that specified by the ICC, provides an elegant solution to the issue of color control.

Microsoft Windows 7 Professional Edition allows selecting a particular color management profile or *color gamut* so the colors in the Tumbling Es or Tumbling Cs charts can be standardized between different computers.

The profile selected for the New Test Set presented in this thesis is the sRGB_IEC61966-2.1.ICC, see Figure 41.

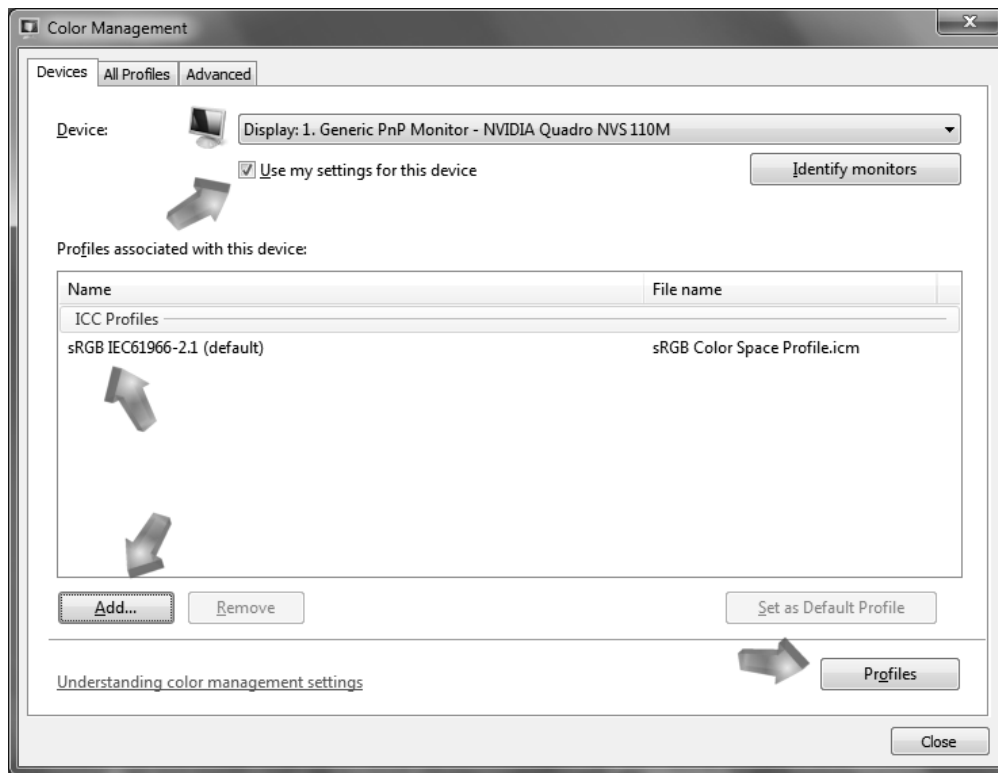


Figure 41. Color Management Option in Windows 7 Professional Edition

To activate in the computer, just click on “Profiles” and select:

sRGB_IEC61966-2.1.ICC

then click in the “Add” button and then select “Use my settings for this device”.

Color Gamut. It is the color range or the various levels of colors that can potentially be displayed by a device. A color gamut can be additive or subtractive.

Additive refers to color that is generated by mixing together primary colors to generate a final color. This is the style used by computers, televisions, and other devices and more often referred to as RGB based on the red, green, and blue colors used to generate the colors.

The most common of the RGB based color gamut is sRGB typically used in all computer displays.

Another color gamut is AdobeRGB that was developed by Adobe to provide a wider range of colors than sRGB.

NTSC was the color space developed for the widest range of colors that can be represented to the human eye.

Device Calibration and Characterization. Color management can be described as consisting of three “C”s:

- Calibration
- Characterization
- Conversion.

The process of calibration involves establishing a fixed, repeatable condition for a device.

For an LCD display, calibration includes adjusting the contrast and brightness controls, see Figure 42:

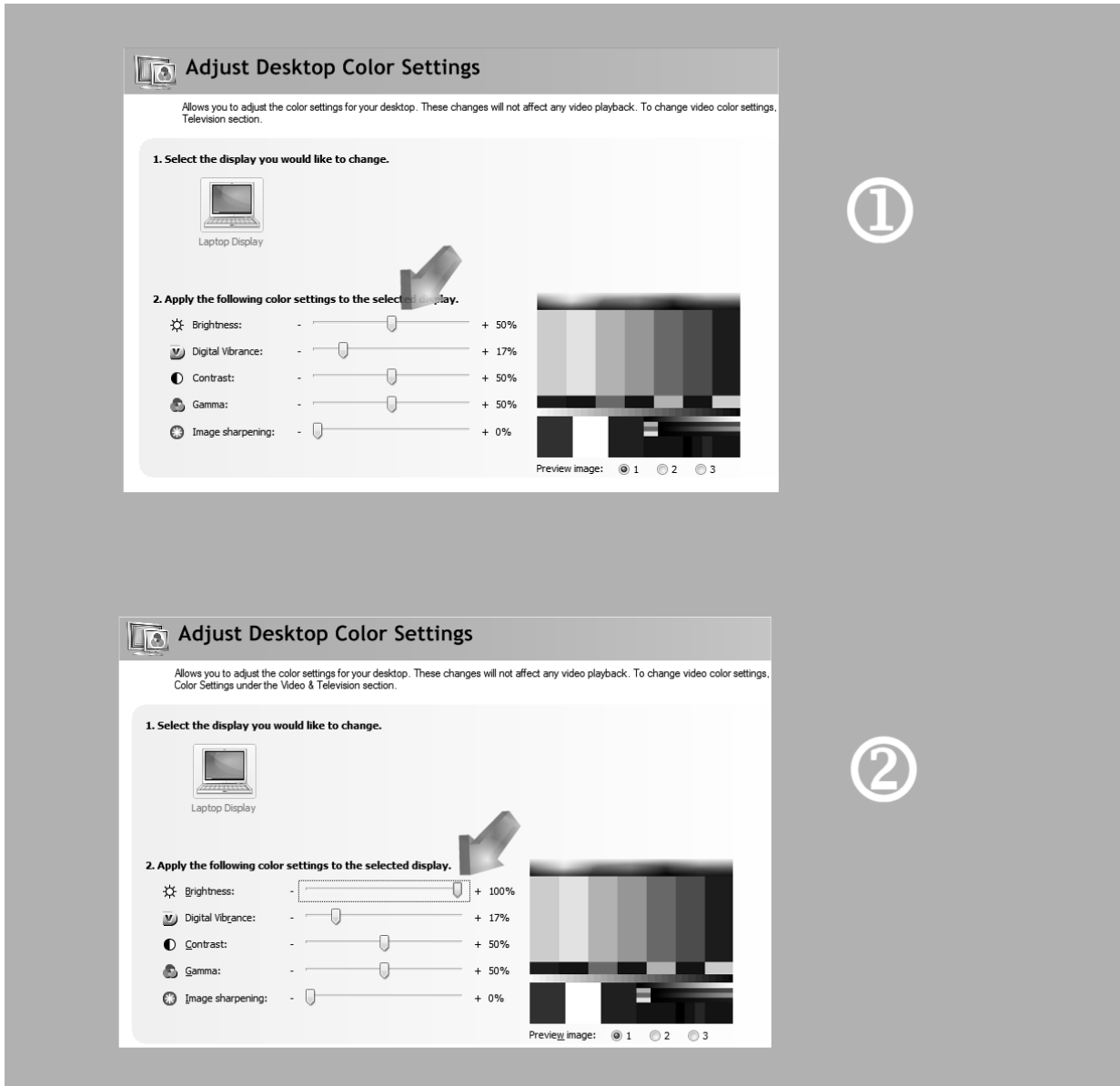


Figure 42. Luminance Adjustment of the Dell Latitude D620 Laptop Video Card

The brightness (luminance) factory default setting ① has been changed to maximum level 100% settings ②.

Characterization is the process of making a profile, sending a sampling of color patches (a test chart) to the device and recording the device's response.

For instance the sRGB_IEC61966-2.1.ICC profile can be used to test the color response of the LCD computer display.

Conversion is a process in which images are converted from one color space to another using a CMM (Color Management Module).

Laptop Screen Luminance. The center of the screen must be in the optical axis and in line with the objective lens to avoid unnecessary changes in the luminance level as the screen luminance varies with the angle of view.

Apparatus Setup (New Test Set)

The apparatus setup refers to the new test set presented in this thesis and the associated benchmarking procedures to test the video imaging system according to the new approach discussed in previous sections.

Several steps indicated in the following set-up procedure will only be needed the first time that a computer is used.

One of the most important steps is to ensure that the correct size of the Tumbling C is obtained in the screen of the particular laptop computer used for the benchmarking test.

Once the screen is calibrated with the appropriate color settings and the Tumbling E or Tumbling C size is correctly determined for a particular screen, the procedures are quite straightforward.

The size of the Tumbling C, see Figure 43, shown in the screen of the laptop, should be measured with a metric ruler and must read exactly 88 mm.

SCREEN CALIBRATION

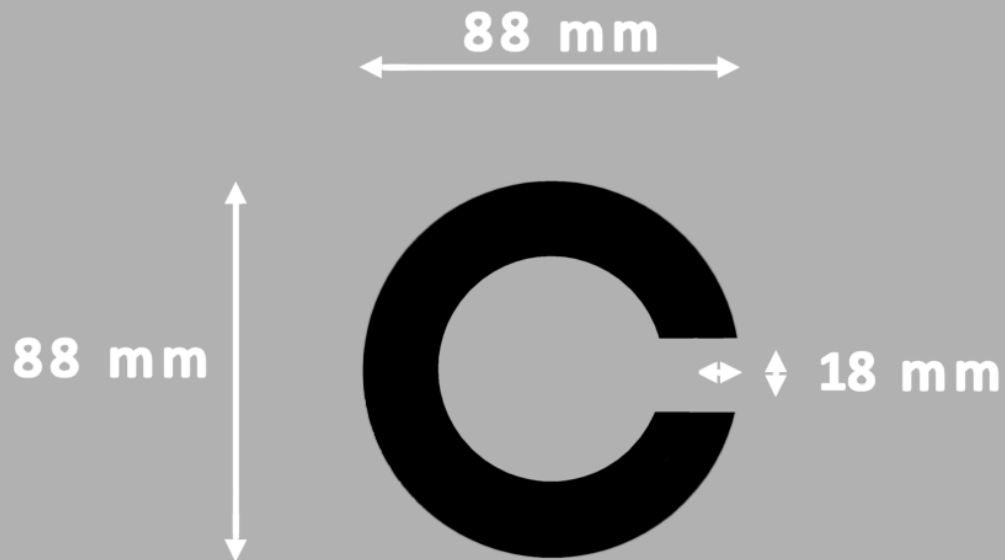


Figure 43. Tumbling C used for screen calibration / Tumbling Cs generator

The Tumbling C shown in Figure 43 can be scaled down to issue all Cs at scale for a particular observation distance, using similar criteria as indicated in Figure 26 for the Tumbling Es.

The height of the Cs should be:

17.6mm at 40 ft

8.8mm at 20 ft

4.4mm at 10 ft

2.2mm at 5 ft

If the direct measurement with a ruler on the screen differs from 88 mm, see Figure 44, a new Tumbling C calibrated for the appropriate LCD screen resolution should be designed.



Figure 44. Display Setup Using the Calibrated C Optotype

The experimental apparatus setup is shown in Figure 2 and Figure 3. The set-up should be carried out according to the following steps:

- Place the laptop computer on a table
- Turn on the computer and load a Tumbling Es or Tumbling Cs generator
- Set the display luminance at maximum by pressing <Fn> and the up-arrow key to increase brightness in the Dell Latitude D620 (other computers may differ)
- Use the Color Management option of Windows 7 to calibrate the monitor using a standard color gamut: as the sRGB_IEC61966-2.1.ICC (see Figure 41)
- Load the Tumbling C to calibrate the display and get the correct size in the screen for the Tumbling C of reference (Figure 44)
- Select the correct size of Tumbling Es or Tumbling Cs for testing distance d
- Turn off the lights
- Place a lux meter at 2 m in front of the laptop and measure the illuminance E_d
- Calculate the illuminance level E_d at 20 ft (6.1 m)
- Estimate the maximum luminance L_s of the screen display and compare to the figure given by the computer manufacturer. If there is a significant discrepancy, review the specifications and see the *Luminance Estimate* in the Results section.
- Place the lux meter, used in the previous steps, in front of the laptop at 0.3 m and secure the light sensor into a bracket or sensor holder.
- Measure the illuminance level E_d and compare it with the exact theoretical value calculated following the method shown in Table 6.
- Without moving the light sensor from its position at 0.3 m from the screen, vary the luminance levels using the luminance charts and determine the linearity of the lux meter at that distance and particular screen luminance

- Place the video camera at the appropriate distance of 20 ft (6.1 m)
- Turn on the light
- Adjust video camera settings to optimum performance (Table 7, Figure 45)

<i>LCL-217HS Settings</i>		
AGC	ON / OFF	
Gamma	ON: 045	OFF: 1
White Balance	ON: AUTO	OFF: FIX
Backlight Compensation	ON: AUTO	OFF: DEACTIVATED

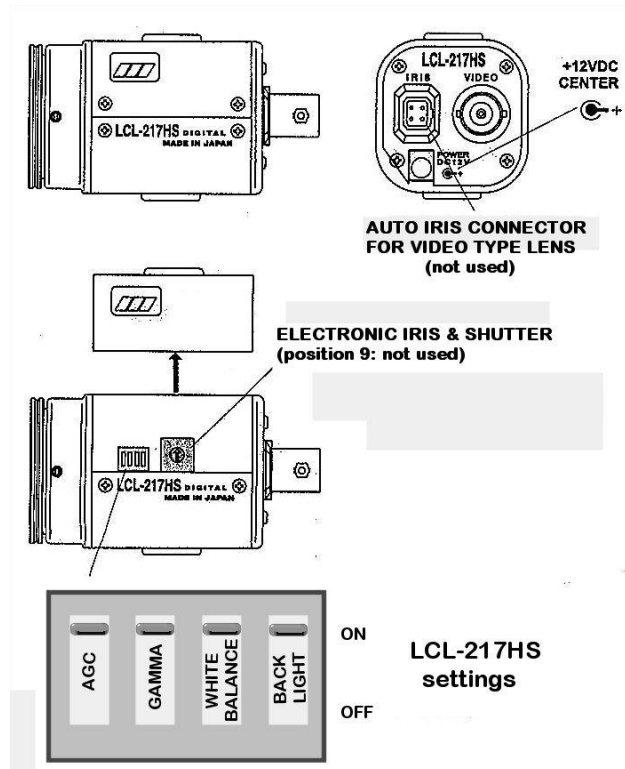


Figure 45. LCL-217HS settings for video quality benchmarking

- Mount the objective lens onto the camera
- Connect the video camera and its power supply
- Turn off the light
- Focus the objective lens for best image in the output monitor of the EVIS
- Select the *F-Stop* until capture a focused image on the card
- Describe the characteristics of the image and check camera specs, see Table 8

Table 8

LCL-217HS CCD Camera Specifications

Sensor Array	1/3" CCD
Picture Elements	768 (H) x 494 (V)
Lens Mount	"CS" mount
Sync System	Internal
Scanning System	2:1 Interlace
Video Output	1.0 V _{p-p} 75 Ω Composite & YC
Resolution	480 TV lines
Min. Illuminance	0.1 lux @ F1.2 (AGC HI)
SNR	≥ 50 dB (AGC OFF)
Power Supply	12 VDC ± 10% ; 180 mA MAX
Operating Temperature	-10°C +40°C (14°F + 104°F)
Weight	85g
Dimensions	1.34 in.*1.34 in.*1.81 in.

- Proceed with the Random Test of Tumbling Es or Tumbling Cs
- Proceed with the Dynamic Test (limit observation time to 3 sec)
- Select E-Chart or C-Chart of different contrast levels
- Select a color E-Chart or C-Chart and test the EVIS
- Load Luminance Filters, see Figure 46 and Figure 47 to reduce the screen luminance level to simulate quarter moon conditions
- Repeat the previous steps as needed

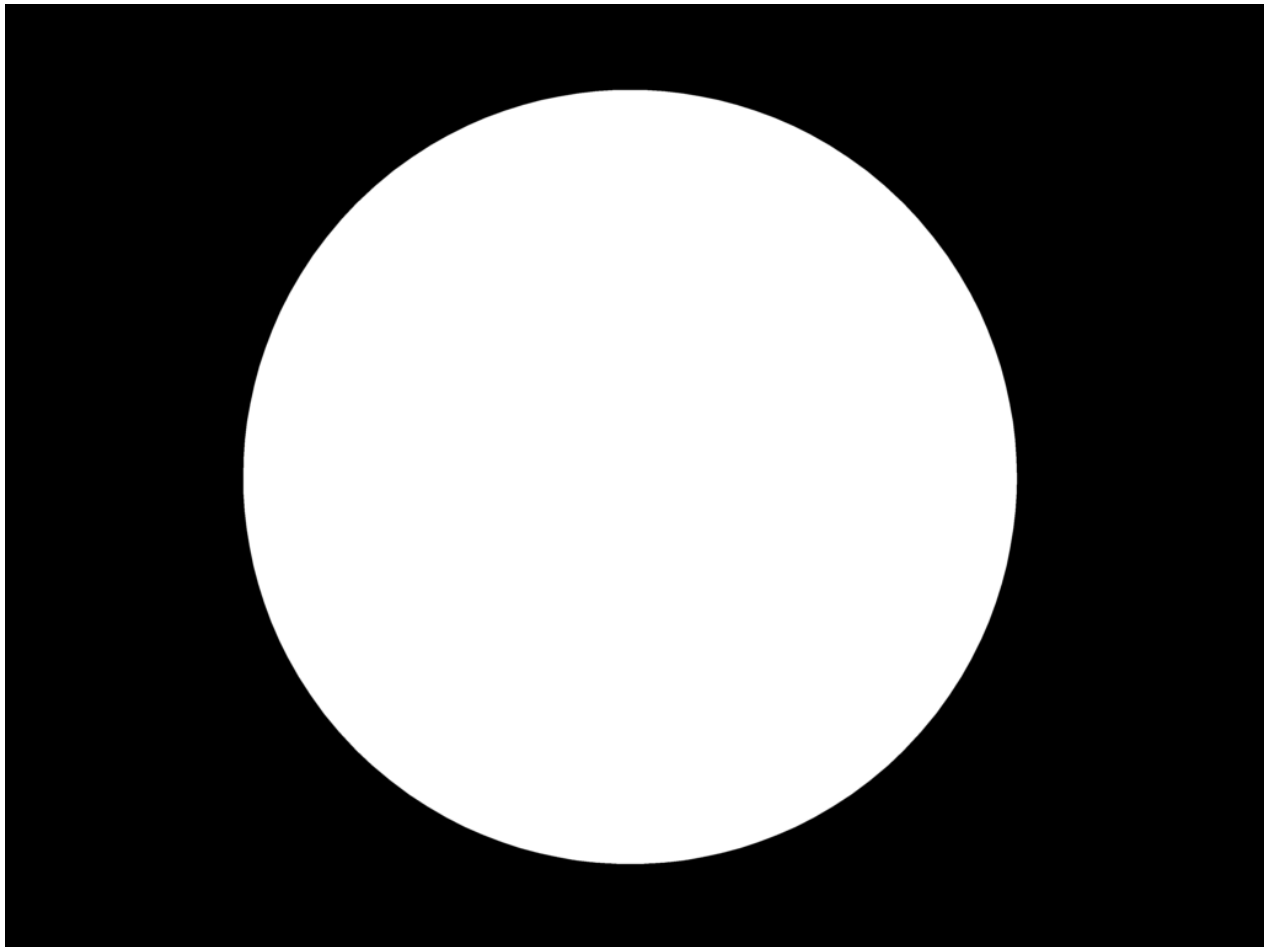


Figure 46. Digital Filter A_s 40% White/60% Black for Luminance L_s Adjustment

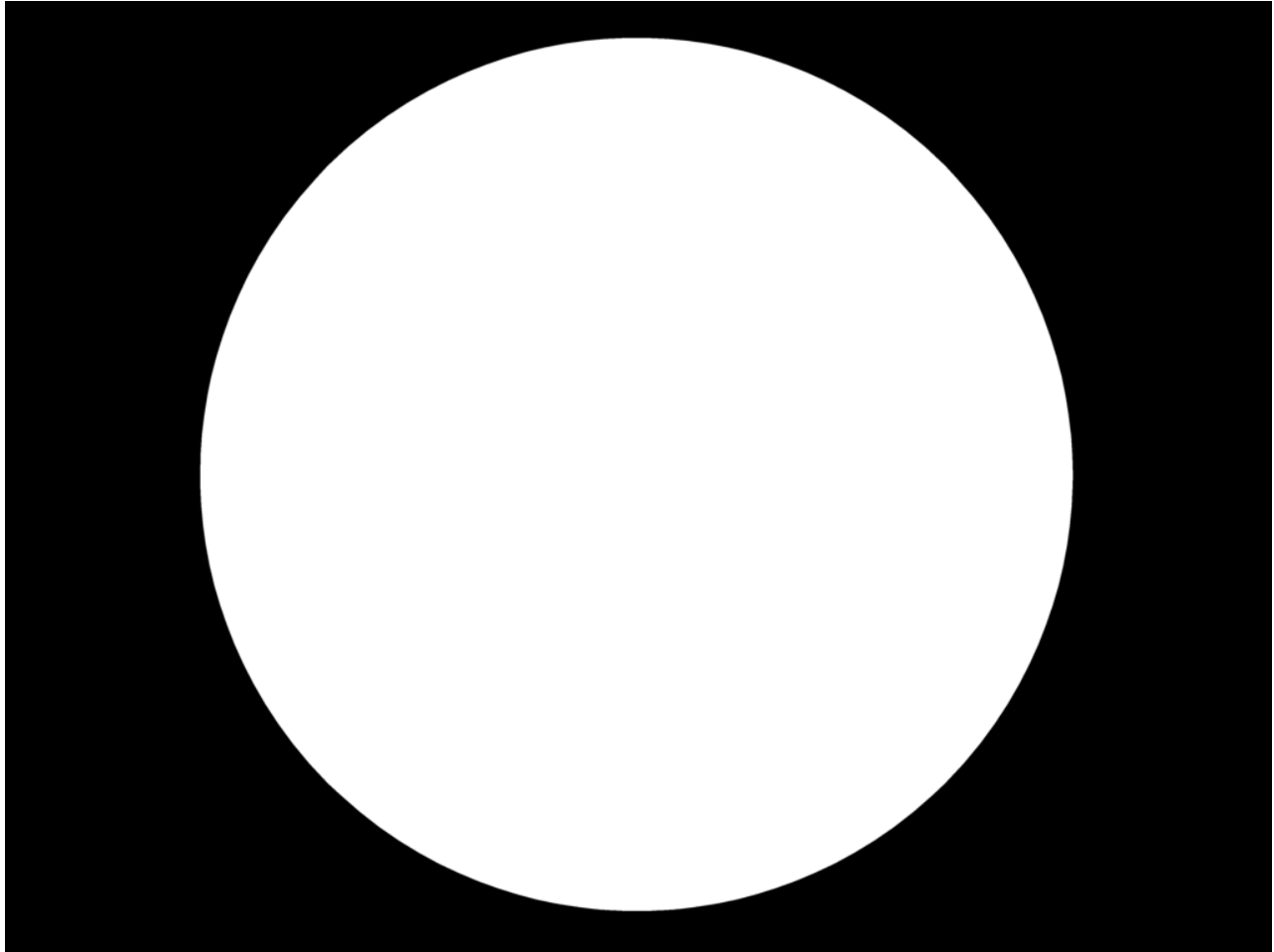


Figure 47. Digital Filter A_s 50% White/50% Black for Luminance L_s Adjustment

The filters shown in Figure 46 and Figure 47 are digital filters that may be designed by using Adobe Photoshop CS or later version and allow to simulate different low light conditions.

For instance, the filter 50% white / 50% black shown in Figure 47 that covers 50% of the radiant surface of the input LCD, will reduce the maximum luminance of the EVIS by 50%.

The maximum luminance for the Dell Latitude D620 is 220 nit (cd/m^2), so when the filter 50% white / 50% black is loaded in the screen, the maximum luminance will be reduced to 110 cd/m^2 .

CHAPTER 3

RESULTS

The Tumbling Es and Tumbling Cs charts were used with grey Es and Cs (contrast 70% or 80%) over black background, instead of black Es over white background, as for instance originally used in the ASTM E2566-08.

Traditional Optotypes vs New Optotypes

The main characteristics considered for the tumbling E optotypes used in traditional video benchmarking methods as the ASTM E2566-08, see Figure 1 are:

- Black Tumbling Es: on White Background
- Different E-Chart for Day & Night: NO
- Contrast Sensitivity: NO
- Color E's: NO
- E-Chart Computer Generated: NO
- Tumbling E's Randomly Generated: NO
- Standard Observer Dynamic Searching: NO – Unlimited Time

In contrast the new testing approach used Tumbling Es and Tumbling Cs as follows:

- Dark Tumbling Es or Cs: on Darker Background
- Different E-Chart / C-Chart for Day & Night: YES
- Contrast Sensitivity: Several levels at night
- Color Es / Cs: YES
- E-Chart / C-Chart computer generated: YES
- Tumbling Es / Cs Randomly Generated: YES
- Standard Observer Dynamic Searching: Limited to 3 sec max.

Grey Es / Cs

At night there are not black targets on white background, but grey targets or color targets (if they are illuminated by artificial lighting) on a dark background.

Day & Night E-Chart / C-Chart

When comparing the performance of video imaging systems, the E-Chart used in ASTM E2566 – 08 for testing the day time Visual Acuity cannot be used to figure out the Visual Acuity in low-light conditions. Thus, when EVIS systems are compared, the new testing approach provides an accurate overall performance of Visual Acuity.

Color Es / Cs

The ASTM E2566 – 08 is used with static E-Charts on the wall. Hence it does not allow benchmarking of different color optotypes (Tumbling Es / Cs) against different backgrounds.

If the objective lens used in a video imaging system has not been properly corrected, chromatic aberration may occur because the focal length in the lens varies according to the wavelength of light, thus the red, green, and blue color form three similar images very close in the display screen that reduces the overall image quality (Ray, 2002). Thus, color benchmarking is also a requirement in EVIS evaluation.

Random Es/Cs

The ASTM E2566 – 08 is intended to be used with static E-Charts, thus the optotypes are in the same position all the time. This test measures only end-to-end capability so the benchmarking evaluation is done by a “standard observer” instead of a machine or optical instrument.

Then the results of the evaluation are dependent on the operator’s subjectivity and sometimes biased judgment. For instance, the operator could memorize the orientation of the tumbling Es on the wall chart and figure out their position without

really seeing the gap in the tumbling Es, which would invalidate the results of the benchmarking.

The new Test Set uses optotypes randomly generated, what prevents a learning curve on the Tumbling Es/Cs and makes impossible for the evaluator to memorize any particular position of the optotypes. Thus, the “standard observer” cannot anticipate whether the gap of the next C or the limbs of the next E will be pointing up, down, left, or right. Figure 48 shows the main new features.



Figure 48. Tumbling Es: Dark Optotypes on Dark Background

Grey Tumbling Es/Cs Main Characteristics

- Grey Tumbling E's: on Darker Background
- Different Es/Cs Chart for Day & Night: YES
- Contrast Sensitivity: Several levels at night
- Color E's: YES
- Es/ Cs Chart Computer Generated: YES
- Tumbling Es/Cs Randomly Generated: YES
- Standard Observer Dynamic Searching: Limited to 3 sec max.

Dynamic Es / Cs

The ASTM E2566 – 08 is intended to be used with static E-Charts, thus the optotypes are in the same position all the time, but in surveillance activities real targets are dynamic and only a limited time for identification and recognition is allowed.

Thus, the time to ascertain the Es/Cs orientation should be limited.

Figure 49 shows three series of Tumbling Cs that will be shown in the output LCD monitor for 3 sec. The “standard observer” will be asked to identify the C-Gap orientation of a Tumbling C located in a different position every single time.

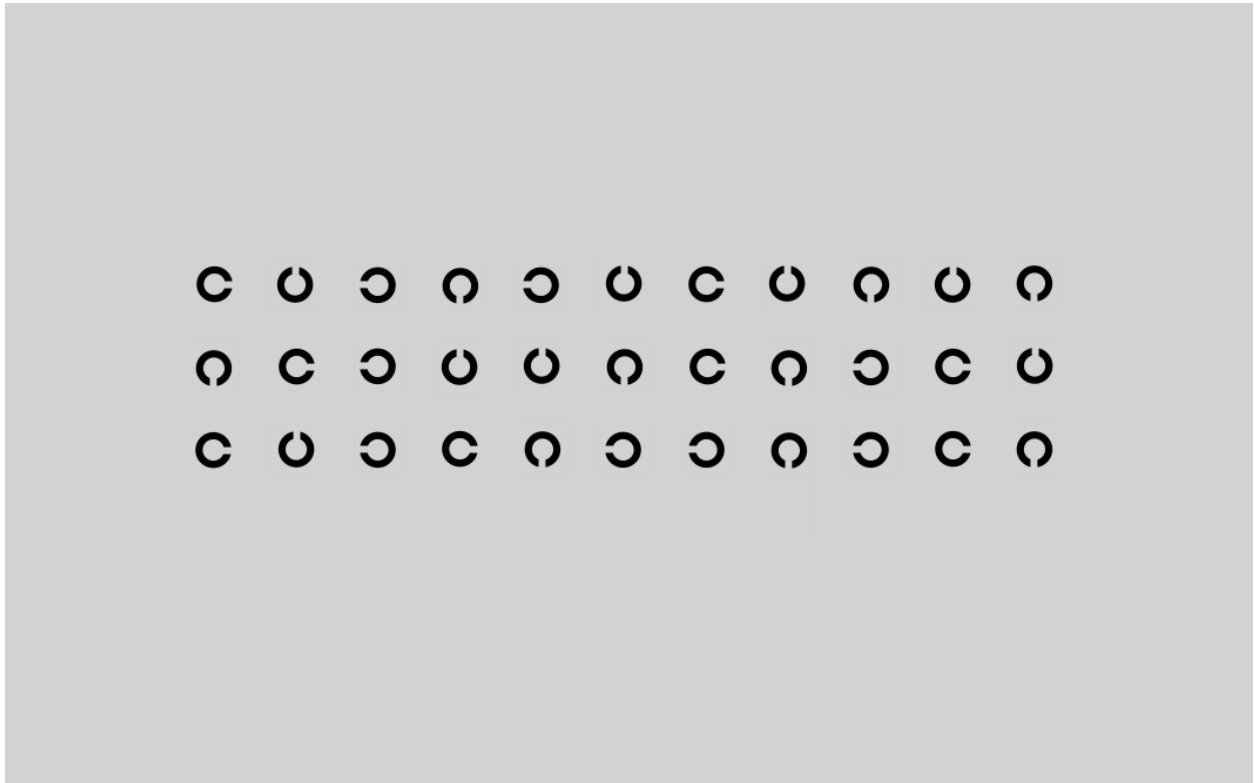


Figure 49. 20/20 Tumbling Cs for C-Gap Identification

LCD Photometric Parameters - Measurements & Estimates

This section illustrates the practical use of the equations and relationships developed in this thesis for the New Test Set and Benchmarking Approach.

It will be demonstrated that when using the lux meter LX1010B at a distance from the LCD monitor $d \geq 2$ m, the key photometric measurements can be obtained.

Screen Display Luminance L_s – Estimate

Let us consider, for instance, the case of a source such as a 14-inch LCD monitor of a laptop Dell Latitude D620 with the following specifications:

Resolution:	1440 x 900 pixels
Display WXGA+ Brightness:	220 nits
Dimensions (W x H):	12 in. x 7.5 in.

The effective screen height is the actual size of Windows 7 desktop screen as the task bar has zero luminance when the screen is the source for testing L_s .

$A_s = 12 \text{ in.} \times 7.25 \text{ in.}$ (effective screen height) = 30.5 cm x 18.4 cm = 561 cm²
 $A_s = 561 \text{ cm}^2 = 0.0561 \text{ m}^2$ is a rectangular area that can be considered equivalent to a circular surface of 0.0561 m² i.e. $A_s = \pi r^2 = 0.0561 \text{ m}^2$ then:

$$r^2 = 0.0561 / \pi = 0.018 \text{ m}^2 \Rightarrow r = 13.4 \text{ cm}$$

Therefore, the formula obtained to calculate the illuminance E_d can be used.

A lux meter model LX1010B can be used to estimate the luminance level L_s of the Dell D620 screen display because, see equation (F03) in Appendix F:

$$E_{LX1010B}(lx) = E_{LX1010B}(lm/m^2) = L_s(lm/m^2 \cdot sr) \frac{A_s}{r^2 + d^2} (sr) \quad (43)$$

The ratio $\frac{A_s}{r^2 + d^2}$ is measured in sr because it is the solid angle ω_s subtended by the source A_s , see for instance ω_s in Figure 50.

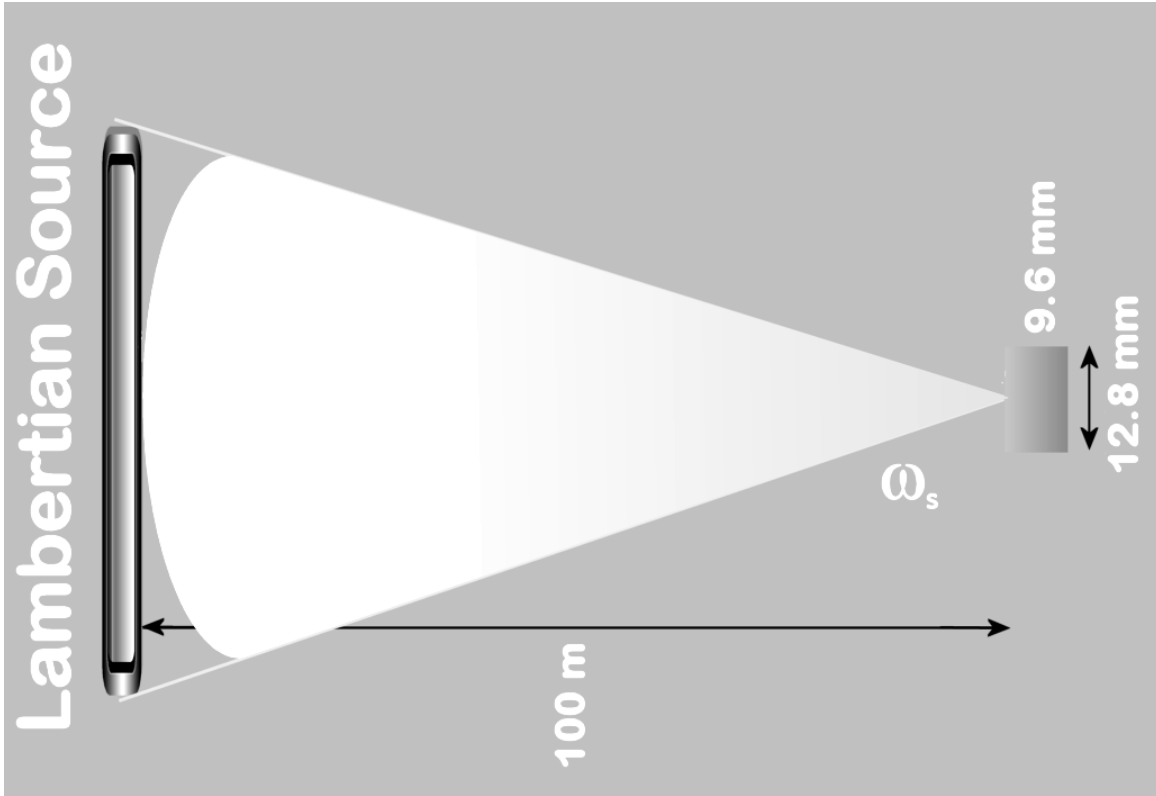


Figure 50. Solid Angle ω_s Subtended by a Lambertian Source

The luminance L_s can be estimated using the approximate equation (43):

$$L_s(\text{cd}/\text{m}^2) = L_s(\text{lm}/\text{m}^2 \cdot \text{sr}) = \frac{E_{LX1010B}(\text{lx})}{\frac{A_s}{r^2+d^2}(\text{sr})} \quad (44)$$

Exact calculations of the irradiance E_d ($E_{LX1010B}$ in this case) and some of the actual readings obtained with the lux meter LX1010B are shown in Table 6.

$$L_s(\text{lm}/\text{m}^2 \cdot \text{sr}) = \frac{E_{LX1010B}(\text{lx})}{\frac{A_s}{r^2+d^2}(\text{sr})} = \frac{3 \text{ lx}}{\frac{.0561 \text{ m}^2}{0.018+2^2 \text{ m}^2}(\text{sr})} = \frac{3 \text{ lm}/\text{m}^2}{.0083 \text{ sr}} = 215 (\text{lm}/\text{m}^2 \cdot \text{sr})$$

$d = 2 \text{ m}$ is the recommended distance to estimate the luminance L_s because the source still provides an illuminance level $E_{LX1010B}(\text{lx}) = 3 \text{ lx}$ that is still within the measuring range limits of the lux meter, see Table 6 for a lux readings list.

The *nit* unit was used long ago but this name is not in general use today (Roberts, 1996), nevertheless the specification of the Latitude Dell D620 indicates the luminance in *nit*.

The *nit* is equivalent to a candle/m² thus the screen display luminance is:

$$L_s = 220 \text{ candle/m}^2 = 220 \text{ lm/m}^2\cdot\text{sr}$$

and the estimated luminance level L_s found using equation (44) was:

$$L_s(\text{cd/m}^2) = 215 \text{ cd/m}^2$$

Thus the error when using the lux meter LB1010B to estimate the luminance level of the Dell Latitude D620 LCD Monitor compared to the nominal figure given by the manufacturer is:

$$\mathcal{E} = 215/220 = 2\%$$

The 2% error could be considered a tolerance from the nominal measurement provided by the manufacturer of the laptop or within the $\pm 5\% + 2d$ accuracy reading of the lux meter manufacturer, see the characteristics of the LB1010B indicated in Table 9.

Consequently, it can be stated that the LCD screen luminance L_s can be measured by using the LX1010B, although it is an illuminance E_d measuring instrument.

The condition is that the measurement is taken at a distance from the LCD monitor:

- a) $d \geq 2$ m to consider valid the LCD approximation to a Lambertian source
- b) $d < 3$ m to get a significant digit reading in the lux meter (see Table 6)

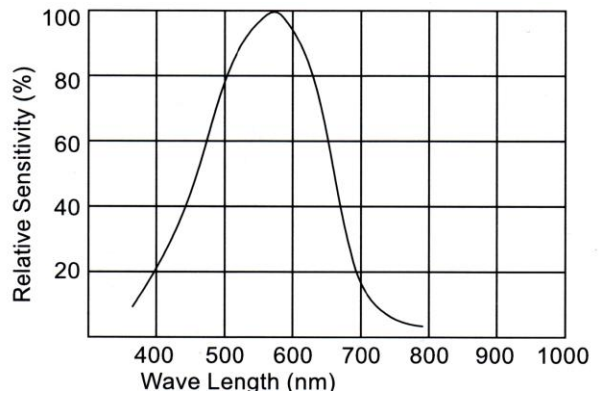
The characteristics of the LX1010B lux meter are indicated in Table 9 and in Figure 51 that shows the Spectral Relative Sensitivity matching the curve in Figure 20.

Table 9

Digital Lux Meter LX1010B Specifications

Display:	18mm (0.7") LCD	
Ranges:	0-50,000 lux; 3 ranges	
0-2,000 lux	Resolution:	1 lux; Accuracy: $\pm 5\% + 2d$
2,000 – 19,900 lux	Resolution:	10 lux; Accuracy: $\pm 5\% + 2d$
19,990-50,000 lux	Resolution:	100 lux; Accuracy: $\pm 5\% + 2d$
Lamp Correction Factor:		
	Mercury	x 1.1
	Fluorescent	x 1.0
	Incandescent	x 1.0
	Daylight:	x 1.0

Figure 51. Spectrum Relative Sensitivity



Sampling Time:	0.4 seconds
Operating Temperature:	0° to 50°C (32° to 122°F)
Operating Humidity:	less than 80% R.H.
Dimensions:	118 x 70 x 29 mm 4.6 x 2.7 x 1.1 in.
Weight (with battery):	200 g
Power Supply:	9 VDC
Current Consumption:	2 mA (approx.)

Screen Display Luminance Control. The luminance level of the Dell Latitude D620 monitor (or any other monitor) can be adjusted by pressing <Fn> and the up-arrow key to increase brightness in the Dell Latitude D620 (other computers may differ) and the irradiance level reduced to $E_d = 0.01$ lx (quarter moon conditions).

It just requires placing a lux meter at a distance $d = 1$ m from the LCD monitor and reducing the screen luminance by using the laptop keyboard and choosing a different option from the default settings in the computer until the lux meter reading is $10 \cdot \frac{1}{10}$ lux = 1 lx, then the irradiance at 20 ft = 6.1 m will be $0.35 \cdot \frac{1}{10} = 0.035$ lx (what approximately simulates quarter moon lighting conditions).

A more accurate method of reducing the luminance is using calibrated digital screen filters:

100 % white / 0% black

85 % white / 15 % black

75 % white / 25 % black

70 % white / 30 % black

65 % white / 35 % black

60 % white / 40 % black

55 % white / 45 % black

50 % white / 50 % black

see Figure 52 and Figure 53.

The size of the white area for each particular filter has been calibrated to amount a specific area of the total surface.

For instance, $A_s = 12$ in. x 7.25 in. (effective screen height) = 30.5 cm x 18.4 cm = 561 cm² thus the white area for filter 75 % white / 25 % black is 22.9 cm x 13.8 cm

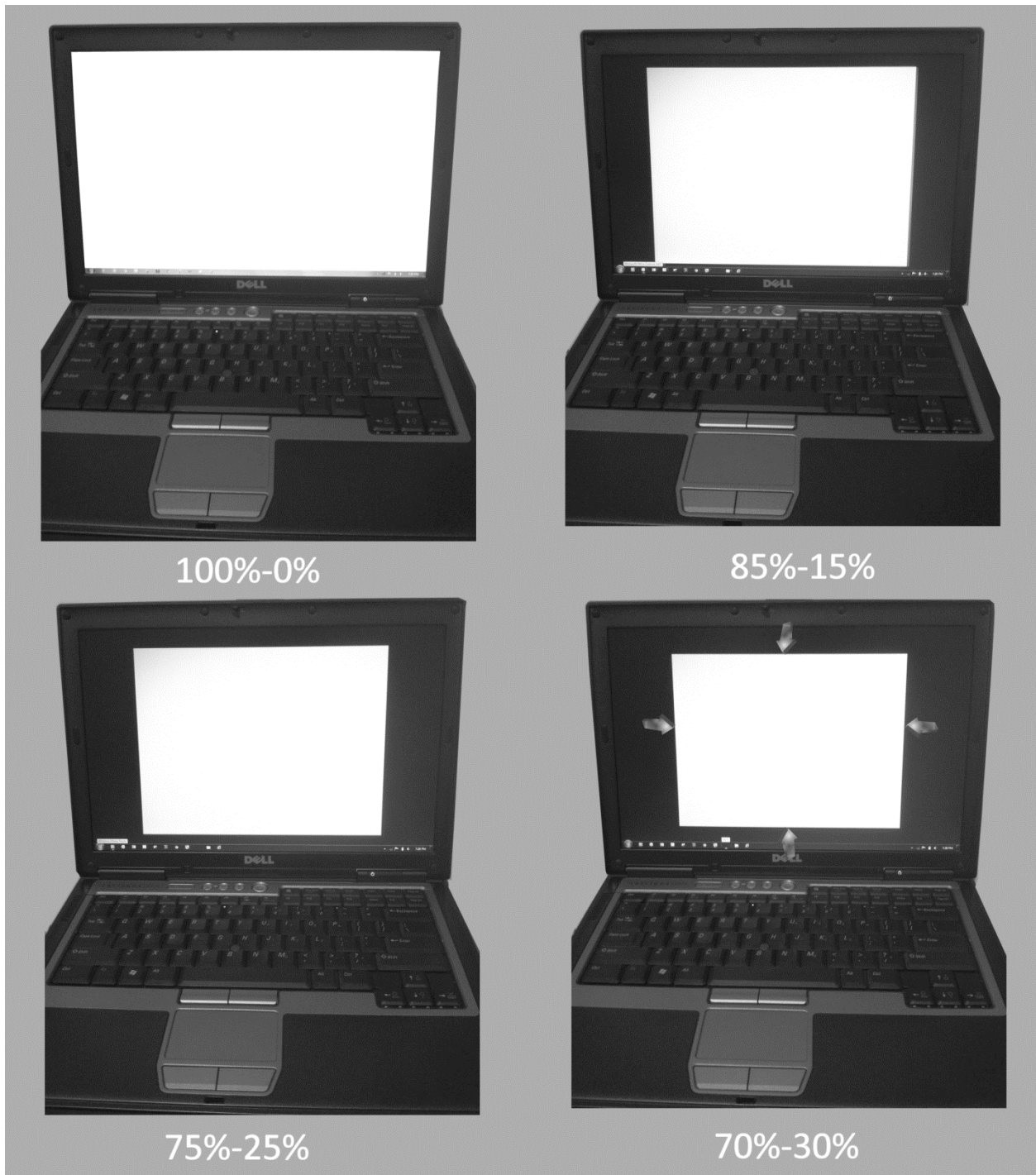


Figure 52. Digital Filters 100% to 70% for a Lambertian Source A_s

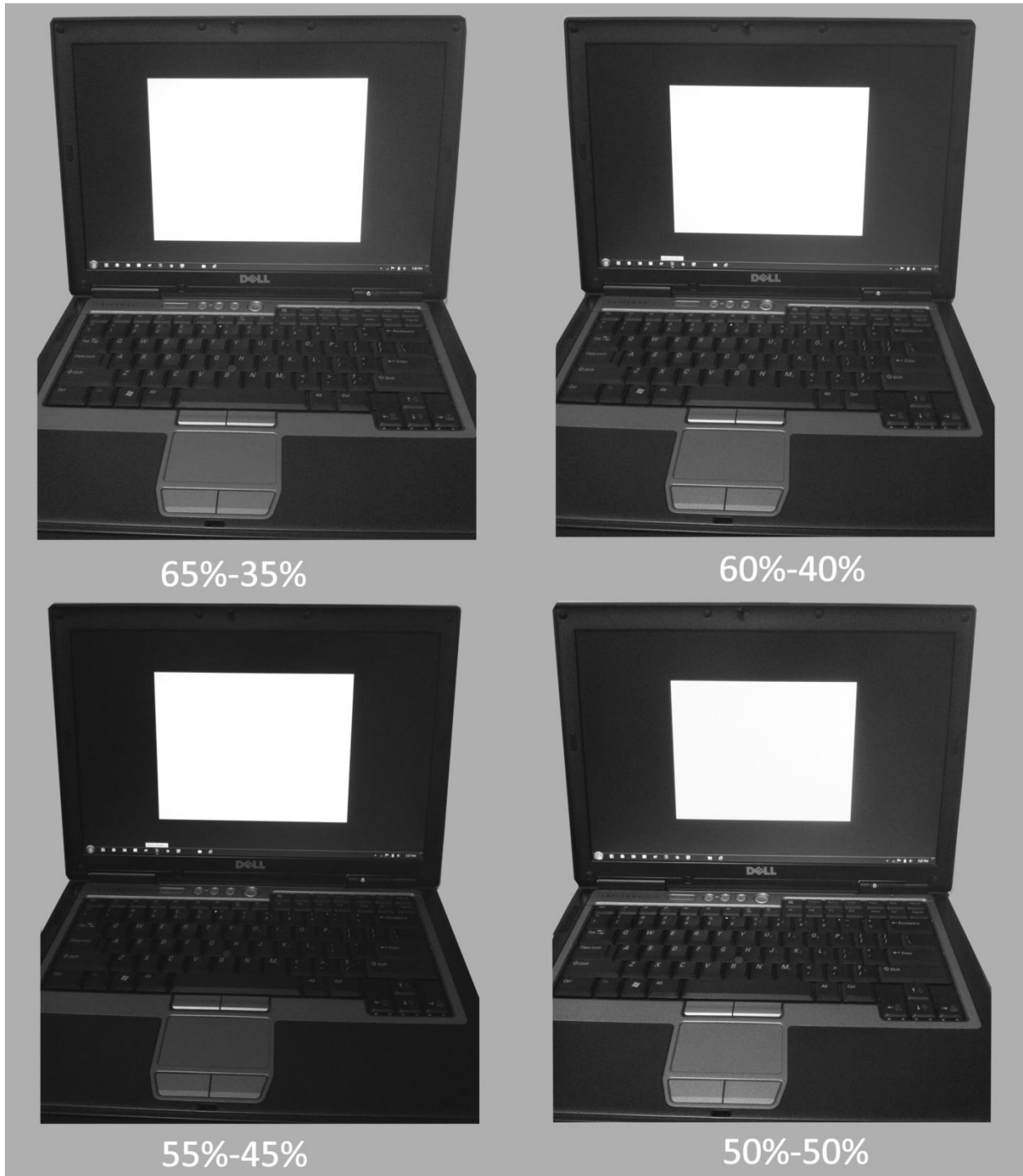


Figure 53. Digital Filters 65 % to 50% for a Lambertian Source A_s

Screen Display Illuminance E_d – Estimate

The equation (F03) in Appendix F and Figure 40 show that the illuminance E_{lens} at the lens for θ small ($2\theta \leq 94^\circ \Rightarrow \theta \leq 47^\circ$) see equation (D14) in Appendix D can be approximated by:

$$E_{lens} \approx L_s \frac{A_s}{d^2 + r^2} \quad (45)$$

The equation (F03) also gives the illuminance E_d at the detector, shown in Figure 50:

$$E_d = E_{lens} \approx L_s \frac{A_s}{d^2 + r^2} \quad (46)$$

The illuminance $E_{LX1010B}$ measured at distance d_1 and d_2 when setting the LCD display luminance control at maximum intensity by acting on the keyboard and on the video card control panel, see Figure 42, will be compared with the theoretical values obtained using the approximate formula for E_d :

$$E_{LX1010B_{d1}} = 220(lm/m^2 \cdot sr) \frac{.0561 m^2}{0.018 + 1.0^2 m^2} (sr) \approx 220 * 0.0551 = 12.1 \text{ lx} ; \quad d_1 = 1.0 \text{ m (40 in.)}$$

$$E_{LX1010B_{d2}} = 220(lm/m^2 \cdot sr) \frac{.0561 m^2}{0.018 + 2.6^2 m^2} (sr) \approx 220 * 0.0083 = 1.8 \text{ lx} ; \quad d_2 = 2.6 \text{ m (102 in.)}$$

$$E_{LX1010B_{(1.0 \text{ m})}} \text{ (calculated)} = 12.1 \text{ lx}; \quad d_1 = 1.0 \text{ m}; \quad E_{LX1010B_{(1.0 \text{ m})}} \text{ (reading)} = 10 \text{ lx}$$

$$E_{LX1010B_{(2.6 \text{ m})}} \text{ (calculated)} = 1.8 \text{ lx}; \quad d_2 = 2.6 \text{ m}; \quad E_{LX1010B_{(2.6 \text{ m})}} \text{ (reading)} = 2 \text{ lx}$$

Thus the measurements obtained with the lux meter LX1010B are quite approximate to the nominal values given by the formula used to calculate E_d .

In Table 6 it is shown that for $d \geq 1 \text{ m}$, the LX1010B is a valid instrument for measuring E_d .

If the display screen is located at $20 \text{ ft} = 6.1 \text{ m}$ ($d^2 = 37.2 \text{ m}^2$) the illuminance is:

$$E_{LX1010B}(\text{lx}) = 220(lm/m^2 \cdot sr) \frac{0.0561 (m^2)}{0.018 (m^2) + 6.1^2 (m^2)} (sr) \approx 220(lm/m^2 \cdot sr) \frac{0.0561 (m^2)}{37.2 (m^2)} = 0.35 \text{ lx}$$

The E reading of 0.35 lx is close to the illuminance level of 0.1 lx that defines full moon conditions, so when the screen display of the laptop Dell Latitude D620 is located at 20 ft (6.1 m) it is equivalent to measure the quality of the video imaging system in low light conditions:

$$\text{Dell Latitude D620: } E_{LX1010B_{(20\text{ ft})}} = 0.35 \text{ lx (full moon conditions)}$$

Another example:

Dell UltraSharp LCD Monitor 1708FP-BLK 17-inch shown in Figure 54:



Figure 54. Dell UltraSharp 1708-BLK/1908-BLK Monitor

has the following specifications:

$$\text{Luminance } L_s = 300 \text{ cd/m}^2$$

$$\text{Radiant Surface } A_s = 0.091 \text{ m}^2 \text{ (0.337 m x 0.270 m)}$$

Dell UltraSharp 1708-BLK can also be approximated to a Lambertian source having constant luminance across the area and used to test the image quality in low

light conditions at 20 ft distance as: $E_{LX1010B_{(20\text{ ft})}} \approx 300 \text{ (lm/m}^2 \cdot \text{sr)} \frac{0.091 \text{ (m}^2\text{)}}{37.2 \text{ (m}^2\text{)}} = 0.74 \text{ lx}$

$$\text{Dell UltraSharp 1708FP-BLK: } E_{LX1010B_{(20\text{ ft})}} \approx 0.74 \text{ lx (full moon conditions)}$$

A Flat Panel Monitor Dell UltraSharp 1708-BLK 17-inch or UltraSharp 1908-BLK 19-inch has a typical brightness (luminance) L_s of 300 cd/m².

Both 17" and 19" has the same luminance L_s and it is constant across the area.

The main characteristics of the LCD Dell UltraSharp monitor are:

Preset Display Area (W x H) 1708-BLK:	337 mm (13.3") x 270 mm (10.6")
	1908-BLK: 380 mm (14.96") x 300 mm (11.81")
Maximum Resolution:	1280 x 1024 pixels
Pixel Pitch 1708-BLK:	0.264 mm
1908-BLK:	0.294 mm
Brightness (Typical):	300 cd/m ²
Color Gamut (Typical):	82% based on CIE1976 (82%) and CIE1931 (72%) test standard
Contrast Ratio (Typical):	800:1
Viewing Angle (Typical):	160° (horizontal) / 160° (vertical)
Response Time (Typical):	5 ms black-to-white
Panel Type & Surface:	TN (twisted nematic) Anti-glare with hard-coat 3H

Illuminance E_d – Estimate for $d \geq 2m$. According to equation (E12) in

Appendix E the estimated E_d value is: $E_d \approx \frac{L_s A_s}{d^2}$ and according to Figure 55 the fraction $\frac{A_s}{d^2}$ is an approximation for the solid angle ω_s see also (D14) in Appendix D.

Thus for $d \geq 2$ m:

$$E_d (\text{lux}) \approx L_s (\text{cd/m}^2) \cdot \omega_s (\text{sr})$$

Example Dell Latitude D620 has: $L_s = 220 \text{ cd/m}^2$; $A_s = 0.057 \text{ m}^2$

$E_d (@ 2 \text{ m}) \approx 220 * 0.057 = 3.1 \text{ lux}$ (as the exact value shown in Table 6 for $d = 2 \text{ m}$).

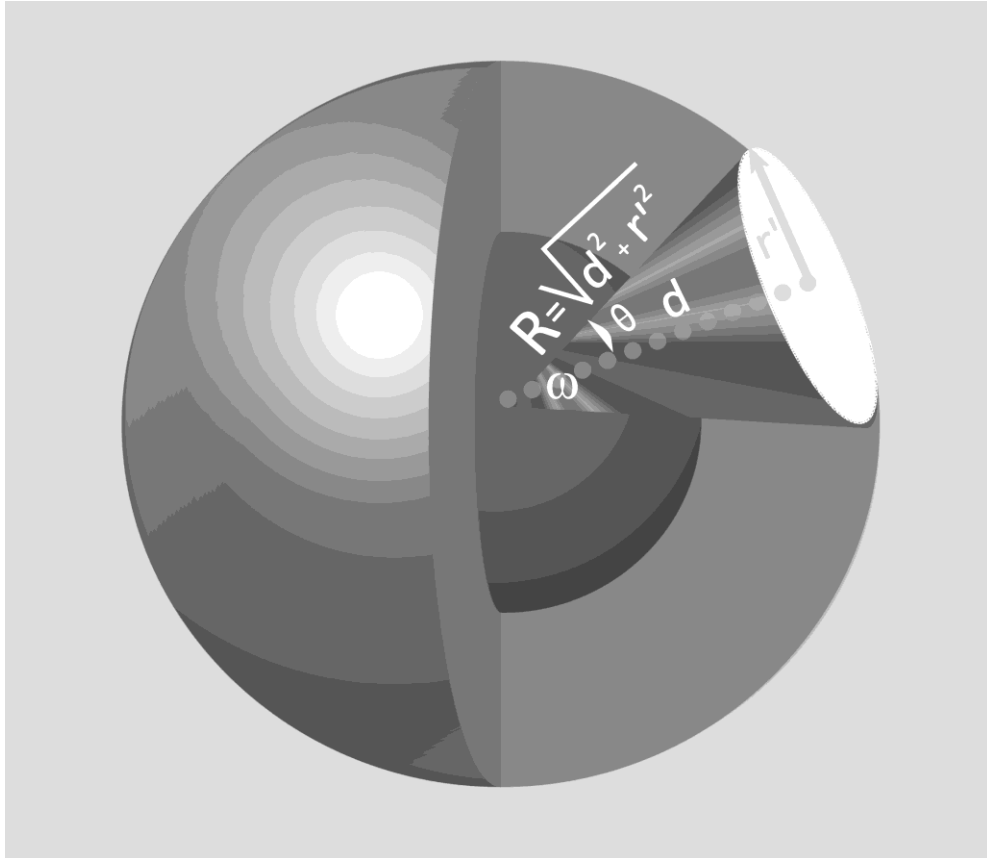


Figure 55. Approximation of a Sphere Cap by a Flat Surface for 2θ Small $\leq 94^\circ$

ω_s Estimate Validation for $d \geq 2\text{m}$. The approximation $\frac{A_s}{d^2} \approx \omega_s$ is based on the following derivation: By definition apex angle = 2θ , see α in Figure 18, thus:

$$2\theta = \frac{2r'}{\sqrt{d^2 + r'^2}} \implies \theta = \frac{r'}{\sqrt{d^2 + r'^2}}$$

Replacing θ in the approximation $\omega \approx \pi\theta^2$ gives (see also (D14) in Appendix D):

$$\omega_s \approx \frac{\pi r'^2}{d^2 + r'^2} = \frac{A_s}{R^2}$$

where A_s is the flat area of the cone's base shown in Figure 55.

A_s is the area of a three dimensional cone cap but it can be approximated to a flat area (two dimensional) when θ is small, see also Appendix D.

In addition $d \gg r$ is a valid approximation as the solid angle subtended by the source: $\omega_s = 0.0083$ is very small, see Figure 17.

When $d^2 \gg r^2$ then $\omega \approx \frac{\pi r^2}{d^2}$ (Greivenkamp, 2004) although this approximation is not always applicable. In the design of the new video imaging test set, the most accurate approximation $\omega \approx \frac{\pi r^2}{d^2 + r^2} = \frac{A_s}{R^2}$ has been used, see Appendix F.

Luminous Intensity I_s - Estimate for $d \geq 2$ m

The Dell Latitude D620 Monitor can be approximated to a Lambertian source, at a distance $d \geq 2$ m see Figure 56 and has $L_s = 220$ cd/m² ; $A_s = 0.057$ m²

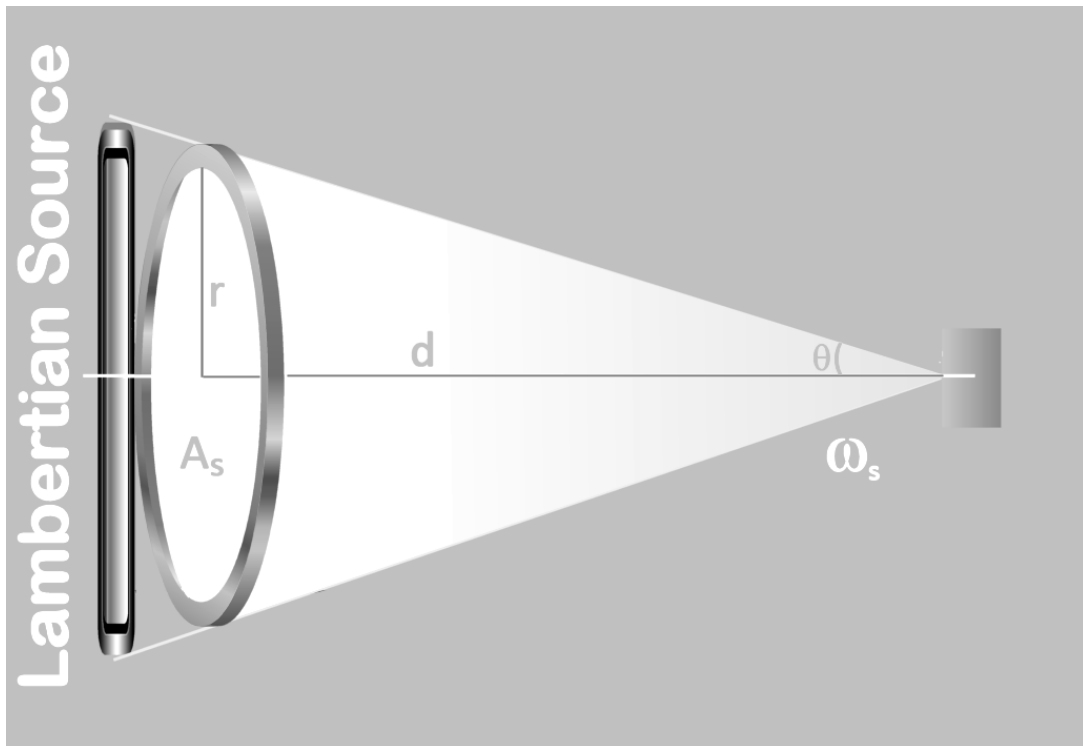


Figure 56. Estimated E_d , I_s and Φ_s at $d \geq 2$ m for the Test Set

A Lambertian source emits radiation with an intensity pattern following only the cosine law:

$$I_s = I_0 \cos \theta; \text{ where } I_0 = L_s A_s \xrightarrow{\theta \text{ small}} I_s \approx L_s A_s$$

$$\theta \text{ small means } \theta \leq 8.5^\circ = 8.5^\circ \cdot \frac{1 \text{ rad}}{57^\circ} = 0.15 \text{ rad}$$

$$\sin \theta = \frac{r}{\sqrt{r^2 + d^2}} \text{ and } \theta \leq 0.15 \implies \sin \theta \approx \theta \implies \theta \approx \frac{r}{\sqrt{r^2 + d^2}} \leq 0.15$$

In the previous section it was shown that the rectangular LCD screen of a Dell D620 is equivalent to a circular area of radius $r = 0.134 \text{ m} \implies r^2 = 0.018 \text{ m}^2$

Therefore:

$$\frac{0.134}{\sqrt{0.018 + d^2}} \leq 0.15 \xrightarrow{\theta \text{ small}} d \geq 0.9 \text{ m}$$

Thus for $d \geq 2 \text{ m}$ the estimated I_s for a Dell Latitude D620 screen display can be estimated using the approximated equation:

$$I_s \approx L_s A_s = 220 \text{ (Lumens/sr} \cdot \text{m}^2) \times 0.057 \text{ m}^2 = 12.54 \text{ (Lumens/sr)}$$

Luminous Power Φ_s - Estimate for $d \geq 2 \text{ m}$

The total luminous power over the radiant hemisphere (solid angle $\pi \text{ sr}$) is:

$$\Phi_s \text{ (Lumens)} = I_s \text{ (Lumens/sr)} \cdot \pi \text{ (sr)} = 12.54 \times 3.1416 = 39.4 \text{ Lumens.}$$

Luminous Emittance M - Estimate

A Lambertian source complies with the following equation at the surface ($d = 0$):

$$M = \pi(\text{sr}) \cdot L(\text{Lumens/sr} \cdot \text{m}^2)$$

hence:

$$M \text{ (Lumens/m}^2) = \pi(\text{sr}) \cdot L(\text{Lumens/sr} \cdot \text{m}^2) = 3.1416 \times 220 = 691.2 \text{ Lumens/m}^2$$

The value found for M provides an alternative method for calculating Φ_s :

$$\Phi_s \text{ (Lumens)} = M \text{ (Lumens/m}^2) \cdot A_s \text{ (m}^2) = 691.2 \times 0.057 \text{ m}^2 = 39.4 \text{ Lumens}$$

A summary of key photometric features measured with the lux meter LB1010B or estimated using the equations developed for the New Test Set follows:

$$L_d = 215 \text{ lm/m}^2\cdot\text{sr} \text{ (estimated)} \qquad L_d = 220 \text{ lm/m}^2\cdot\text{sr} \text{ (nominal value)}$$

$$E_d = 3.1 \text{ lux @ } d = 2 \text{ m (estimated)} \qquad E_d = 3 \text{ lux @ } d = 2 \text{ m (measured)}$$

$$I_s = 12.54 \text{ lm/sr (estimated)}$$

$$\Phi_s = 39.4 \text{ lm (estimated)}$$

$$M = 691.2 \text{ lm/m}^2 \text{ @ } d = 0 \text{ m (LCD surface) (estimated)}$$

The accuracy of the equations used to estimate the values of L_d and E_d is manifest after comparing them to the nominal and measured values respectively.

Illuminance E_d in Terms of the Objective Lens F-Stop

In Appendix F, equation (F11) there was shown the following approximation for E_d the irradiance at the detector:

$$E_d = \frac{\Phi_d}{A_d} \approx \frac{\pi L_s}{4F_{stop}^2 + \left(\frac{2r'}{D}\right)^2} \quad (47)$$

where $2r'$ is the sensor array format and D is the lens entrance pupil.

If the format of the sensor array equals the lens entrance pupil, as it is typically the case in surveillance video systems that include a 1/2-format fixed objective lens with 1X magnification and 1/2-inch format CCD, then $2r' = D$ and according to equation (F12) in Appendix F:

$$E_d = \frac{\Phi_d}{A_d} \approx \frac{\pi L_s}{4F_{stop}^2 + 1} \quad (48)$$

Thus using equation (F12):

$$E_d \text{ (lx)} = E_d \text{ (lm/m}^2\text{)} = \frac{\Phi_d}{A_d} \approx \frac{\pi(sr)L_s\left(\frac{\text{lm}}{\text{m}^2}\cdot\text{sr}\right)}{4F_{stop}^2 + 1} \quad (49)$$

$$E_d = \frac{\Phi_d}{A_d} \approx \frac{\pi 220}{4(1.4)^2 + 1} = \frac{691}{8.84} = 78 \text{ lx}$$

that is the illuminance at 0.38 m approximately because using equation (46) to calculate $E_d @ 0.378 \text{ m}$ gives:

$$E_d(\text{lx}) = 220(\text{lm}/\text{m}^2 \cdot \text{sr}) \frac{0.0561 (\text{m}^2)}{0.018 (\text{m}^2) + 0.378^2 (\text{m}^2)} (\text{sr}) \approx 77 \text{ lx @ } 0.378 \text{ m}$$

The lens used in the prototype of the video imaging system discussed in this document has the following characteristics:

Objective Lens \varnothing 25 mm

$F/1.4$

Magnification: 1X

FOV: 40°

The Lambertian source has a radiant surface:

$$A_s = 30.5 \text{ cm} \times 18.4 \text{ cm (effective height)}$$

equivalent to a circular surface of $.0561 \text{ m}^2$ so:

$$r^2 = 0.018 \text{ m}^2 \Rightarrow r = 13.4 \text{ cm}$$

According to Figure 7:

$$\text{FOV: } 40^\circ \Rightarrow \theta/2 = 20^\circ = 20^\circ \cdot \frac{1 \text{ radian}}{57^\circ} = 0.35 \text{ radian}$$

$$\tan 20^\circ = \tan 0.35 \text{ rad} = \frac{13.4 \text{ cm}}{37.8 \text{ cm}} = 0.35 \text{ rad}$$

The FOV of the objective lens covers the whole Lambertian surface A_s , so the equation (48) provides the same result that the equation (46) used to calculate more accurate figures for E_d :

$$E_d = 78 \text{ lx @ } 0.378 \text{ m}$$

Illuminance E_d in Terms of E_{lens} and Lens FOV

In Appendix F it is shown the derivation of equation (F18), another useful equation to calculate the illuminance E_d at the detector as a function of FOV and F - $Stop$ that are typically known parameters of any lens:

$$E_d = E_{lens} \frac{A_{lens}}{A_d} \approx \frac{E_{lens}}{(FOV * F_{stop})^2} \quad (50)$$

The lens used in the prototype of the video imaging system discussed in this document has the following characteristics:

Magnification: 1X ; FOV : 40° ; Objective Lens \varnothing 25 mm ; $F/1.4$

$$FOV: 40^\circ \implies FOV = 40^\circ * \frac{1 \text{ radian}}{57^\circ} = 0.7 \text{ rad}$$

$$FOV * F\text{-}Stop = 0.7 * 1.4 \approx 1$$

Thus for the prototype video imaging system: $E_d \approx E_{lens}$

The illuminance measured at distances d_1 and d_2 with a lux meter LX1010B, see Table 9, and setting the LCD display luminance control at maximum is:

$$E_{LX1010B_{(1.0 \text{ m})}} = 10 \text{ lx} ; d_1 = 1.0 \text{ m} \implies E_d \approx E_{LX1010B_{(1.0 \text{ m})}} = 10 \text{ lx} ; d_1 = 1.0 \text{ m}$$

$$E_{LX1010B_{(2.6 \text{ m})}} = 2 \text{ lx} ; d_2 = 2.6 \text{ m} \implies E_d \approx E_{LX1010B_{(2.6 \text{ m})}} = 2 \text{ lx} ; d_2 = 2.6 \text{ m}$$

Lux Meter LX1010B Linearity

The lux meter has been tested at a close distance to figure out its relative linearity response.

Table 10 shows that linearity starts at distance $d \geq 11.4 \text{ cm}$ (4.50 in.) for $A_s = 75\%$ although according to the data in Table 6 to obtain correct E_d readings the minimum distance starts at $d \geq 1 \text{ m} \approx 40 \text{ in.}$

Table 10

LX1010B Lux Meter - E_d (lx) Measurements Linearity Test.

E_d has been measured for different percentages of white surface A_s on the LCD monitor

The readings show that linearity starts at $d \geq 11.4$ cm (4.50 in.) for $A_s = 75\%$

inch	meter	cm	100%	85%	75%	65%	60%	55%	50%
0.00	0.000	0.0	165	163	163	163	163	163	163
1.00	0.025	2.5	159	158	158	158	158	155	155
2.00	0.051	5.1	153	152	148	146	146	135	127
4.50	0.114	11.4	127	118	111				
			<i>E_d as function of A_s</i>	118/127 = 93%	111/127 = 85%				
5.80	0.147	14.7	107	98	89				
			<i>E_d as function of A_s</i>	98/107 = 92%	89/107 = 84%				
11.80	0.300	30.0	60	52	45				
			<i>E_d as function of A_s</i>	52/60 = 87%	45/60 = 75%				
39.37	1.000	100.0	10	8	6				
			<i>E_d as function of A_s</i>	8/10 = 80%	6/10 = 60%				

d: distance to the LCD screen

LCD Viewing Angle

In Table 6 it is shown that E_d (measured) equals to E_d (exact calculation) at a distance $d \geq 2$ m for a screen size with dimensions $W \times H = 30$ cm \times 19 cm such as the LCD monitor of the Dell Latitude D620.

The solid angle ω subtended by the radiant surface A_s (dimensions in cm) at a distance of 300 cm (3 m) is:

$$\omega_s = A_s / d^2 = (30 \times 19) / 300^2 = 0.0067$$

That means that the reading of the lux meter LX1010B is accurate provided the solid angle subtended by a radiant source is equal or lesser than 0.0067.

The equivalence between surface and distance for a constant solid angle figure could be used as follows:

$$\omega_s = A_s / d^2 = (30 \times 19) / 300^2 = (3 \times 1.9) / 30^2 = 0.0067$$

Thus, the readings of the LX1010B obtained for the whole surface of the Dell Latitude D620, $A_s = 30$ cm \times 19 cm at a distance of 300 cm should be the same as for a radiant cell $C_s = 3$ cm \times 1.9 cm at a distance of 30 cm.

The dimensions $C_s = 3$ cm \times 1.9 cm can be approximated to 3 cm \times 2 cm what allows the whole screen to be divided into 90 cells C_s of dimensions 3 cm \times 2 cm.

It also has been demonstrated that the illuminance E_d on the light sensor can be estimated, see equation (46), at a distance $d \gg r$ by $E_d \approx L_s \frac{A_s}{d^2 + r^2}$

Thus the E_d reading obtained at 300 cm for the whole screen A_s should be also applicable to one cell C_i at 30 cm in the optical axis, see Figure 57.

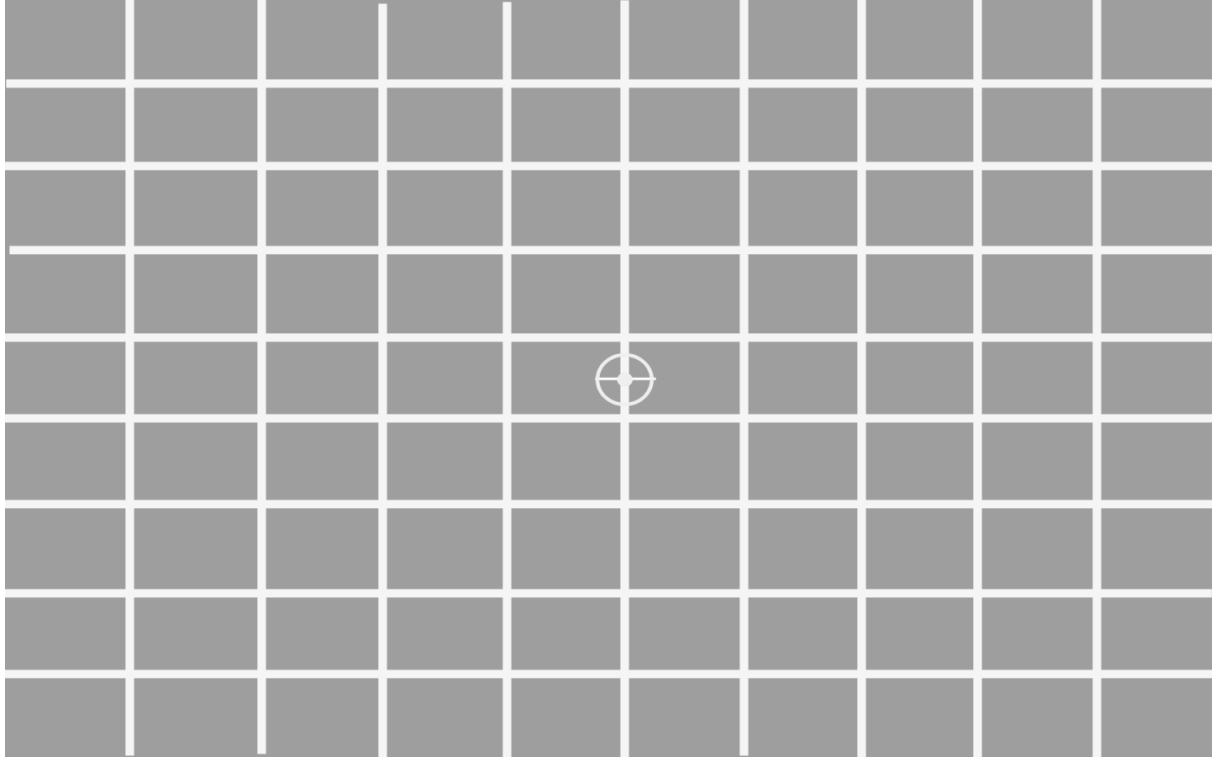


Figure 57. The Geometrical Center in the Dell Latitude D620 Monitor

It can be considered that any elemental cell in the screen shown in Figure 57 could be measured with the LX1010B by only taking into account the cosine-to-the-fourth law for the angle θ_x between the optical axis and the geometric center of the particular cell.

Hence, according to equation (E18) the reading E_{di} of any cell will be:

$$E_{di} \approx L_s \omega_s \cos^4 \theta_x \quad (51)$$

and the total illuminance:

$$E_d \approx L_s \omega_s \cos^4 \theta_1 + \dots + L_s \omega_s \cos^4 \theta_{90} = L_s \omega_s \sum_{i=1}^{90} \cos^4 \theta_i \quad (52)$$

In Figure 58 it is shown that the radii r_1 , r_{21} , r_{56} , and r_{61} from the center have the same length, thus the cells #1, 21, 56, and 61 generate the same illuminance:

$$E_{d1} = E_{d21} = E_{d56} = E_{d61} \text{ on the light sensor} \quad (53)$$

45				41	16	17	18	19	20
					11	12	13	14	15
					6	7	8	9	10
60				56	1	2	3	4	5
j	i	h	g	f	a	b	c	d	e
65				61	21				25
80				76	36				40

Figure 58. Same Illuminance E_{di} for Symmetric Cells Around the Geometric Center

Similar case occurs for cells #20, 40, 45 and 80: $E_{d20} = E_{d40} = E_{d45} = E_{d80}$.

Analog criteria applies to cells #a, f and cells #b, g. Thus:

$$E_d \approx L_s \omega_s \sum_{i=1}^{90} \cos^4 \theta_i = 4 L_s \omega_s \sum_{i=1}^{20} \cos^4 \theta_i + 2 L_s \omega_s \sum_{i=a}^e \cos^4 \theta_i \quad (54)$$

In Table 11 it is shown the value of $\cos^4 \theta_i$ for each radius r_i where the length has been measured directly, Figure 59, on the screen of the Dell Latitude D620 and calculated using the following equation:

$$\cos^4 \theta_i = \left(\frac{d}{\sqrt{d^2 + r_i^2}} \right)^4 = \frac{d^4}{(d^2 + r_i^2)^2} \quad (55)$$

where d is the distance from the light sensor to the center of the screen and r_i is the distance to the geometric center.

Table 11

Cosine-To-The-Fourth Power - E_d Estimate at Short Distance

d (cm)		cm r_i	cm^2 $(d^2+r_i^2)$	cm^4 $(d^2+r_i^2)^2$	FOV	$d^4 / (d^2+r_i^2)^2$
30	1	2.5	906.25	821289.06	1	0.986254459
	2	5.0	925.00	855625.00	1	0.946676406
	3	7.5	956.25	914414.06	1	0.885813149
ω_s (sr) 0.0067	4	10.5	1010.25	1020605.06	1	0.793646857
	5	13.5	1082.25	1171265.06	1	0.691559943
L_s (cd/m ²) 220	6	4.5	920.25	846860.06	1	0.956474435
	7	6.0	936.00	876096.00	1	0.924556213
	8	8.5	972.25	945270.06	1	0.856897972
	9	11.0	1021.00	1042441.00	1	0.777022393
	10	14.0	1096.00	1201216.00	1	0.674316692
	11	6.5	942.25	887835.06	1	0.912331619
	12	7.6	957.76	917304.22	1	0.883022213
	13	9.6	992.16	984381.47	1	0.822851738
	14	12.0	1044.00	1089936.00	1	0.743162901
	15	14.8	1119.04	1252250.52	1	0.646835426
	16	8.7	975.69	951970.98	1	0.850866277
	17	9.5	990.25	980595.06	1	0.826029042
	18	11.2	1025.44	1051527.19	1	0.770308181
	19	13.3	1076.89	1159692.07	1	0.698461272
	20	15.8	1149.64	1321672.13	1	0.612860014
					Σ	16.2599472
					$E_{d_a} =$	95.86864871
a		1.5	902.25	814055.06	1	0.995018688
b		4.5	920.25	846860.06	1	0.956474435
c		7.5	956.25	914414.06	1	0.885813149
d		10.5	1010.25	1020605.06	1	0.793646857
e		13.5	1082.25	1171265.06	1	0.691559943
					Σ	4.322513072
					$E_{d_b} =$	12.74276854
TOTAL					$E_d =$	109



Figure 59. The Radii r_1 to r_{20} and r_a to r_b Directly Measured on the Dell D620 Screen

The method indicated in Table 11 gives a value for $E_d = 109$ lx that is very similar to the value $E_d = 115$ lx obtained using the exact formula as shown in Table 6 but the actual reading with the LX1010B was $E_d = 60$ lx.

Table 12 explains the reason for a lower E_d : the values calculated using equation (55) consider that their impact on the E_d value indicated in equation (54) from cells with $r_i \geq 8.5$ cm has been cancelled, namely $r_i \geq 8.5$ cm \implies FOV = 0

Table 12

Cosine-To-The-Fourth Power - E_d Correct Readings at Short Distance

d (cm)		cm r_i	cm^2 $(d^2+r_i^2)$	cm^4 $(d^2+r_i^2)^2$	FOV	$d^4 / (d^2+r_i^2)^2$
30	1	2.5	906.25	821289.06	1	0.986254459
	2	5.0	925.00	855625.00	1	0.946676406
	3	7.5	956.25	914414.06	1	0.885813149
ω_s (sr) 0.0067	4	10.5	1010.25	1020605.06	0	0
	5	13.5	1082.25	1171265.06	0	0
L_s (cd/m ²) 220	6	4.5	920.25	846860.06	1	0.956474435
	7	6.0	936.00	876096.00	1	0.924556213
	8	8.5	972.25	945270.06	1	0.856897972
	9	11.0	1021.00	1042441.00	0	0
	10	14.0	1096.00	1201216.00	0	0
	11	6.5	942.25	887835.06	1	0.912331619
	12	7.6	957.76	917304.22	1	0.883022213
	13	9.6	992.16	984381.47	0	0
	14	12.0	1044.00	1089936.00	0	0
	15	14.8	1119.04	1252250.52	0	0
	16	8.7	975.69	951970.98	1	0.850866277
	17	9.5	990.25	980595.06	0	0
	18	11.2	1025.44	1051527.19	0	0
	19	13.3	1076.89	1159692.07	0	0
	20	15.8	1149.64	1321672.13	0	0
Σ						8.202892743
$E_{d_y} =$						48.36425561
	a	1.5	902.25	814055.06	1	0.995018688
	b	4.5	920.25	846860.06	1	0.956474435
	c	7.5	956.25	914414.06	1	0.885813149
	d	10.5	1010.25	1020605.06	0	0
	e	13.5	1082.25	1171265.06	0	0
Σ						2.837306272
$E_{d_x} =$						8.364378889
$E_d = 60$ lx (measured)			TOTAL		$E_d =$	57

FOV = 0 for $r_i > 8.7$ cm gives a E_d value of 57 lx, very similar to $E_d = 60$ lx calculated making FOV = 0 in the spreadsheet that was used to simulate the display-detector properties at closer distance.

FOV = 0 means, see Figure 60, that the influence of cell i on the reading of the light sensor is irrelevant.

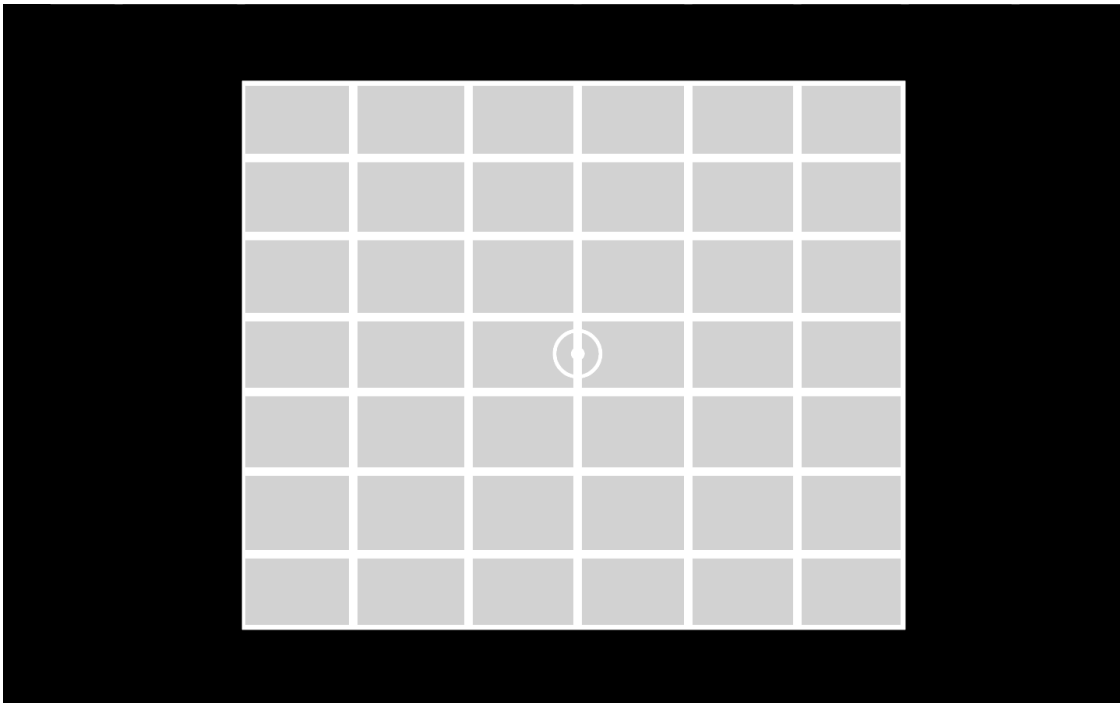


Figure 60. A Lux Meter Placed at $d = 30$ cm Is Not Affected by Corner Screen Cells

Measuring E with the lux meter LX1010B at $d = 30$ cm is equivalent to deactivate some cells on the screen i.e. FOV = 0 for $r_i > 8.7$ cm.

It is due to the combined effects of:

- a reduced field of view of the light sensor and
- the viewing angle of the LCD (an important parameter to define in non-emissive types of displays such as LCDs)

There are limitations inherent to the LCD technology and the viewing angle can help characterize the display more accurately.

LCDs usually have their viewing angle defined as minimum contrast ratio over a certain angle (Sharp Corporation, 1993).

For instance the Flat Panel Monitor Dell UltraSharp 1708-BLK, see Figure 54, has vertical and horizontal viewing angles of 160°.

Thus, operating a lux meter must take into account that the measurements obtained with this device needs correction.

The correction factor can be calculated by using the method described in this section, and a spreadsheet similar to the one shown in Table 12, for the particular monitor used in benchmarking EVIS has been created after ascertaining the:

- a) Correct A_s
- b) Equivalent ω_s at a distance d ; and
- c) Radii r_i have been determined

LCD refresh rate

The refresh rate refers to how many times per second a frame is drawn in the screen. For an LCD monitor, the rate is typically 60 Hz or 120 Hz.

A high refresh rate makes a real difference when watching a movie or sports, where a picture moves quickly as the image may show a defect called “motion blur”.

Nevertheless, the benchmarking method developed for the New Test Set uses dynamic images lasting up to 3 sec in the screen.

The time the Tumbling Es/Cs are shown is long enough for the motion blur effect not to be noticeable.

Thus the refresh rate of 60 Hz that is the default value in Microsoft Windows 7 operating system will suffice when using a laptop monitor in the new test set.

CHAPTER 4

CONCLUSIONS AND RECOMMENDATIONS

Limitations and Recommendations for Future Research

Even though the new test set and the benchmarking approach has been extensively tested in order to derivate the mathematical formulae and physical principles applicable in its design, still a number of practical tests involving different “standard observers” have to be implemented. Basically the tests will consist of requesting that different users test several video imaging systems while random oriented Tumbling Cs or Es are shown for a brief period of time (2 or 3 seconds) and ascertaining the reliability of the observers responses.

A Weibull probability function should be fitted to the data and the reliability of the observer responses statistically tested (Driggers, 2003).

The threshold will be defined as the contrast level between the Cs or Es and their background at which the observers scores 75% correct.

Conclusions

It has been demonstrated that the proposed new test set that also includes a new benchmarking approach (US Patent pending) is more accurate and versatile than the current test sets and benchmarking methods used to test image quality and video imaging systems.

Image quality can be quantified using the Extended Video Imaging System (EVIS) configuration defined in this manuscript and taking into account the photometric and visual parameters that characterize a “standard observer”.

The New Test Set has several advantages over the current testing systems:

- 1) It is a very compact and portable system that can be used in any laboratory or in the field
- 2) It allows benchmarking of video imaging systems with any lens fixed or zoom lens, as the objective lens does not require to be mounted in any special adapter to aim to a radiant source
- 3) It allows all members of a “standard observer team” to benchmark the system at the same time, thus reducing the occurrence of biased diagnostics
- 4) EVIS calibration is fast
- 5) It is a very cost-effective approach as it can be implemented in any laptop once the appropriate set of Tumbling Es/Cs has been built for the particular screen display in use
- 6) It allows color image benchmarking
- 7) It allows contrast sensitivity benchmarking
- 8) It allows dynamic detection and recognition benchmarking
- 9) It also allows any of the traditional resolution charts such as the USAF1951 to be used in high-light and low-light level conditions
- 10) It allows checking up the visual acuity of the “standard observer” by using the 20/20 Tumbling Es/Cs before the observer proceeds to benchmarking the video imaging system
- 11) It allows benchmarking two video imaging systems at the same time by placing both systems in tandem and aiming at the same Tumbling Es/Cs
- 12) It allows simulation in the laboratory of low-light conditions such as full moon or quarter moon
- 13) It is easy to use
- 14) Training and qualifying a “standard observer” takes less than 10 minutes.

REFERENCES

- Al-Azzawi, A. (2007). *Photonics: Principles and practices*. CRC Press
ISBN: 978-0-8493-8290-1
- ASTM E2566–08. *Standard test method for determining visual acuity and field of view of on-board video systems for tele-operation of robots for urban search and rescue applications*. Available from
<http://www.astm.org/Standards/E2566.htm>
- Bailey, H.H. (1970). *Target detection through visual recognition: A quantitative model*. Santa Monica, CA: Rand
- Bass, M. (1994, September 1). *Chapter 24. Radiometry and photometry*. Handbook of Optics, Vol. 2: Devices, measurements, and properties, 2nd Ed. ISBN 978-0070479746
- Chaves, J. (2008). *Introduction to non imaging optics*. CRC Press 2008.
ISBN: 978-1-4200-5429-3. DOI: 10.1201/9781420054323.pt1
- Conrad, J. (2000). Getting the right exposure when photographing the moon.
Retrieved from <http://www.calphoto.com/moon.htm>
- Cowan, S. (1982). *Understanding infinite Series and Fourier series*. Handbook of modern electronics math. Englewood Cliffs, NJ.: Prentice-Hall, ISBN 0-13-380485-2
- DiLaura, D. (2011). Photopic and scotopic lumens. Retrieved from
<http://www.visual-3d.com/Education/LightingLessons/LightingLessons.aspx>
- Driggers, R.G. (2003). *Electro-optical imaging systems performance measurement*. Encyclopedia of Optical Engineering. Vol. 1. New York, NY: Marcel Dekker, ISBN 0-8247-4258-8

- Ginsburg, A. (1982, December 28). *Spatial frequency and contrast sensitivity test chart*. U.S. Patent # 4365873
- Greivenkamp, J.E. (2004). *Field guide to geometrical optics*. Bellingham, WA: SPIE The International Society for Optical Engineering. ISBN 0-8194-5297-7
- Johnson, J. (1966). Analytical description of night vision devices. *Proceedings of the seminar on direct viewing electro-optical aids to night vision*. Biberman, L., Editor. Institute for Defense Analyses Study S254, Oct, 1966
- Kalloniatis, M., & Luu, C. (2007). Visual acuity. Retrieved from <http://webvision.med.utah.edu/book/part-viii-gabac-receptors/visual-acuity/>
- K-Light Laboratories (2011). Photometric testing & calibration services. Retrieved from <http://www.klightlab.com/luminance.html>
- Lenhardt, K., & Kreuznach, B. (2005). Optical measurement techniques with telecentric lenses. Retrieved from http://www.schneiderkreuznach.com/pdf/div/optical_measurement_techniques_with_telecentric_lenses.pdf
- MIL-STD-150A (1959, May 12). Military standard photographic lenses. Retrieved from [http://www.everyspec.com/MIL-STD/MIL-STD+\(0100+-+0299\)/download.php?spec=MIL-STD-150A.016197.PDF](http://www.everyspec.com/MIL-STD/MIL-STD+(0100+-+0299)/download.php?spec=MIL-STD-150A.016197.PDF)
- Palmer, J.M. (1995, February). Getting intense on intensity. *Optics and photonics news*. p 6. Retrieved from <http://www.optics.arizona.edu/Palmer/intenopn.html>
- Palmer, J.M. (2003, October). Radiometry & photometry FAQ. Retrieved from <http://www.optics.arizona.edu/palmer/rpfaq/rpfaq.htm> downloadable ver. 1.1
- Ray, S. F. (2002). *Applied photographic optics*. 3rd Ed. Woburn, MA: Elsevier Science. ISBN 0 240 51540 4

- Roberts, D.A. (1996). *Radiometry/photometry: A guide to speaking the language of radiometry and photometry*. The photonics design and applications handbook.
- Rolyn Optics Company, (n.d.). Optical Formulae. Retrieved on Sep 1, 2011 from http://www.rolyn.com/images/Rolyn%20Optics_OpticalFormulae.pdf
- Sharp Corporation, (1993). Liquid crystal displays. *LCD application note*. Reference Code SMT92023
- Simon, C. (1965). Rapid acquisition of radar targets from moving and static displays. *Human Factors*, Vol. 7, June 1965
- Steedman, W., & Backer, C. (1960). Target size and visual recognition. *Human Factors*, Vol. 2, Aug. 1960
- Strouse, W. (2003, October). How visual acuity is measured. Retrieved from <http://www.mdsupport.org/library/acuity.html>
- Tyler, J. A. ("n.d."). OTM I lecture: Visual acuity. Retrieved from http://www.nova.edu/hpd/otm/otm-a/guestlects/visual_acuity.htm
- Thompson, B.J., & Malacara, D. (2001). *Handbook of optical engineering*. CRC Press
ISBN: 978-0-8247-9960-1
- Vision Sciences Research Corp. (2002). FAQs. Retrieved from <http://contrastssensitivity.net/faqs.html>
- Walree, P., (2002-2011). Vignetting. Retrieved from <http://toothwalker.org/optics/vignetting.html>
- Weber, J., Humphrey, F. & Silver, A. (1998). The optics of light & vision. Marchon Eyewear. <http://www.cpsection.org/education/descriptions.html>

APPENDIXES

Appendix A

Language of Light - Definitions

Brightness	<p>Is a term commonly misused when specifying luminance.</p> <p>Brightness is purely a psycho-physiological attribute when the human eye has adapted to a particular radiation level. Brightness is not a measurable parameter.</p>
Chrominance	<p>Is the physical combination of the dominant wavelength (hue) and purity (saturation).</p>
CIE System	<p>The chart is based on the supersaturated primaries of red, blue, and green. Any color can be characterized by its x and y coordinates. The chart assumes all colors are generated by equal radiance sources, which puts white at the center of the chart.</p>
Color	<p>The CIE System describes the three dimensional color features: luminance, hue, and saturation in a two-dimensional chart.</p>
Contrast Ratio	<p>Is the defined as $\text{max. luminance} / \text{min. luminance}$</p> <p>All ambient and display parameters must be defined in order to calculate a meaningful ratio. Another factor is the area for the measurement.</p>
Entrance Pupil	<p>Is the image of the aperture stop seen through all lens elements in front of it and from a position on the optical axis</p>
Exit Pupil	<p>Is the image of the aperture stop that an observer sees when the observer looks into the lens from the rear</p>

Foot-candle (fc)	<p>The foot-candle is a unit to measure incident light.</p> <p>It is the illuminance on a surface one foot distant from a source of one Candela; 1 fc = 1 lm/ft² (Lumens/sq. foot)</p>
Foot-lambert (fL)	<p>The unit used to measure the emitted light from a surface.</p> <p>For a perfect reflecting and diffusing surface, the number of foot-lamberts will be equal to the number of foot-candles.</p>
<i>F-Stop</i>	<p>It is the measure of the aperture of a given lens. Each <i>F-Stop</i> jump indicates a 50% reduction in the amount of light a lens is able to transmit (Transmittance).</p> <p>Typical <i>F-Stop</i> : 1.4 2 2.8 4 5.6 8 11</p> <p>Transmittance: 100% 50% 25% 12.5% 6.3% 3% 1.5%</p>
Gamma	<p>It is the measure of the grey scale in a television picture.</p> <p>A numerical factor used in the television system to indicate how the light values are expanded or compressed. A gamma with a value of 1 (one) indicates a linear characteristic. While a gamma with a value of less than 1 indicates that there is a compression in the level changes of the white components of the signal.</p>
Gamma Correction	<p>The introduction of a nonlinear output / input characteristic for the purpose of changing the effective value of the gamma.</p>
Grey Scale	<p>A series of tones that range from true black to true white; it is usually expressed in 10 steps</p>
Hue	<p>Is the dominant wavelength of the color as subjectively perceived by the human eye</p>
Illuminance	<p>Is the amount of light incident on a particular area</p>

IRE	<p>Institute of Radio Engineers</p> <p>An IRE unit is 1% of the voltage from blanking to peak white in the video signal.</p>
IRE Scale	<p>An oscilloscope scale that applies to composite video levels.</p> <p>Typically there are 140 units in one volt</p> <p>(1 IRE = 1000 mV/140 IRE = 7.14 mV).</p>
Luminance	<p>Luminance is defined as the quantitative measure of brightness and is measured in English units as foot-lamberts (fL) and in SI (International System) units as Candela/m².</p> <p>Luminance is also defined as the amount of light intensity perceived by the eye as brightness (referred to as “Y”).</p>
Luminance Signal	<p>The portion of the composite video signal that represents the brightness of the black and white information</p>
Lux	<p>1 lux \approx 0.1 fc ; 1 fc = 10.764 lux \approx 11 lux</p>
Pixel	<p>The smallest resolvable spatial-information element on any display. The pixel can be subdivided further to achieve color. Each red, green, and blue element is referred to as subpixel. The spatial dimension of pixel can be defined by the pixel size and pixel pitch.</p> <p>Fill factor is another parameter used when image quality measurements are taken over an area (more than one pixel).</p>
Radiance	<p>Is a measure of the rate of energy flow from an electromagnetic source usually measured in power units: watts or joules / second</p>

Reflected Light	<p>The scene luminance (“brightness”) reflected from a scene.</p> <p>Usually it represents 5 to 95 percent of the incident light, and it is expressed in foot-lamberts.</p>
Resolution	<p>There are numerous methods to measure resolution, and the same method must be used when comparing two displays to each other.</p> <p>When describing a LCD display, for instance, 640 x 480 is not the resolution. This should be referred to as the display format.</p> <p>For discretely addressed displays such as LCDs, resolution is usually measured in resolvable elements per unit measurement: pixels (dots/inch)</p> <p>For analog addressable displays such as CRTs, resolution can be defined as above or more accurately as the spatial frequency (lines/inch or lines/mm) at which an observer can no longer discriminate for instance the light and dark bars of a square wave pattern such as the USAF 1951 chart.</p>
Response Time	<p>Is the time it takes a pixel to change state from on to off (“black” to “white”). This time includes all electrical and physical delays.</p> <p>It is defined as the transition time from the 10% level to the 90% level luminance output.</p> <p>In LCDs, because the rise and decay times are usually unequal, both are specified; τ_r (10%-90%), τ_d (90%-10%)</p> <p>Rise and decay times may be combined to give a total response time.</p>

Saturation	<p>It is the degree to which the hue of a color subjectively appears to be undiluted by its complimentary color to form white.</p> <p>If there is no trace of apparent white in the color, it is said to be fully saturated.</p>
Solid Angle (ω)	<p>$\omega = A/R^2$ A solid angle is the ratio of the sphere surface area enclosed to the square of the radius. Unit: Steradian : sr</p>
Viewing Angle	<p>Is an important factor in nonemissive display such as a LCD.</p> <p>This angle is specified by its x and y direction on the face of the display. LCDs usually have their viewing angle defined as minimum contrast ratio over a certain angle.</p>
Vignetting	<p>Indicates an unintended darkening of the image corners in a photographic image. Most photographic lenses exhibit optical vignetting to some degree. The effect is strongest when the lens is used wide open. Its origin relates to the simple fact that a lens has a length. Obliquely incident light is confronted with a smaller lens opening than light approaching the lens head-on.</p>
White light	<p>It is equal luminance level across the visible spectrum that gives white its color.</p> <p>Equal radiance levels across the visible spectrum, however, will give a magenta color.</p>

Appendix B

Optical Vignetting

Optical Vignetting is a reduction in the size of the entrance pupil for off-axis objects due to physical constraints of lens diameters.

Entrance Pupil

It is the image of the aperture stop seen through all lens elements in front of it and from a position on the optical axis. See Figure 9.

Exit Pupil

It is the image of the aperture stop that an observer sees when he looks into the lens from the rear.

There are two fundamental rays to consider in the geometric representation of a thin lens: on-axis meridional ray and principal meridional ray

On-Axis Meridional Ray: A ray from the object plane, on the optical axis, to the image plane, also on the optical axis.

Principal Meridional Ray: A meridional ray from the edge (or any other off-axis point) on the object to the corresponding point on the image.

The planes on which the on-axis meridional ray crosses the optical axis are conjugates to the object and image planes (Thompson & Malacara, 2001)

Any thin lens at these positions does not affect the path of the on-axis meridional ray but affects the path of the principal ray. This lens is called a field lens and the diameter of the field lenses determines the diameter of the image (field).

By stopping a principal ray with a certain height, we have an effect called vignetting, see Figure 8. In a multiple element lens, the rear elements are shaded by elements in front of them, what reduces the effective lens opening for off-axis incident light, see Figure 10.

Appendix C

Natural Vignetting

Compared with the image center, the irradiance (amount of light) getting in the corners of the sensor array is less than in the center of the image, see Figure 61.

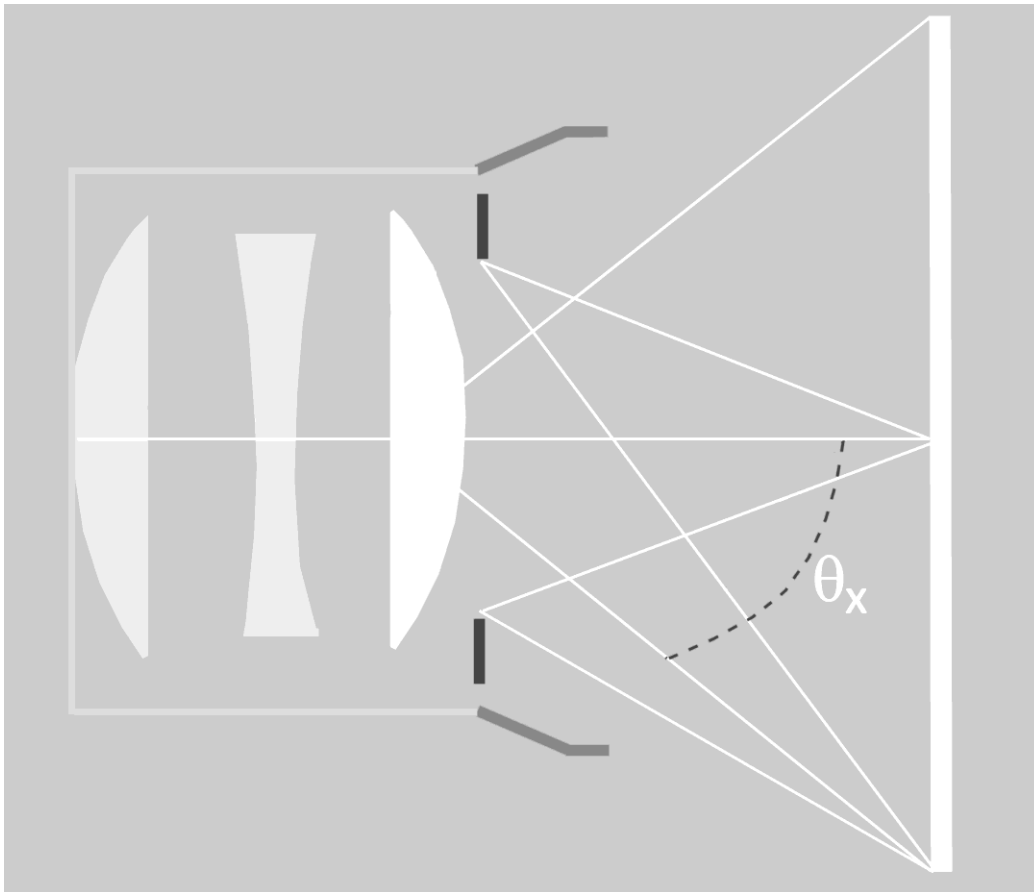


Figure 61. Natural Vignetting

- 1) Light has longer way to travel to the corner
- 2) Exit pupil seen by the off-axis is elliptical and has smaller apparent area
- 3) Lambert's law: light strikes the corner at an angle

There are three reasons (Walree, 2011) which lead to a *cosine-to-the-fourth illuminance falloff*:

- 1) There is a $\cos^2(b)$ factor due to the inverse square law: the light has a longer way to travel to the image corner.
- 2) The pupil seen by the off-axis point is not round but elliptical and has a smaller area than the round pupil seen by the image center.

This yields another $\cos(b)$ factor. Note however that this cosine factor is approximate. It needs refinement when the pupil diameter is not small compared to its distance from the sensor array.

- 3) While the light hits the image center at normal incidence, it strikes the image corner at the angle b . This yields another $\cos(b)$ factor.

The last effect relates to Lambert's law and can be compared with a late afternoon sun that heats the earth less than the sun at noon because the same beam of sunlight is spread over a larger area.

The combined effect of all cosine factors is a: *cosine-to-the-fourth illuminance falloff towards the image corners*, as shown in Figure 61.

The performance graphic shown in Figure 14 provided by Zeiss for one of its manufactured objective lenses, considering the relative illuminance of the center image to be the 1.0 value, shows at full aperture of the iris ($F/2.8$) the corner relative illuminance to the center is 0.2 what in terms of *F-Stop* means the corner receives about 25% illuminance.

Thus the $F/2.8$ lens is equivalent to an $F/5.6$ lens when looking at the borders of the image (see Appendix B) what is considerably lower *F-Stop* than the full aperture.

Appendix D

Solid Angle Equations

Solid Angle (ω) is defined as the ratio of a portion of the area *on the surface of a sphere* to the square of the sphere radius R .

The sphere is defined by the vertex (usually the center of a luminous body) and the center of the surface (usually an aperture detector), see Figure 10.

The portion of the whole space of a sphere of radius R about a given point (the center of the sphere) bounded by a conical surface with its vertex at that point is *measured by the area cut by the bounding surface from the sphere*.

A solid angle ω defines a sector of unit sphere ($R = 1$) in analog manner a planar angle θ defines the length of an arc on a unit circle (Sharp Corporation, 1993), see Figure 11.

The planar angle is measured in degrees or radians and the solid angle in Steradians (sr).

The solid angle ω of a cone with apex angle 2θ (planar angle), sets a spherical cap on the unit sphere with a solid angle:

$$\omega = 2\pi (1 - \cos\theta) \tag{D01}$$

where θ is half the apex angle (Greivenkamp, 2004).

Solid Angle Equivalent Identities

As indicated by Zalewski (as cited in Bass, 1994) for $R = 1$ the equivalence identity applies:

$$\omega = 2\pi (1 - \cos\theta) = 4\pi \sin^2(\theta/2) \tag{D02}$$

The equivalent representations for the solid angle ω can be demonstrated using the following trigonometric identity (Cowan, 1982):

$$\frac{1}{2} (1 - \cos 2\theta) = \sin^2\theta \tag{D03}$$

Now, replacing θ by $\theta/2$ gives:

$$\frac{1}{2}(1 - \cos 2\theta) = \sin^2\theta \implies \frac{1}{2}(1 - \cos\theta) = \sin^2(\theta/2) \implies (1 - \cos\theta) = 2\sin^2(\theta/2)$$

Thus the equation (D03) can be rewritten as:

$$(1 - \cos\theta) = 2\sin^2(\theta/2) \quad (\text{D04})$$

and $2\pi(1 - \cos\theta) = 4\pi\sin^2(\theta/2)$ as indicated in equation D02.

For $R \neq 1$ the area of the spherical cap is:

$$A = 4\pi R^2 \sin^2(\theta/2) \quad (\text{D05})$$

although the solid angle is independent of the distance R as by definition:

$$\omega = A/R^2 = 4\pi\sin^2(\theta/2) \quad (\text{D06})$$

thus an entire sphere, regardless the size of its radius, has a solid angle:

$$\omega = 4\pi \text{ Steradians} = 12.56 \text{ sr} \quad (\text{D07})$$

Solid Angle Identities Based on Planar Angle Definitions

Defining the solid angle ω by making reference to $\theta/2$ (half apex angle) as indicated by Zalewski (as cited in Bass, 1994) or setting θ as the entire apex angle (Ray, 2002), leads to two equivalent definitions.

If apex angle = 2θ then the solid angle is:

$$\omega = 4\pi\sin^2(\theta/2) \quad (\text{D08})$$

If apex angle = θ then the solid angle is:

$$\omega = \pi\sin^2(\theta) \quad (\text{D09})$$

Both (D08) and (D09) are found alternatively in technical literature and the reference used for the apex angle θ has to be figured out first to avoid confusion when using derivations and formulae obtained in each reference system.

The Taylor series (Cowan, 1982) for $\sin\theta$ and $\cos\theta$ provide the following approximations for small values of the apex angle θ :

$$\sin\theta = \theta - \frac{\theta^3}{3!} + \frac{\theta^5}{5!} - \dots \quad \xrightarrow{\theta \text{ small}} \sin\theta \approx \theta \quad (\text{D10})$$

$$\cos\theta = 1 - \frac{\theta^2}{2!} + \frac{\theta^4}{4!} - \dots \quad \xrightarrow{\theta \text{ small}} \cos\theta \approx 1 - \frac{\theta^2}{2!} \implies \theta^2 \approx 2(1 - \cos\theta) \quad (\text{D11})$$

Thus for small apex angle values, the solid angle equations give the same results and:

$$\omega = 2\pi(1 - \cos\theta) \approx \pi\theta^2 = \frac{A_s}{d^2 + r^2} \quad (\text{D12})$$

$$\omega = 4\pi\sin^2(\theta/2) \approx 4\pi(\theta/2)^2 = \pi\theta^2 = \frac{A_s}{d^2 + r^2} \quad (\text{D13})$$

a) (D12) and (D13) are equivalent and $\omega \approx \pi(\theta)^2$ is valid for apex angle $2\theta < 94^\circ$

b) for θ small: $\pi\theta^2$ (see Figure 55, Figure 62 and Table 13) is given by A_s/R^2 :

$$2\theta = \frac{2r'}{\sqrt{d^2 + r^2}} \implies \pi\theta^2 = \pi \frac{r'^2}{d^2 + r^2} = \frac{A_s}{d^2 + r^2} = \frac{A_s}{R^2} = \omega_s \quad (\text{D14})$$

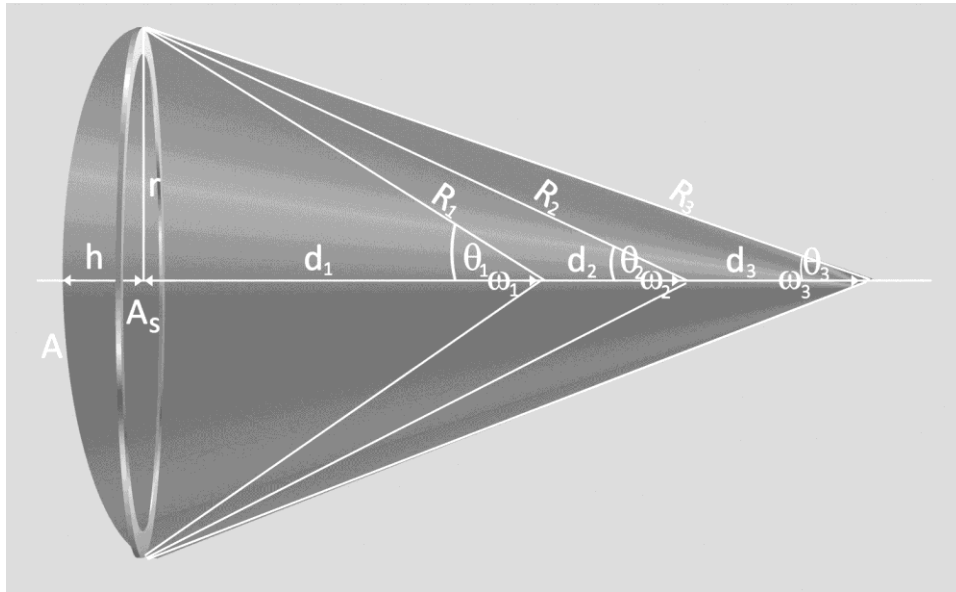


Figure 62. The approximation $\omega \approx \pi(\theta)^2 \rightarrow A$ (cone cap) $\approx A_s$ (flat circle) $= \pi r^2$

$$d_1 = 0.2 \text{ m} \implies \omega_1 \text{ (sr)} = 1.41 \quad \theta_1 \text{ (rad)} = 0.6831 \quad ; \quad 2\theta_1 \text{ (}^\circ\text{)} = 78.3^\circ$$

$$d_2 = 2.0 \text{ m} \implies \omega_2 \text{ (sr)} = 0.0141 \quad \theta_2 \text{ (rad)} = 0.0670 \quad ; \quad 2\theta_2 \text{ (}^\circ\text{)} = 7.7^\circ$$

$$d_3 = 20.0 \text{ m} \implies \omega_3 \text{ (sr)} = 0.000141 \quad \theta_3 \text{ (rad)} = 0.0067 \quad ; \quad 2\theta_3 \text{ (}^\circ\text{)} = 0.77^\circ$$

Table 13

Solid Angle ω - Apex Angle 2θ - Validity of $\omega \approx \pi(\theta)^2$ Approximation

$$\omega = 2\pi(1 - \cos\theta) = 4\pi\sin^2(\theta/2)$$

$$\theta = \arccos(1 - \omega/2\pi) = 2\arcsin\sqrt{(\omega/4\pi)}$$

$$\theta \approx r/d \Rightarrow d \approx r/\theta$$

	solid angle ω	planar angle θ (rad)	planar angle θ°	apex angle $2\theta^\circ$	θ (rad)	$\sin(\theta)$	$\omega \approx \pi(\theta)^2$ approx	Dell D620 $r = 0.134\text{m}$ d (m)	error
4 π	12.5664	3.1416	180.0	360	3.14	0.00	31.01	approx not valid	
	10.7250	2.3559	135.0	270	2.36	0.71	17.44	approx not valid	
2 π	6.2832	1.5708	90.0	180	1.57	1.00	7.75	approx not valid	
	4.00	1.1989	68.7	137.4	1.20	0.93	4.52	0.11	13%
	2.00	0.8207	47.0	94.0	0.82	0.73	2.12	0.16	6%
	1.41	0.6831	39.1	78.3	0.68	0.63	1.47	0.20	4%
	0.90	0.5418	31.0	62.1	0.54	0.52	0.92	0.25	2%
	0.80	0.5101	29.2	58.5	0.51	0.49	0.82	0.26	2%
	0.70	0.4765	27.3	54.6	0.48	0.46	0.71	0.28	2%
	0.60	0.4406	25.2	50.5	0.44	0.43	0.61	0.30	2%
	0.50	0.4016	23.0	46.0	0.40	0.39	0.51	0.33	1%
	0.40	0.3587	20.6	41.1	0.36	0.35	0.40	0.37	1%
	0.30	0.3103	17.8	35.6	0.31	0.31	0.30	0.43	1%
	0.20	0.2530	14.5	29.0	0.25	0.25	0.20	0.53	1%
	0.10	0.1786	10.2	20.5	0.18	0.18	0.10	0.75	0%
	0.09	0.1695	9.7	19.4	0.17	0.17	0.09	0.79	0%
	0.08	0.1597	9.2	18.3	0.16	0.16	0.08	0.84	0%
	0.07	0.1494	8.6	17.1	0.15	0.15	0.07	0.90	0%
	0.06	0.1383	7.9	15.8	0.14	0.14	0.06	0.97	0%
	0.05	0.1262	7.2	14.5	0.13	0.13	0.05	1.06	0%
	0.04	0.1129	6.5	12.9	0.11	0.11	0.04	1.19	0%
	0.03	0.0978	5.6	11.2	0.10	0.10	0.03	1.37	0%
	0.02	0.0798	4.6	9.1	0.08	0.08	0.02	1.68	0%
	0.014100	0.0670	3.8	7.7	0.07	0.07	0.01	2.00	0%
	0.006280	0.0447	2.6	5.1	0.04	0.04	0.01	3.00	0%
	0.001515	0.0220	1.3	2.5	0.02	0.02	0.002	6.10	0%
	0.000141	0.0067	0.4	0.8	0.01	0.01	0.0001	20.00	0%

Appendix E

Radiant Power Transfer from Source to Detector

Nonimaging optical systems, instead of an object, have a light source and instead of an image they have a receiver.

Instead of an image of the source, the optic produces a prescribed illuminance (or irradiance) pattern on the receiver.

Nonimaging optics are used to describe some of the characteristics of the video imaging systems (Chaves, 2008) such as the radiant power transfer from the source to the sensor array.

The intensity I of the radiation is defined as the flux per unit solid angle. The radiometric quantity is given in watts per Steradian (W/sr) and the photometric quantity in Candelas where $1 \text{ cd} = 1 \text{ lm/sr}$.

The radiation flux L per unit projected area and per unit solid angle is called radiance and is measured in watts per square meter per Steradian ($\text{W/m}^2\cdot\text{sr}$).

The corresponding photometric quantity is the luminance L_v measured in Lumens per square meter per Steradian ($\text{lm/m}^2\cdot\text{sr}$) equal to Candelas per square meter (cd/m^2).

Lambertian Source – Uniformly Radiant Areas

Consider the particular case in which the radiance L (or luminance L_v) of a surface A is uniform and constant throughout the whole area.

A source having a radiance that is uniform across its surface and uniformly emits in all directions from its surface is called a Lambertian source as indicated by Zalewski (as cited in Bass, 1994). Such a surface (Chavez, 2008) emits or intercepts radiation with an intensity pattern following only the cosine law:

$$I = LA\cos\theta \quad (\text{E01})$$

where:

$$LA = I_s \quad (E02)$$

θ is the angle in any particular direction with the axle of the surface and for a Lambertian source L is constant across its surface so the factor LA is constant.

Thus the intensity I is only function of the angle θ in a particular direction:

$$I = I_s \cos\theta \quad (E03)$$

In practice, if we consider a source located far enough from the observer and that the angle θ_s varies in a small range from θ_1 to θ_2 , as shown in Figure 39 the approximation to a Lambertian source is correct.

Radiant Transfer Between a Circular Source and Detector

Considering the simpler case of a source and a detector, the radiant flux Φ is described by the following equation:

$$\Phi = \iint \frac{L \cos\theta_s \cos\theta_d}{d^2} dA_s dA_d \quad (E04)$$

Radiant Transfer Between a Lambertian Source and Detector

For a Lambertian source the equation (E04) can be simplified, as $L = L_s$ constant across the surface and the radiant flux Φ of the source can be described as:

$$\Phi_s = L_s \iint \frac{\cos\theta_s \cos\theta_d}{d^2} dA_s dA_d \quad (E05)$$

where d is the distance between the source and the detector, and the subscripts s and d denote the source and detector, respectively.

According to Zalewski (as cited in Bass, 1994), it is assumed the detector is cosine corrected, i.e. it responds equally to radiation at any point across its surface and from any direction.

For a Lambertian source, the Radiant Exitance M_s is equivalent to:

$$M_s [\text{watt/cm}^2] = \pi [\text{sr}] L_s [\text{watt/cm}^2 \cdot \text{sr}] \quad (E06)$$

so for the source-detector configuration shown in Figure 39, the angle $\theta_s = \theta_2 - \theta_1 \approx 0$ then $\cos\theta_s \approx 1$ where L_s is the Radiance of the Lambertian source.

The units in the dimensional equations are:

$$M \text{ by definition} \Rightarrow [\text{watt}/\text{cm}^2]$$

$$\pi \Rightarrow [\text{sr}]$$

$$L \text{ by definition} \Rightarrow [\text{watt}/\text{cm}^2 \text{ sr}]$$

thus:

$$\pi L \Rightarrow [\text{watt}/\text{cm}^2] \quad (\text{E07})$$

A distance source can be approximated to a Lambertian radiator, thus for a distance source:

$$M_s \approx \pi L_s \quad (\text{E08})$$

The radiant transfer between a circular source and detector is a particular case in common configurations to many optical systems and it is assumed that the centers of the source and detector are located along the same optical axis.

The radius of the Lambertian source and the detector are r_s and r_d respectively and the distance between centers is d , see Figure 50.

In this case the exact solution of the equation for the radiant flux Φ of a Lambertian source is:

$$\Phi_s = L_s \iint \frac{\cos\theta_s \cos\theta_d}{d^2} dA_s dA_d = \frac{2L_s(\pi r_s r_d)^2}{r_s^2 + r_d^2 + d^2 + \sqrt{(r_s^2 + r_d^2 + d^2)^2 - 4r_s^2 r_d^2}} \quad (\text{E09})$$

but $(\pi r_s r_d)^2 = \pi r_s^2 \pi r_d^2 = A_s A_d$ thus the equation (E08) can be rearranged as:

$$\Phi_s = \frac{2L_s(\pi r_s r_d)^2}{r_s^2 + r_d^2 + d^2 + \sqrt{(r_s^2 + r_d^2 + d^2)^2 - 4r_s^2 r_d^2}} = \frac{2L_s A_s A_d}{r_s^2 + r_d^2 + d^2 + \sqrt{(r_s^2 + r_d^2 + d^2)^2 - 4r_s^2 r_d^2}} \quad (\text{E10})$$

Considering an ideal system in the air (refraction index $n = 1$) and without energy absorption, the principle of energy conservation establishes that the radiance L and the $A\omega$ product or throughput are conserved (Greivenkamp, 2004).

Thus the radiant flux Φ_d falling on the detector equals the radiant flux Φ_s emitted by the source, and the illuminance E_d on the detector can be written as:

$$E_d = \frac{\Phi_d}{A_d} = \frac{2L_s A_s}{r_s^2 + r_d^2 + d^2 + \sqrt{(r_s^2 + r_d^2 + d^2)^2 - 4r_s^2 r_d^2}} \quad (\text{E11})$$

This is the fundamental equation to calculate the illuminance E_d on a detector from a Lambertian radiator of area A_s and luminance L_s located at distance d from the detector.

In Table 6 it is shown the calculations for the New Test Set.

The equation (E11) provides exact figures, but if $4r_s^2 r_d^2 \ll (r_s^2 + r_d^2 + d^2)^2$ it can be approximated as follows:

$$E_d \approx \frac{L_s A_s}{r_s^2 + r_d^2 + d^2} \approx \frac{L_s A_s}{d^2} \approx L_s \omega_s \quad (\text{E12})$$

if $d^2 \gg r_s^2 + r_d^2$ namely, the radii are completely negligible with respect to the distance.

For a distance $d \geq 20$ ft (6 meter) a radiant source seen from a small detector as shown in Figure 39 complies with $\cos\theta_s \approx 1$ and $d^2 \gg r_s^2 + r_d^2$ so the configuration can be approximated to a Lambertian source.

$\frac{A_s}{d^2}$ is the solid angle ω_s subtended by the area A_s of the Lambertian source

having its vortex in the detector see Figure 50, thus:

$$\Phi_d \approx L_s A_d \omega_s$$

Now considering other grouping:

$\frac{A_d}{d^2}$ is the solid angle ω_d subtended by the area A_d of the detector having its

vortex in the source see Figure 63, thus:

$$\Phi_d \approx L_s A_s \omega_d$$

which is an alternative equation to describe the radiant flux Φ_d falling on the detector.

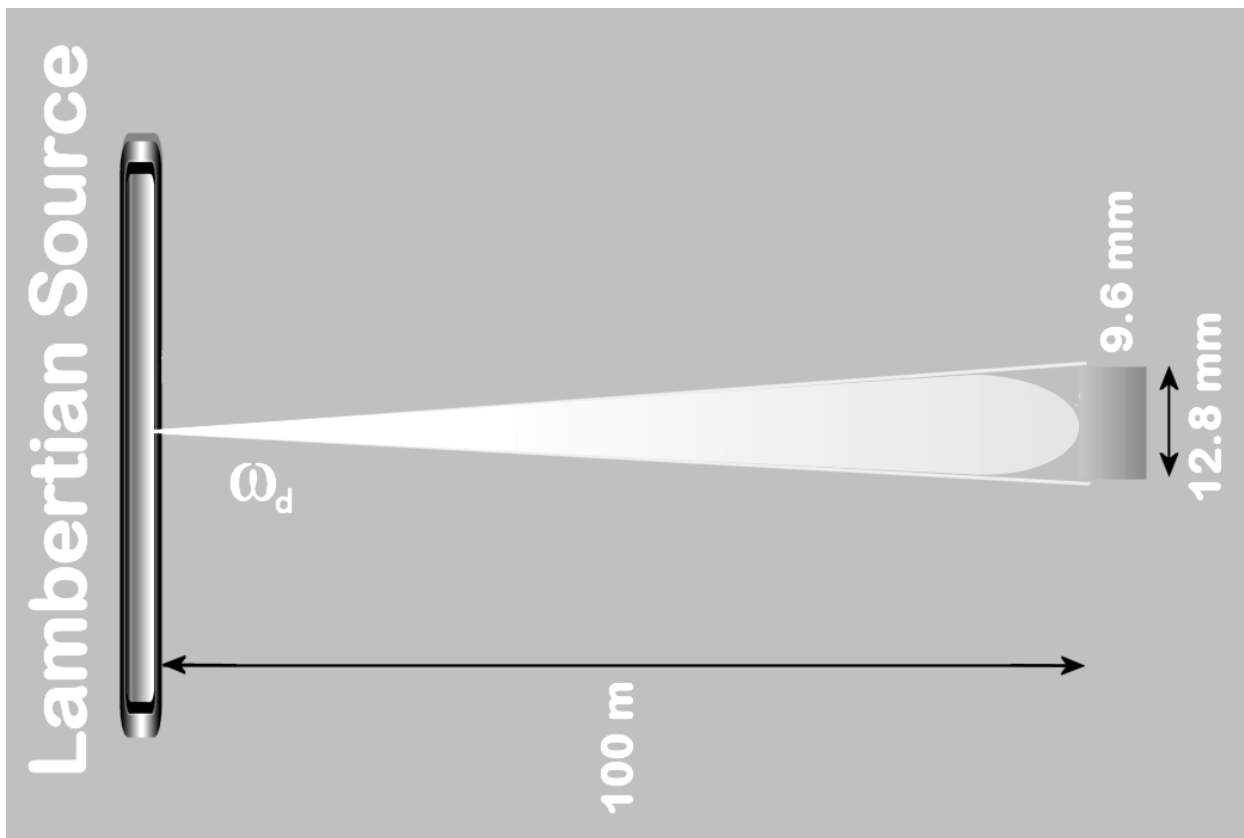


Figure 63. Solid Angle ω_d Subtended by the Detector

The detector shown in Figure 63 could be a 1" format CCD sensor array of dimensions $W \times H = 12.8 \text{ mm} \times 9.6 \text{ mm}$.

So in summary, the radiant flux Φ_d falling on the detector can be described by the following equations:

$$\Phi_d \approx L_s A_d \omega_s = L_s A_s \omega_d \quad (\text{E13})$$

Taking into account that the solid angle ω_s subtended by the source at the detector is $\omega_s = 4\pi \sin^2(\theta_{max}/2)$ the equation (E13) can be written as:

$$\Phi_d \approx L_s A_s \omega_d = L_s A_d \omega_s = L_s A_d 4\pi \sin^2(\theta_{max}/2)$$

Thus the irradiance at the detector E_d is:

$$E_d = \frac{\Phi_d}{A_d} = L_s 4\pi \sin^2(\theta_{max}/2) \quad (\text{E14})$$

and replacing the relationship $L_s A_d \omega_s = L_s A_s \omega_d$ from equation (E13) into (E14) gives the following formula for the irradiance E_d see Figure 56:

$$E_d = \frac{\Phi_d}{A_d} \approx L_s \omega_s = L_s \omega_d \frac{A_s}{A_d} \quad (\text{E15})$$

If the detector is moved off-axis by a distance x , the ray from A_s to A_d will then be at an angle θ_x and $\theta_{x'}$ with respect to the normal at both surfaces as follows:

$$\theta_x = \theta_{x'} = \theta = \text{atan}\left(\frac{x}{d}\right) \quad (\text{E16})$$

The radiant power at a distance x away from the axis decreases by the fourth power of the cosine of the angle formed between the normal to the surface and the ray so the radiant power at a position x off-axis, according to Zalewski (as cited in Bass, 1994) can be described by:

$$\Phi_x \approx \frac{L_s A_s A_d}{d^2} \cos^4 \theta_x \quad (\text{E17})$$

Thus, the irradiance at the detector using Φ_d and the cosine-to-the-fourth approximation is:

$$E_d = \frac{\Phi_d}{A_d} \approx L_s \omega_s \cos^4 \theta_x = L_s \omega_d \frac{A_s}{A_d} \cos^4 \theta_x \quad (\text{E18})$$

Consider for instance a geometrical configuration with:

- a) An extended source and a detector in the same axle so $\theta_x = 0$
- b) The extended source has surface $A_s = 10 \text{ cm} \times 10 \text{ cm}$

$$\text{Radiance } L_s = 3 \text{ W/cm}^2 \cdot \text{sr}$$

- c) The detector is a 1" CCD format sensor array of $A_d = 12.8 \text{ mm} \times 9.6 \text{ mm}$

For ease of calculations the CCD dimensions will be approximated to 10 mm x 10 mm.

The detector is located at an axial distance d of 20 ft (610 cm) or further from the source.

These settings define a Lambertian source as $\theta_s = 2 \arctan\left(\frac{10/2 \text{ cm}}{610 \text{ cm}}\right) = 0.016$.

It has been demonstrated that at if the distance $d \geq 20 \text{ ft}$ the power density emitted by a radiating surface could be approximated Lambertian if its intensity I can be considered constant across the surface.

Now, if the distance d is increased, for instance to 100 meters, how much power will fall on a 1" format CCD sensor array?

First we calculate the solid angle ω_d subtended by the area A_d of the detector having its vortex in the source, see Figure 63:

$$A_d = (10 \text{ mm} \times 10 \text{ mm})^2 = (10 \text{ mm} \times 10^{-3} \frac{\text{m}}{\text{mm}})^2 = 10^{-4} \text{ m}^2$$

$$\omega_d = A_d / d^2 = 10^{-4} \text{ m}^2 / (100 \text{ m})^2 = 10^{-8} \text{ sr}$$

We multiply the solid angle ω_d by the area A_s of the source and the radiance L_s of the source to obtain the radiant power Φ_d on the detector:

$$\Phi_d = L_s A_s \omega_d = 3 \text{ (W/cm}^2 \text{sr)} \times 100 \text{ cm}^2 \times 10^{-8} \text{ sr} = 3 \times 10^{-6} \text{ W} = 3 \mu\text{W}$$

The radiant power Φ_d can also be represented as a function of ω_s as follows:

$$\Phi_d = L_s A_s \omega_d = L_s A_s A_d / d^2 = L_s A_d A_s / d^2 = L_s A_d \omega_s$$

$$A_s = (10 \text{ cm} \times 10 \text{ cm}) = (10 \text{ cm} \times 10^{-2} \frac{\text{m}}{\text{cm}})^2 = 10^{-2} \text{ m}^2$$

The solid angle ω_s subtended by the extended source having its vortex in the detector is, see Figure 50:

$$\omega_s = A_s / d^2 = 10^{-2} \text{ m}^2 / (100 \text{ m})^2 = 10^{-6} \text{ sr}$$

$$A_d = (10 \text{ mm} \times 10 \text{ mm}) = (10 \text{ mm} \times 10^{-1} \frac{\text{cm}}{\text{mm}})^2 = 1 \text{ cm}^2$$

$$\Phi_d = 3 \text{ (W/cm}^2\text{sr)} \times 1 \text{ cm}^2 \times 10^{-6} \text{ sr} = 3 \times 10^{-6} \text{ W} = 3 \text{ }\mu\text{W as calculated before.}$$

Thus, the power Φ_d from an approximated Lambertian source that falls on the detector can be represented as described in equation (E13) by:

$$\Phi_d = L_s A_d \omega_s$$

or alternatively by:

$$\Phi_d = L_s A_s \omega_d$$

A comparison between the CCD sensor array of a 1" format and 2/3" format shows that the areas A_d of the detectors have the following ratio:

$$A_{d_{2/3}} / A_1 = (\frac{2}{3}w * \frac{2}{3}h) / (w * h) = \frac{4}{9}$$

Thus radiant power transfer from the Lambertian source to a CCD sensor array of 2/3" format is 4/9 of the power transferred to a 1" format: $\Phi_{d_{2/3}} / \Phi_{d_{1"}} = 4/9 = 0.445$ considering that $\omega_{s_{2/3}} \approx \omega_{s_{1"}}$ because $d = 100\text{m} \gg$ detector width (12.8mm).

The SNR of the video imaging system if 2/3" CCD is used instead of 1" will be:

$$\text{SNR}_{2/3"} = 10 \log_{10} (4/9 \frac{P_{\text{signal}}}{P_{\text{noise}}}) \tag{E19}$$

$$\text{SNR}_{2/3"} = 10 \log_{10} (4/9 \frac{P_{\text{signal}}}{P_{\text{noise}}}) = 10 \log_{10} (\frac{P_{\text{signal}}}{P_{\text{noise}}}) + 10 \log_{10} (0.445) = \text{SNR}_{1"} - 3.52 \text{ dB}$$

$$\text{SNR}_{2/3''} = \text{SNR}_{1''} - 3.52 \text{ dB} \quad (\text{E20})$$

where P_{signal} is the useful energy in watts and P_{noise} is the noise internally created by the CCD and also indicated in watts.

A comparison between the CCD sensor array of a 2/3" format and 1/3" format shows that the areas A_d of the detectors have the following ratio:

$$A_{d_{1/3''}} / A_{d_{2/3''}} = \left(\frac{6}{11}w * \frac{6}{11}h \right) / (w * h) = \frac{36}{121}$$

Radiant Power Transfer from source to a CCD sensor array of 1/3" instead of 2/3" format: $\Phi_{d_{1/3''}} / \Phi_{d_{2/3''}} = 36/121 = 0.298$.

The comparative SNR of the video imaging system if 1/3" CCD is used will be:

$$\text{SNR}_{1/3''} = 10\log_{10}\left(36/121 \frac{P_{\text{signal}}}{P_{\text{noise}}}\right) = 10\log_{10}\left(\frac{P_{\text{signal}}}{P_{\text{noise}}}\right) + 10\log_{10}(0.298) = \text{SNR}_{2/3''} - 5.25 \text{ dB}$$

$$\text{SNR}_{1/3''} = \text{SNR}_{2/3''} - 5.25 \text{ dB} \quad (\text{E21})$$

Typical CCDs used for CCTV applications are 1/3" and 1/4". So, in this case:

$$A_{d_{1/4''}} / A_{d_{1/3''}} = \left(\frac{3}{4}w * \frac{3}{4}h \right) / (w * h) = \frac{9}{16} \text{ and } \Phi_{d_{1/4''}} / \Phi_{d_{1/3''}} = 9/16 = 0.5625$$

If both sensor arrays have the same fill factor and are manufactured with similar technologies, the SNR of the video imaging system using a 1/4" CCD will be:

$$\text{SNR}_{1/4''} = 10\log_{10}\left(9/16 \frac{P_{\text{signal}}}{P_{\text{noise}}}\right) = \text{SNR}_{1/3''} - 2.5 \text{ dB}$$

$$\text{SNR}_{1/4''} = \text{SNR}_{1/3''} - 2.5 \text{ dB} \quad (\text{E22})$$

The cumulative SNR decrease of 1/4" CCD compared to 1" CCD format will be:

$$\text{SNR}_{1/4''} = \text{SNR}_{1''} - 3.52 - 5.25 - 2.5 \text{ dB} = \text{SNR}_{1''} - 11.27 \text{ dB}$$

In summary, the cumulative SNR decrease between 1/4" CCD and 1" CCD is:

$$\text{SNR}_{1/4''} = \text{SNR}_{1''} - 11.27 \text{ dB} \quad (\text{E23})$$

Appendix F

Irradiance Levels at Different Stages of a Video Imaging System

Considering an ideal lens in the air (refraction index $n = 1$) and without energy absorption, the principle of energy conservation establishes that the radiance L and the $A\omega$ product or throughput are conserved (Greivenkamp, 2004).

Thus, in a video imaging system, see Figure 40, the radiant flux Φ_d falling on the detector equals the radiant flux Φ_{lens} falling on the lens which equals the radiant flux Φ_s emitted by the source.

The following approximations (Greivenkamp, 2004) are considered:

- First-order optics so optical systems are supposed without aberrations
- Gaussian approximation and paraxial optics equations
- Objectives are lens element combinations typically used to image distant objects and the simple objective is represented by a thin lens.
- Thin lens is an approximation, so the thickness of the lens is negligible because the source is placed a distance $d \gg f$ (lens focal distance).

Thus, a thin lens has optical power but no thickness and the image distance $q \approx f$ (the rear focal length).

The paraxial equations are approximations based on first order relationships of an optical system (Greivenkamp, 2004) that assumes that all ray angles are small, so $\tan\alpha \approx \alpha$. However, according to lens manufacturers the paraxial equations are sufficiently accurate for the vast majority of situations (Rolyn, n.d.) and are the approximations that will be used to derivate the equations for the irradiance levels at different stages of the video imaging system.

It also can be argued that the Gaussian model of ray pencil limitations may not be applied in reality because in general the Entrance Pupil and Exit Pupil aberrations

are large, but indeed only the centers of the pupils to develop the projection model are used (Lenhardt & Kreuznach, 2005).

Irradiance E_{lens} at the Objective Lens

The radiant flux either emitted or reflected from a source approximated to a Lambertian radiator, see Figure 64, and falling Φ_{lens} on the objective lens may be calculated by multiplying the radiance L_s of the source A_s and the solid angle of the lens ω_{lens} to obtain:

$$\Phi_{lens} = L_s A_s \omega_{lens} \tag{F01}$$

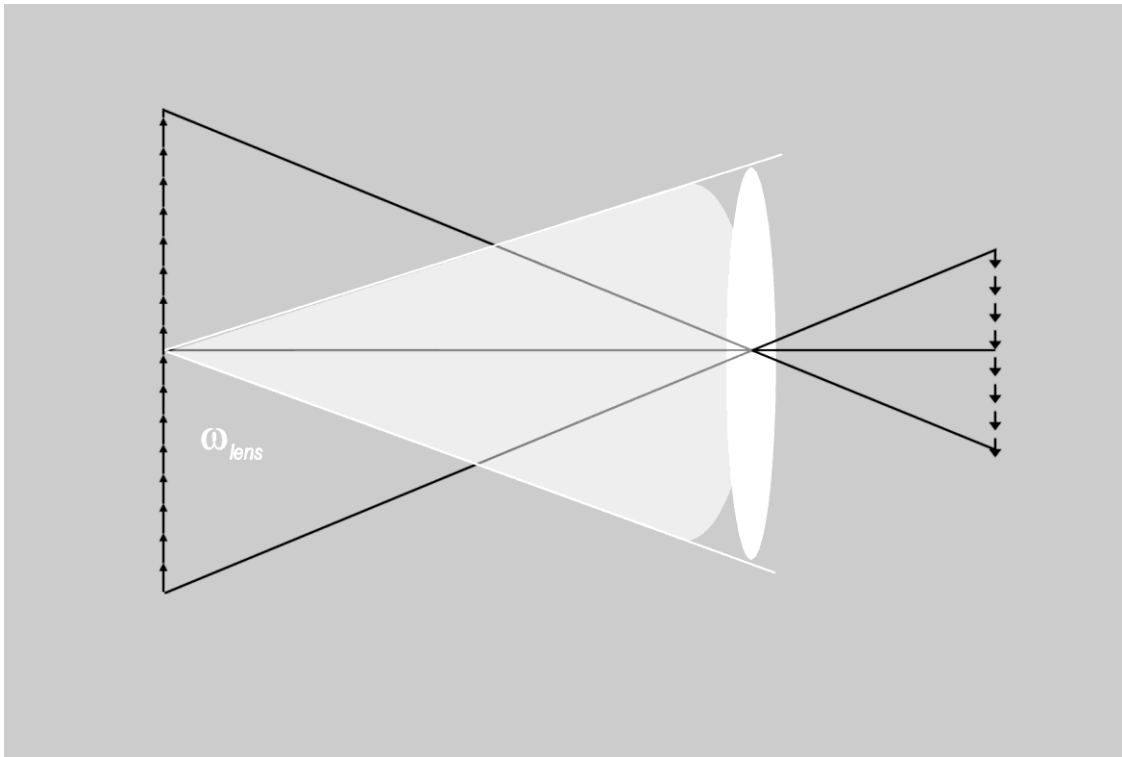


Figure 64. Solid Angle ω_{lens} Subtended by the Lens

According to Figure 64 and Figure 65 the following equation applies:

$$A_s \omega_{lens} = A_s A_{lens} / d^2 = A_{lens} A_s / d^2 = A_{lens} \omega_s$$

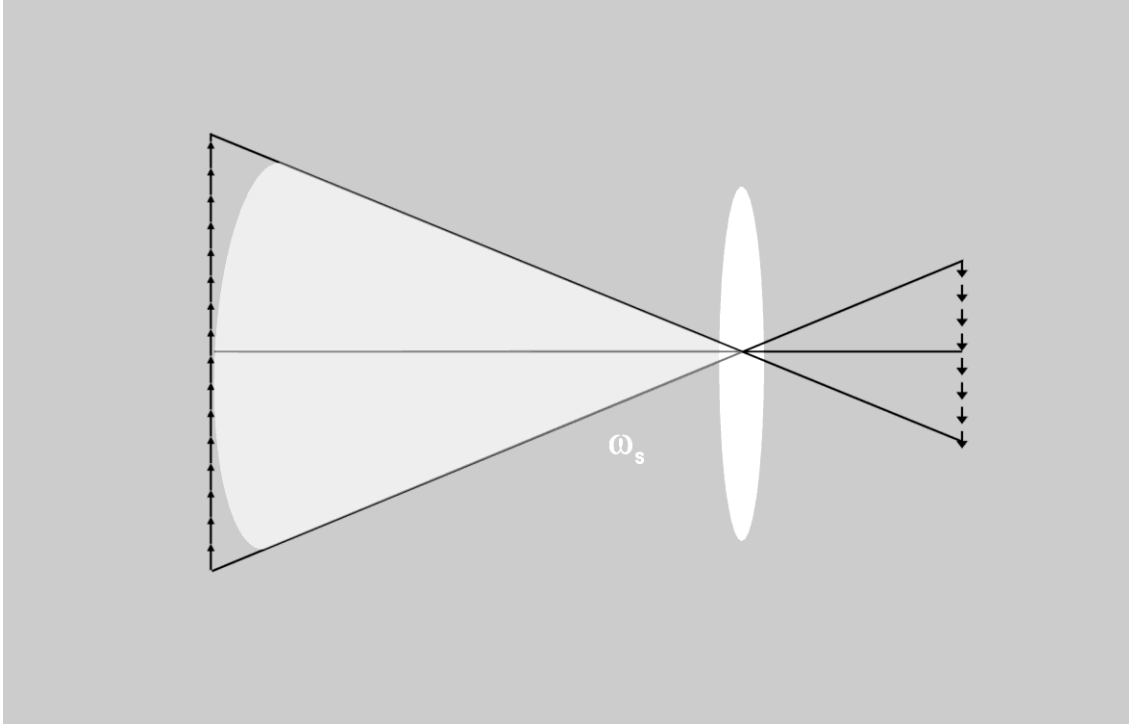


Figure 65. Solid Angle ω_s Subtended by the Source

Hence the radiant power on the lens can be stated as:

$$\Phi_{lens} = L_s A_s \omega_{lens} = L_s A_{lens} \omega_s = L_s A_{lens} 4\pi \sin^2(\theta_{max}/2) \quad (\text{F02})$$

because the solid angle ω_s subtended by the source at the lens is $\omega_s = 4\pi \sin^2(\theta_{max}/2)$

and the irradiance at the lens $E_{lens} = \frac{\Phi_{lens}}{A_{lens}} = L_s 4\pi \sin^2(\theta_{max}/2)$ can be approximated by:

$$E_{lens} \xrightarrow{\theta \text{ small}} E_{lens} \approx L_s \pi \theta_{max}^2 = L_s \pi \left(\frac{r}{\sqrt{d^2 + r^2}} \right)^2 = L_s \pi \frac{r^2}{d^2 + r^2} = L_s \frac{A_s}{d^2 + r^2} = L_s \omega_s \text{ (see Figure 55)}$$

where $A_s \approx \pi r^2$ is the flat area of the circular source cross section instead of its cone cap (see earlier derivation of equation (D14) in Appendix D).

Thus for θ small E_{lens} is given by (see Figure 40):

$$E_{lens} \approx L_s \frac{A_s}{d^2 + r^2} \quad (\text{F03})$$

Irradiance E_d in Terms of the Objective Lens F -Stop

Taking into account the Lens Equation (Al-Azzawi, 2007) see Figure 66:

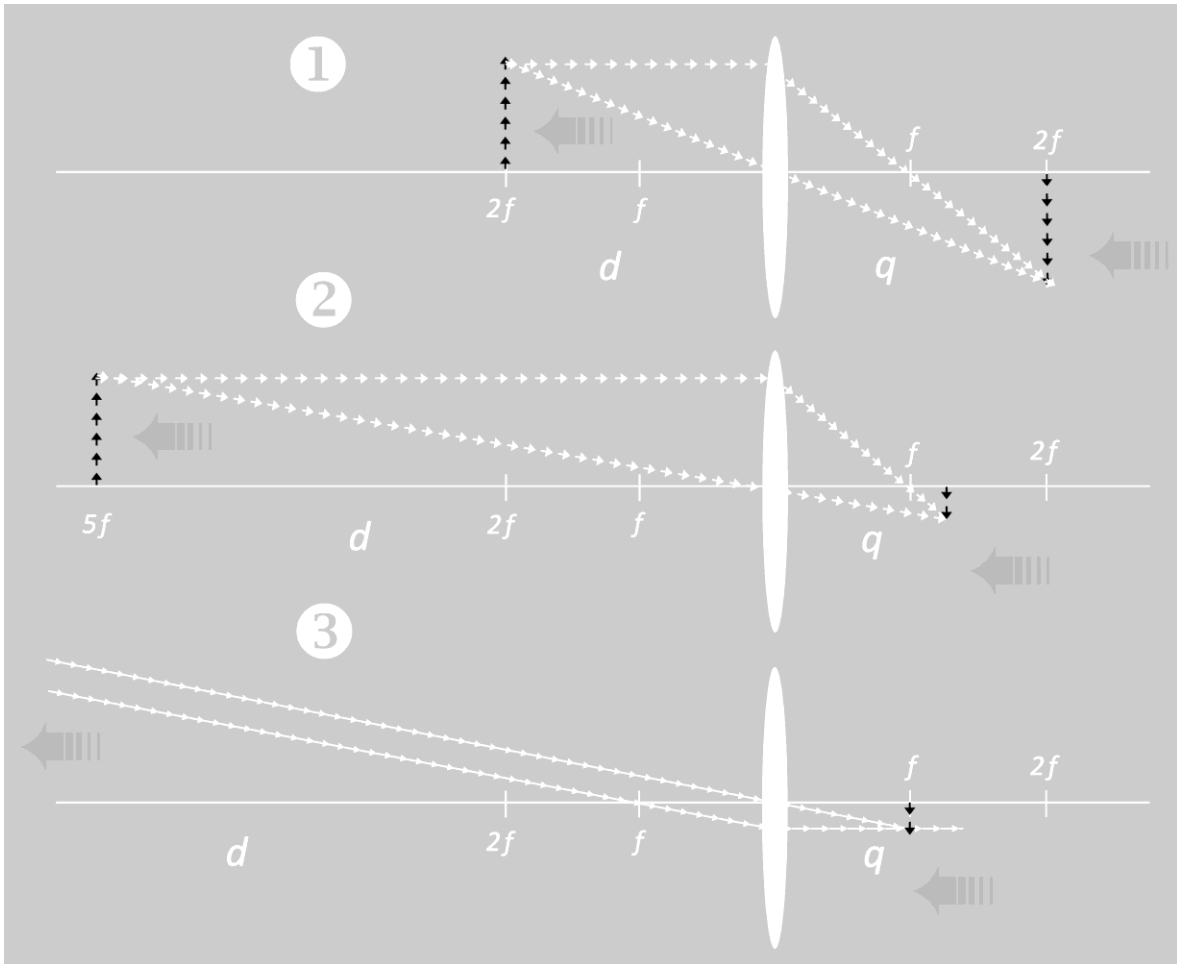


Figure 66. Image Formation by a Converging Thin Lens

d : distance between the lens and the object

q : distance where the image is located

The principal axis is calibrated in terms of f units being:

f : the lens focal distance

$2f$: twice the lens focal distance, etc.

The basic equation for thin lenses is:

$$\frac{1}{d} + \frac{1}{q} = \frac{1}{f}$$

and

$$\frac{1}{q} \rightarrow \frac{1}{f} \xrightarrow{d \rightarrow \infty} q \rightarrow f$$

Also:

$$d = 2f \implies \frac{1}{q} = \frac{1}{f} - \frac{1}{2f} = \frac{2}{2f} - \frac{1}{2f} = \frac{1}{2f} \implies q = f$$

then:

$$2f \leq d \leq \infty \implies 2f \geq q \geq f$$

Cases 1, 2, and 3 in Figure 66 illustrate that if the same object is placed farther away, then the image gets smaller and closer to f the focal point of the lens.

In the limit $d \rightarrow \infty \implies q \rightarrow f$. Optical infinity is considered for $d \geq 20$ ft (6 m).

The irradiance E_d can be described as a function of $F\text{-Stop} = \frac{f}{D}$ where f is the lens focal distance and D is the lens Entrance Pupil, see Figure 40, based on the thin lens approximation as follows:

$$A_{lens} \approx \pi \left(\frac{D}{2}\right)^2 \text{ then } F\text{-Stop} = \frac{f}{D} \implies \pi \left(\frac{D}{2}\right)^2 = \frac{\pi f^2}{4F\text{stop}^2} \implies$$

$$A_{lens} \approx \frac{\pi f^2}{4F\text{stop}^2} \quad (\text{F04})$$

Considering that $\omega_s = 4\pi \sin^2(\theta_{max}/2)$ the radiant power on the lens can be rewritten as:

$$\Phi_{lens} = L_s A_s \omega_{lens} = L_s A_{lens} \omega_s = L_s \frac{\pi f^2}{4F\text{stop}^2} 4\pi \sin^2(\theta_{max}/2) \quad (\text{F05})$$

Now, taking into account the Lens Equation (Al-Azzawi, 2007), see Figure 66:

$$\frac{1}{d} + \frac{1}{q} = \frac{1}{f} \quad (\text{F06})$$

Considering the geometrical relationship $\frac{r'}{r} = \frac{q}{d}$ where r and r' are the radii of the source and detector respectively, see Figure 40, the equation (F06) can be rewritten as:

$$q = f \left(1 + \frac{r'}{r} \right) \approx f \quad (\text{F07})$$

Thus:

$$q \xrightarrow{r' \ll r} f$$

when $r' \ll r$ the distance q can be approximated to f and the image plane is located at f

Namely, the image plane is located at the focal distance f when the ratio $\frac{r'}{r}$ of the radii r' and r of the detector surface and the source area is very small.

Then using equation (F07) $q \approx f$ for $\frac{r'}{r} \ll 1$ the solid angle ω_d , see Figure 40, can be approximated as follows:

$$\omega_d \approx \frac{A_d}{\left(\sqrt{f^2 + r'^2} \right)^2} \quad (\text{F08})$$

The exact equation, see Figure 17, for the solid angle is: $\omega_d = 4\pi \sin^2(\theta_{max}/2)$ and

$$\omega_d = 4\pi \sin^2(\theta_{max}/2) \approx \frac{A_d}{\left(\sqrt{f^2 + r'^2} \right)^2} \quad (\text{F09})$$

Therefore it can be stated that:

$$A_d \approx (f^2 + r'^2) 4\pi \sin^2(\theta_{max}/2) \quad (\text{F10})$$

For a lossless lens: $\Phi_d = \Phi_{lens}$ and replacing the previous equations in E_d :

$$\begin{aligned} E_d &= \frac{\Phi_d}{A_d} = \frac{\Phi_{lens}}{A_d} \approx \frac{Ls \frac{\pi f^2}{4F_{stop}^2} 4\pi \sin^2(\theta_{max}/2)}{(f^2 + r'^2) 4\pi \sin^2(\theta_{max}/2)} = \frac{Ls \frac{\pi f^2}{4F_{stop}^2}}{(f^2 + r'^2)} = \frac{\pi Ls f^2}{(f^2 + r'^2) 4F_{stop}^2} = \\ &= \frac{\pi Ls f^2}{f^2 4F_{stop}^2 + r'^2 4F_{stop}^2} = \frac{\pi Ls}{4F_{stop}^2 + \left(F_{stop} \frac{2r'}{f} \right)^2} = \frac{\pi Ls}{4F_{stop}^2 + \left(\frac{2r'}{D} \right)^2} \end{aligned}$$

where in the last part of the equation it has also been used the definition of $F\text{-Stop} = \frac{f}{D}$

Thus for $\frac{r'}{r} \ll 1$ the illuminance E_d can be approximated as follows:

$$E_d = \frac{\Phi_d}{A_d} \approx \frac{\pi L S}{4F_{stop}^2 + \left(\frac{2r'}{D}\right)^2} \quad (\text{F11})$$

where $2r'$ is the sensor array format and D is the lens entrance pupil.

If the format of the sensor array equals the lens entrance pupil, as it is typically the case for surveillance video imaging systems which include a 1/2-format fixed objective lens with 1X magnification and 1/2-inch format CCD, then $2r' = D$ and

$$E_d = \frac{\Phi_d}{A_d} \approx \frac{\pi L S}{4F_{stop}^2 + \left(\frac{2r'}{D}\right)^2} = \frac{\pi L S}{4F_{stop}^2 + 1} \quad (\text{F12})$$

Irradiance E_d in Terms of E_{lens} and Lens FOV

Another useful equation for the irradiance level E_d at the lens using $\Phi_d = \Phi_{lens}$ will be deduced:

$$E_d = \frac{\Phi_d}{A_d} = \frac{\Phi_d A_{lens}}{A_d A_{lens}} = \frac{\Phi_{lens} A_{lens}}{A_d A_{lens}} = \frac{\Phi_{lens} A_{lens}}{A_{lens} A_d} = E_{lens} \frac{A_{lens}}{A_d} \quad (\text{F13})$$

Using the thin lens approximation:

$$A_{lens} = \pi \left(\frac{D}{2}\right)^2 = \pi \frac{f^2}{4F_{stop}^2}$$

and

$$A_d = \pi r'^2$$

hence:

$$\frac{A_{lens}}{A_d} = \frac{1}{4F_{stop}^2} \left(\frac{f}{r'}\right)^2 = \frac{1}{\left(\frac{2r'}{f} F_{stop}\right)^2} \quad (\text{F14})$$

According to Figure 40:

$$\tan(\theta_{max}) = \frac{r'}{f} \xrightarrow{\theta \text{ small}} \tan(\theta_{max}) \approx \theta_{max} = \frac{r'}{f} \implies \frac{2r'}{f} = 2\theta_{max} \quad (\text{F15})$$

and based on the definition of Angle of View, shown in Figure 7, the lens angle of view FOV in Figure 40 will be $FOV: \theta = 2\theta_{max}$

Thus:

$$\frac{2r'}{f} = FOV \quad (F16)$$

and replacing equation (F16) in equation (F14) it gives:

$$\frac{A_{lens}}{A_d} = \frac{1}{\left(\frac{2r'}{f}F_{stop}\right)^2} = \frac{1}{(FOV * F_{stop})^2} \quad (F17)$$

Thus the irradiance E_d at the detector can be indicated as follows:

$$E_d = E_{lens} \frac{A_{lens}}{A_d} \approx \frac{E_{lens}}{(FOV * F_{stop})^2} \quad (F18)$$

Appendix G

Summary of Key Equations and Relationships

Following is a list of key equations and relationships from Appendixes D, E, and F:

$$\text{apex angle} = \theta \quad \omega = \pi \sin^2(\theta) \quad (\text{D09})$$

$$\text{apex angle} = 2\theta \quad \omega = 4\pi \sin^2(\theta/2) \quad (\text{D08})$$

$$2\theta \text{ small } (\leq 94^\circ) \quad \omega_s \approx \pi \theta^2 = \frac{A_s}{R^2} = \frac{A_s}{d^2 + r^2} \quad A_s \text{ (flat)} = \pi r^2 \quad (\text{D14})$$

$$E_d = \frac{\Phi_d}{A_d} = \frac{2L_s A_s}{r_s^2 + r_d^2 + d^2 + \sqrt{(r_s^2 + r_d^2 + d^2)^2 - 4r_s^2 r_d^2}} \quad (\text{E11})$$

$$E_d \approx \frac{L_s A_s}{r_s^2 + r_d^2 + d^2} \approx \frac{L_s A_s}{d^2} \approx L_s \omega_s \quad (\text{E12})$$

$$\Phi \approx L_s A_d \omega_s = L_s A_s \omega_d \quad (\text{E13})$$

$$E_d = \frac{\Phi_d}{A_d} \approx L_s \omega_s \cos^4 \theta_x = L_s \omega_d \frac{A_s}{A_d} \cos^4 \theta_x \quad (\text{E18})$$

$$E_{lens} \approx L_s \frac{A_s}{d^2 + r^2} \quad (\text{F03})$$

$$E_d = \frac{\Phi_d}{A_d} \approx \frac{\pi L_s}{4F_{stop}^2 + \left(\frac{2r'}{D}\right)^2} \quad (\text{F11})$$

$$E_d = \frac{\Phi_d}{A_d} \approx \frac{\pi L_s}{4F_{stop}^2 + \left(\frac{2r'}{D}\right)^2} = \frac{\pi L_s}{4F_{stop}^2 + 1} \quad (\text{F12})$$

$$E_d = E_{lens} \frac{A_{lens}}{A_d} \approx \frac{E_{lens}}{(FOV * F_{stop})^2} \quad (\text{F18})$$

VITA

JOAQUIN RAVENTOS

Personal Data: Place of Birth: Barcelona, Spain
U.S. Citizen

Education: B.S., Electronics Engineering
Telecommunications Engineering School, Polytechnic
University of Barcelona, 1979
Thesis: The Underlying Mathematical Theory and
Principles to Designing Multiple-Band Equalizers
Awarded: Summa cum laude

M.S., Engineering Technology
East Tennessee State University, Dec 2011
Thesis: New Test Set for Video Quality Benchmarking
Entrepreneurial Leadership Certificate
East Tennessee State University, Dec 2011

Professional Experience: Electronics Engineer
Philips Electronics, Barcelona, Spain, 1980-1987
Manufacturing Consultant
CL/EY, Barcelona, Spain, 1987-1992
Owner – Operator
QTIC, Miami, Florida, 1992-1998
Vice President Engineering / Sales
Nightline, Inc., Miami, Florida, 1998 – Present

Honors and Awards: Golden Key International Honour Society